Structure and Function of Protein-only RNase P

by

Michael J. Howard

A dissertation submitted in partial fulfillment
of the requirements for the degree of
Doctor of Philosophy
(Biological Chemistry)
in the University of Michigan
2015

Doctoral Committee:

Professor Carol A. Fierke, Chair
Professor David. R. Engelke
Associate Professor Patrick J. O'Brien
Associate Professor Bruce A. Palfey
Professor Nils G. Walter

Dedication

To those in an honest pursuit to understand how nature works.

Acknowledgements

My time as a graduate student has been enjoyable, and this is in large part due to my mentor Carol Fierke, who granted me with freedom to make valuable mistakes but did not let me stray too far. Her breadth of scientific knowledge, patience, and compassion are a continual source of inspiration.

I would also like to thank past and present members of the Fierke lab for creating a great work environment. I particularly would like to thank members of the RNase P group for help, reagents, comments, and discussions (Wan Lim, Xin Liu, Yu Chen, Bradley Klemm, and Nancy Wu). Also great thanks to Markos Koutmos who has been almost like a second mentor to me. Chapter 2 would not have been possible without his expertise.

Additionally, I would like to thank the Biological Chemistry department, both administrators and faculty members, for creating a great environment for learning.

I would also like to acknowledge my family and friends for their support. In particular my father's skepticism, my mother's strong work ethic, and their shared reverence for nature are attributes that have shaped my life and brought me here. Furthermore, I would like to acknowledge a friend of the family, Riley Mahar, whose passion for science and critic thinking really sparked my interest in science.

And my fiancé, Ashley Konal, who shares my scientific curiosity and will partake in discussions about my ideas concerning enzymes, evolution, and life. Thanks for all the love, support, and encouragement.

Table of Contents

List of Figures

List of Tables

Abstract

Transfer RNA is essential for deciphering the genetic code. Transcribed as a precursor, containing extra nucleotides on its 5’ and 3’ termini, tRNA must undergo several enzymatic processing steps before functioning in protein translation. One of the first steps in tRNA maturation is removal of the 5’ extraneous sequence, which is catalyzed by ribonuclease P (RNase P). In all domains of life RNase P can be found composed of a single catalytic RNA which associates with a varying number of proteins. However, a protein-only RNase P (PRORP) has evolved for functioning within genome containing organelles such as the mitochondrion and chloroplast, and the nucleus of land plants and some protist.

This work investigates the molecular function of PRORP. The crystal structure of PRORP1 from *Arabidopsis* reveals three domains: a pentatricopeptide repeat (PPR) domain tethered to a metallonuclease domain through a structural-zinc binding site. The pH and metal dependence of PRORP1 catalyzed pre-tRNA hydrolysis with wild-type and active site mutants is consistent with PRORP1 using a two-metal ion mechanism with a metal hydroxide nucleophile to catalyze phosphodiester bond hydrolysis. Interestingly, this proposed catalytic mechanism is similar to the RNA-based RNase P mechanism, providing evidence for the mechanistic convergence of two different macromolecules, RNA and protein. Furthermore, examination of the reactivity of the three PRORP isozymes with a number of pre-tRNAs of different organellar origin demonstrates that the plant PRORP isozymes have overlapping substrate specificities but varying cleavage fidelities. Overall this work provides an understanding of the molecular function of PRORP enzymes and lays the foundation for understanding the more complicated human mitochondrial protein-only RNase P.

Chapter 1 [1]
Introduction

Background

Gene expression involves the processes of transcription and protein translation, the so called central dogma of biology. Transfer RNA (tRNA) is an essential molecule in protein translation that acts as an adaptor of the genetic code, relating a nucleotide sequence to an amino acid. tRNA primary transcripts are extensively processed and modified before they participate in translation. One of the initial steps in precursor-tRNA (pre-tRNA) processing is the removal of extra nucleotides flanking the 5' and 3' ends. Ribonuclease P (RNase P) is the endonuclease responsible for catalyzing 5' end cleavage (Figure 1-1) (1). In eukaryotes, RNase Z catalysis removal of the extra nucleotides on the 3' end of tRNA (2). After end processing, the tRNA undergoes a series of enzymatic processing events including CCA addition to the 3' end, nucleotide modifications, and aminoacylation (2). Some tRNAs contain intron sequences encoded within the tRNA body that are catalytically removed by nucleases and ligated as part of their maturation process (3). The enzymes involved in tRNA maturation are essential for life, with the exception of a majority of the tRNA base modification enzymes (2).

RNase P is arguably one of the more intriguing enzymes found within the tRNA maturation pathway because it is a ribonucleoprotein (RNP) complex. The RNA component is responsible for the catalytic activity and associates with either 1, 5 , or 10 proteins in Bacteria, Archaea and Eukaryotes, respectively (Figure 1-2) (4). To date, the archeon *Nanoachaeum equitans* is the only known organism without RNase P, presumably because the tRNAs in this organism are transcribed without leader

[1] Some contents in this Chapter are taken from a point-of-view article: Howard,M.J., Liu,X., Lim,W.H., Klemm,B.P., Fierke,C.A., Koutmos,M. and Engelke,D.R. (2013) RNase P enzymes: divergent scaffolds for a conserved biological reaction. *RNA Biol*, **10**, 909–14.

sequences (5). The RNA components in Bacteria, Archaea, and Eukaryotic nuclear RNase P are structurally related (6), highlighting the conservation of this ribozyme throughout life.

RNA-Based RNase P

Studies on $tRNA^{Tyr}$ in the early 70's revealed that it is produced as a precursor-tRNA, with extra nucleotides flanking the 5' and 3' ends of the mature tRNA. Thus, researches reasoned that to generate functional tRNA, nuclease activity must catalyze removal of these extra nucleotides. A search for this activity in *Escherichia coli* revealed a 5'endonuclease activity, which generates products containing a 5' phosphate mature tRNA and a 3' hydroxyl-terminated leader (7). Because the nuclease cleaved pre-tRNA, it was named RNase P. Subsequent studies revealed that bacterial RNase P is composed of a catalytic RNA and a small protein (8). Sidney Altman was awarded the Nobel Prize in chemistry for the discovery of catalytic RNA, which was shared with Thomas Cech for his studies on the *Tetrahymena* ribozyme.

Since its discovery, bacterial RNase P has remained a model system for understanding how RNA performs catalysis. This is due in part to its minimal number of components: bacterial RNase P is composed of a ~400 nt RNA (P RNA) component which associates with an ~120 amino acid protein (P protein). Additionally, bacterial RNase P is the only naturally occurring ribozyme discovered to date that catalyzes multiple-turnovers and does not require proteins for activity *in vitro* (8). The RNA component alone is fully catalytic in high salt, however *in vivo* the protein component is required for viability (8). The protein component increases the substrate and magnesium affinity for the P RNA (9,10).

There are two major reasons why enzymes are fascinating: enzymes catalyze reactions rapidly and have specificity for their substrates. These two reasons are particularly interesting with regard to RNA-based RNase P because it uses RNA as the macromolecule to accomplish these tasks. Devoid of many of the functional groups that amino acids contain, RNase P utilizes magnesium cofactors to catalyze phosphodiester bond hydrolysis (11). RNA-based RNase P is proposed to use a classic two-metal ion

mechanism (12). In this proposed mechanism, metal I activates a water molecule and/or stabilizes the hydroxide nucleophile for attack of the scissile phosphate, both metal ions

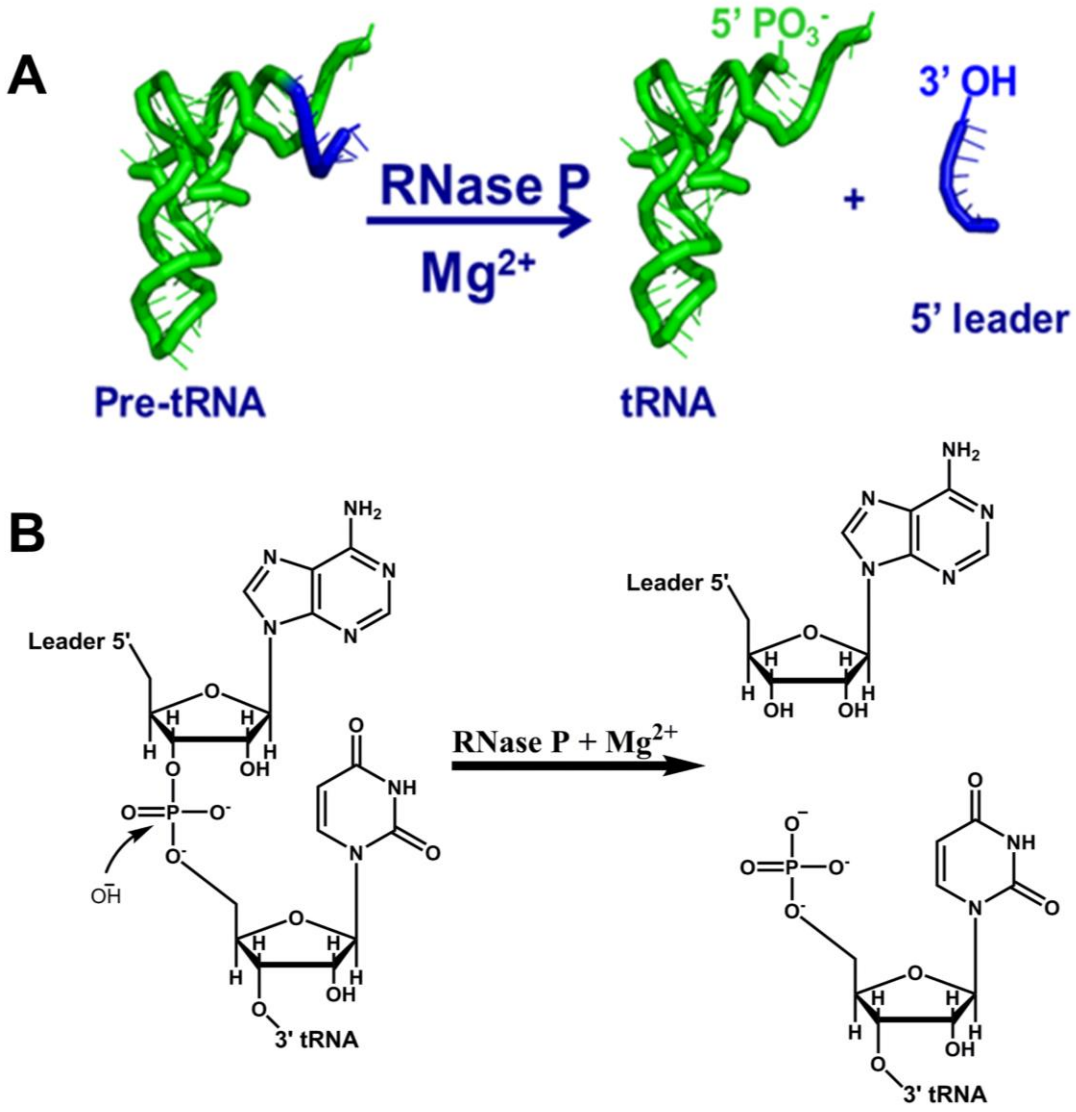

Figure 1-1. RNase P catalyzes 5' end maturation of Pre-tRNA. A. RNase P catalyzes the removal of the 5' leader from precursor-tRNA generating a mature 5' phosphate tRNA. The leader sequence is shown in blue. B. RNase P uses metal ions to catalysis phosphodiester bond hydrolysis.

stabilize the negative charge build up in the transition state, and metal II acts as an electrophilic catalyst stabilizing the 3’ oxyanion leaving group (12). Thus, the RNA component is proposed to bind and orient metal ions to achieve catalysis, with no direct use of functional groups involved in stabilizing the transition state.

RNase P recognizes over 20 different pre-tRNAs substrates, thus the molecular recognition determinants of RNase P has to be shared among the different pre-tRNAs. These interactions include: base stacking and pairing between P RNA and the elbow region (D and T-loops), nucleotides within the leader sequence, the acceptor stem, and the CCA of the 3’ end of pre-tRNA (13,14). Additionally, the P protein interacts with the leader through both electrostatic and hydrogen bonding interactions (15). These interactions were confirmed in the crystal structure of *Thermotoga maritima* RNase P in complex with tRNA and a product leader (14).

Discovery of Protein-only RNase P

Given the ubiquity and conservation of RNA-based RNase P, it seemed unlikely that a protein-only version would exist. Indeed, propositions of a protein-only RNase P functioning within organelles was meet with harsh skepticism (16). The first evidence for a protein-only RNase P came from spinach chloroplast where partial purifications of RNase P activity was detected showing sedimentation coefficients characteristics similar to a protein and displaying a stereochemical difference in chemistry compared to the RNA-based enzyme (17,18). Similarly, the RNase P activity from human mitochondria was shown to be insensitive to nuclease treatment and have a distinct substrate specificity as compared to the nuclear RNase P (19). However, because the genetic identity of this activity remained unknown, for many, the burden of proof was not satisfied. Until the paradigm was finally shifted when Rossmanith and colleagues demonstrated, through a series of partial purifications and proteomic techniques, that human mitochondrial RNase P is composed of three proteins: tRNA m1G methyltransferase (MRPP1/TRMT10C), hydroxysteroid 17-β dehydrogenase 10 (MRPP2/SDR5C1), and a metallonuclease (MRPP3/PRORP) (20).

The Evolution of PRORP

The discovery of the genetic identity of protein-only RNase P in humans allowed for identification of protein-only RNase P genes within other organisms. The characterization of PRORP enzymes in various eukaryotic lineages provides insight into the evolution of PRORP enzymes, including hints as to its origin and history.

In contrast to the multi-subunit human mitochondrial RNase P, the RNase P in the mitochondria/chloroplasts of most plants, algae, and some protists is predicted to be a single protein enzyme (PRORP) (21,22) . This was first shown in *A. thaliana*, where three isoforms are found: PRORP1, 2, and 3. PRORP1 localizes to the mitochondria and chloroplasts, whereas PRORP2 and 3 localize to the nucleus (21). All three of these enzymes catalyze pre-tRNA processing in their respective localized organelles and *in vitro* (23). Attempts to identify RNase P RNA genes in plant genomes by sequence homology have not yielded any potential candidates for a canonical nuclear RNase P (24-26). This suggests that *A. thaliana* may be devoid of an RNA-based RNase P thereby catalyzing 5' end processing using only PRORP enzymes (27). Alternatively, the plant RNase P RNA may be non-canonical, thus making it hard to identify by sequence homology searches. Evidence in support of this hypothesis comes from RNase P activity detected by immunoprecipitation of the protein POP1, which is a shared protein component of MRP and nuclear RNase P in other eukaryotes (28).

The protozoan *Trypanosoma brucei* harbors two PRORP isoforms, both of which catalyze 5' pre-tRNA processing activity *in vitro* (22). One isoform (PRORP1) localizes to the nucleus and the second (PRORP2) to the mitochondrion. Strikingly, *T. brucei* PRORP1 can substitute for yeast nuclear RNase P *in vivo*, demonstrating that a single protein can complement a RNP complex composed of 9 proteins and a ~400 nucleotide catalytic RNA (22). In addition, this result shows that *T. brucei* PRORP1 catalyzes all of the other non-canonical, yet vital functions of nuclear yeast RNase P, which may include processing of non-canonical RNAs. It has also been shown that *Arabidopsis* PRORP1 can complement for the loss of *E. coli* RNase P *in vivo* (21).

Similar to *Arabidopsis*, the moss, *Physcomitrella patens,* also contains three PRORP enzymes and no apparent gene encoding the catalytic RNA component for the RNA-dependent version of RNase P (29). However, in *P. patens* two PRORP enzymes localize

to the mitochondria and chloroplast and one to the nucleus (29). Furthermore, knockout of the nuclear PRORP in *P. patens* is not lethal, suggesting a yet unidentified RNase P activity in the nucleus or potential dual localization of one or both of the organellar PRORPs (29). The two PRORPs (PpPPR_67 and PpPPR_104) that are proposed to localize to the mitochondria and chloroplast are significantly longer than PRORPs from other organisms, 791 and 993 amino acids, respectively. For comparison, the plant PRORPs are 572, 528, 576 amino acids and human PRORP is 583 amino acids in length. These extra amino acids are located at the N and C-termini and contain no identifiable domains. Further biochemical characterization will need to be performed to understand the function of this extra matter.

Ostreococcus tauri, an alga and one of the smallest eukaryote species, may be a living transitional organism representing the possible switch from RNA- to protein-based RNase P activity. The chloroplast and mitochondrial genomes of *O. tauri* encode distinct individual RNase P RNA genes and the nucleus encodes both a bacterial-like RNase P protein component, and a PRORP enzyme (30). The organellar RNase P RNAs are expressed *in vivo,* however under *in vitro* conditions catalysis of pre-tRNA cleavage is not observed even when associated with the nuclear encoded bacterial-like protein*. O. tauri* is the only organism studied thus far, that encodes RNase P RNAs in both organellar genomes and contains a nuclear encoded PRORP. The localization of the nuclear encoded PRORP is currently unknown. Thus, further studies are required to help understand why *O. tauri* has retained the organellar encoded RNase P RNA genes.

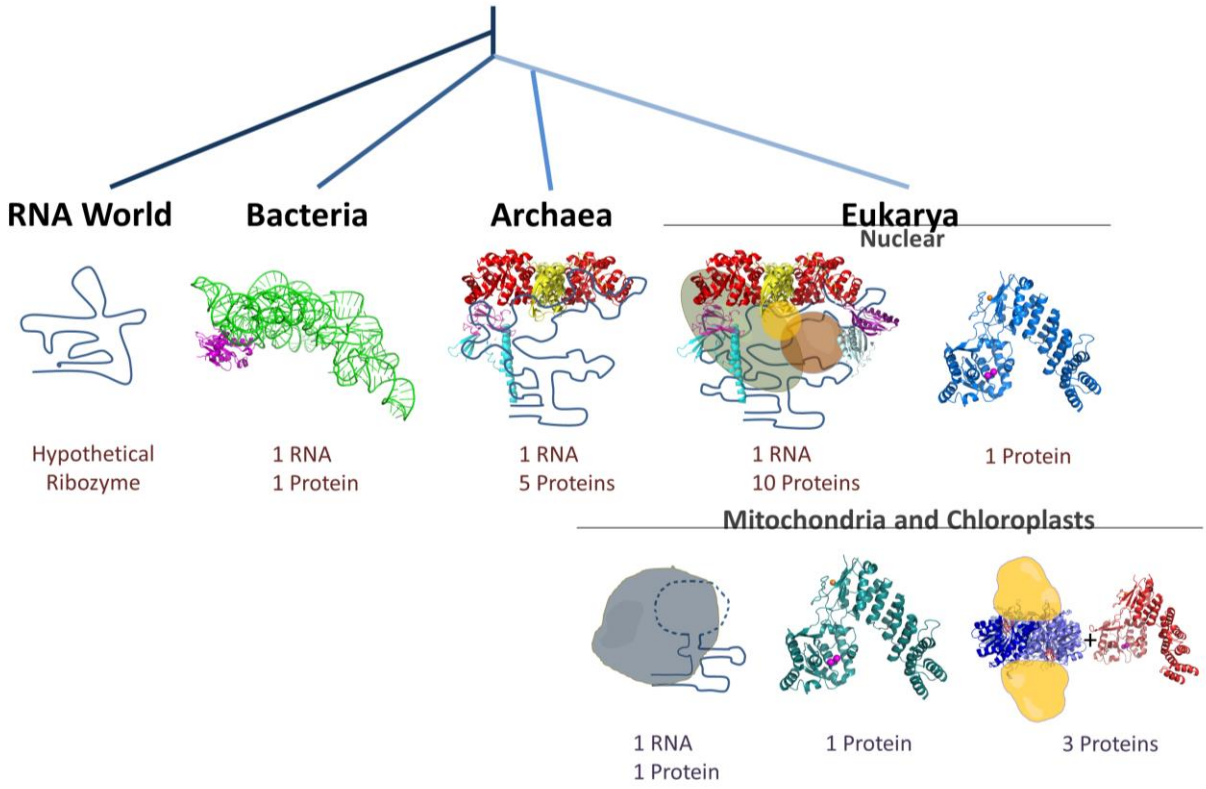

Figure 1-2. RNase P is conserved in all 3 domains of life. Bacterial RNase Ps consists of 1 RNA (green) and 1 protein (magenta) (pdb 3Q1R). Model of archaeal RNase P which contains 1 RNA (secondary structure in blue) and at least 4 proteins (red: PH1877 (PDB 2CZV), yellow: PH1481 (PDB 2CZV), magenta: PH1771 (PDB: 2ZAE), cyan: PH1601 (PDB 2CZV). Proteins are arbitrary positioned. Most eukaryal nuclear RNase Ps are RNP based (left) which contain 1 RNA (blue) and at least 9 proteins (4 archaeal homologs, green: POP1, brown: POP3, purple: POP6 (PDB 3IAB), silver: POP7 (PDB 3IAB), orange: POP8). The proteins are arbitrary positioned. Some nuclear RNase Ps are proposed to be protein-only with homology to PRORP1 (i.e. *T. brucei* and *A. thaliana*; structure of PRORP1 shown). Mitochondrial and chloroplast RNase Ps from left to right: yeast; plants, some algae, and some protists (*A. thaliana* and *T. brucei*); mammals (human). The mitochondrial yeast RNase P contains 1 RNA (blue) and 1 large protein, RPM2, (gray). Plant, some algae, and protists mitochondrial/chloroplast RNase Ps are single proteins (teal) that have homology to *A. thaliana* PRORP1. Mammalian mitochondrial RNase Ps consists of 3 nuclear encoded proteins TRMT10C, (MRPP1) , SDR5C1 (MRPP2), and PRORP (MRPP3) shown in yellow cartoon, blue tetramer (PDB 1U7T), and red (homology model based of *A. thaliana* PRORP1), respectively. The positioning of the TRMT10C/SDR5C1 subunits has not yet been demonstrated.

As mentioned previously, mammalian mitochondrial RNase P enzymes utilize three protein components for efficient pre-tRNA cleavage. The three protein components include: a tRNA-methyltransferase (TRMT10C), a dehydrogenase (SDR5C1), and the PRORP nuclease. The methyltransferase and dehydrogenase form a complex with a proposed stoichiometry of 2:4 and the metallonuclease does not tightly associate with either subunit (20,31). The tRNA methyltransferase activity of TRMT10C is activated by SDR5C1. However, the catalytic activity of either the methyltransferase or the

dehydrogenase is not required for pre-tRNA cleavage catalyzed by PRORP (31). The reason for the additional protein components in mammalian mitochondrial RNase P could be a result of the non-canonical tRNA structures that mitochondrial-encoded tRNAs form (32). Thus, one possible explanation for the requirement of TRMT10C and SDR5C1 to activate PRORP activity is that the TRMT10C-SDR5C1 complex associates with a pre-tRNA substrate to induce conformational changes required for pre-tRNA cleavage catalyzed by PRORP. The role of the TRMT10C-SDR5C1 complex in human mitochondrial RNase P is one of the biggest questions in the field.

Analyzing the inventory of PRORP enzymes described above, an interesting evolutionary history emerges. First, all PRORP enzymes discovered are nuclear encoded and are absent in bacterial and archaeal genomes, suggesting they evolved within eukaryotic evolution. PRORP genes can be found in distant eukaryotic linages, plants, metazoans, and excavates, suggesting PRORP genes were present in the early diversification of eukaryotes (Figure 1-3). However, no genes for PRORP are apparent in the fungal, amoebozoa, and chromalveolates lineages suggesting that these lineages possibly lost PRORP, potentially through direct competition with RNA-based RNase P. Taken together, I and others propose that PRORP evolved for functioning in the mitochondria during early eukaryotic evolution. Cech and colleagues have termed this organelle-triggered diversification (33). Possible reasons why the organellar genome did not retain a RNA-based RNase P could be that there was strong evolutionary pressure to downsize organellar genomes, which would allow for rapid replication and give regulatory control to the nucleus (34). But why not just import the nuclear RNase P into the mitochondria? Some possible explanations to this answer include difficulties in importing a large structured RNA and differences in substrate recognition. However, there must be some evolutionary advantage distinct from mitochondrial acquisition, because PRORP also overtook the nuclear RNA-based RNase P, as seen in plants and trypanosomes.

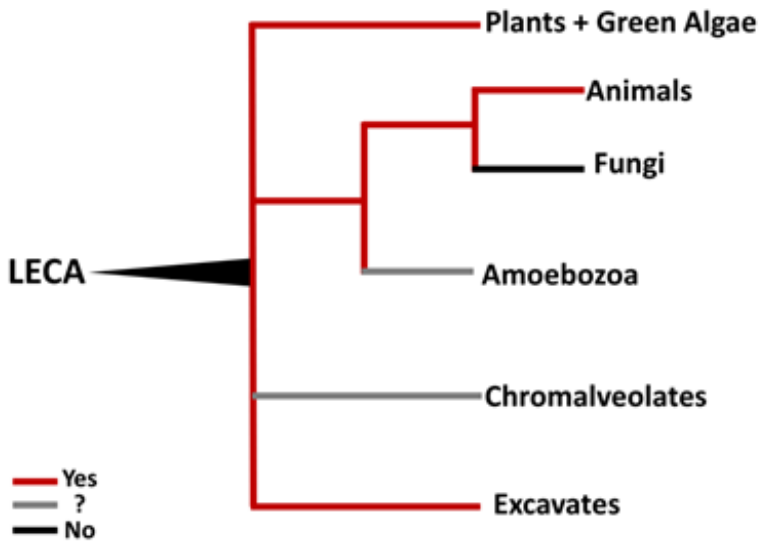

Figure 1-3. The evolution of PRORP. The main eukaryotic lineages are shown (tolweb.org), originating from the last eukaryotic common ancestor (LECA). Black lines indicate lineages where PRORP genes have not been identified in nuclear genomes. Grey lines indicate lineages where no obvious *prorp* genes are found through blast searches using human or *Arabidopsis* PRORPs on representive organisms (*Dictyostelium discoideum* for Amoebozoa and *Tetrahymena thermophila* for Chromalveolates). Red lines represent linages containing *prorp* genes.

Conclusions and Significance

PRORP represents a new class of enzyme that has replaced the function of RNA-based RNase P. The origin of PRORP may have been initiated by the acquisition of organelles during early eukaryotic evolution (~2 BYA). This provides a unique situation where one can ask fundamental questions about the nature of catalysis and substrate recognition between two different macromolecules, RNA and protein. Furthermore, the RNA world hypothesis proposes that proteins overtook the function of most catalytic RNAs, the mechanisms underlying this replacement could provide fundamental insights into protein evolution and the origin of modern cells. PRORP represents a model system for exploring this proposed shift from RNA to protein, an event that likely happened numerous times during the course of evolution. Additionally, the enzymes and pathways for RNA processing in organelles is largely unknown and mutations within mitochondrial tRNAs and within RNase P can manifest as diseases within humans (35). Thus, an understanding of PRORP function can provide insight into the molecular basis of diseases originating from dysfunctional mitochondrial RNA processing.

Objectives

The overall objective of this research is to understand the molecular function of the newly discovered PRORP. Since PRORP represents an entirely new nuclease, very little was known about how it performs catalysis and recognizes substrates. Therefore, chapter 2 describes the crystal structure of PRORP1 and identifies important domains and residues involved in substrate binding and catalysis. In chapter 3, using the crystal structure as a guide, we probed the catalytic mechanism of PRORP using mutants and variations in pH and metal concentrations. In chapter 4, the substrate specificity of the three plant PRORPs with four different pre-tRNAs and model RNA substrates are examined. Taken together, this work provides an understanding of this new class of enzyme, provides insight into understanding the more complicated human mitochondrial RNase P, and potentially provides a foundation for understanding the basis for mitochondrial disease states that arise through dysfunction in RNA processing.

References

1. Xiao, S., Scott, F., Fierke, C.A. and Engelke, D.R. (2002) Eukaryotic ribonuclease P: a plurality of ribonucleoprotein enzymes. *Annu Rev Biochem*, **71**, 165-189.
2. Phizicky, E.M. and Hopper, A.K. (2010) tRNA biology charges to the front. *Genes & development*, **24**, 1832-1860.
3. Paushkin, S.V., Patel, M., Furia, B.S., Peltz, S.W. and Trotta, C.R. (2004) Identification of a human endonuclease complex reveals a link between tRNA splicing and pre-mRNA 3' end formation. *Cell*, **117**, 311-321.
4. Walker, S.C. and Engelke, D.R. (2008) A protein-only RNase P in human mitochondria. *Cell*, **135**, 412-414.
5. Randau, L., Schröder, I. and Söll, D. (2008) Life without RNase P. *Nature*, **453**, 120-123.
6. Ellis, J. and Brown, J. (2009) The RNase P family. *RNA biology*, **6**, 362-369.
7. Robertson, H.D., Altman, S. and Smith, J.D. (1972) Purification and properties of a specific Escherichia coli ribonuclease which cleaves a tyrosine transfer ribonucleic acid precursor. *Journal of Biological Chemistry*, **247**, 5243-5251.
8. Guerrier-Takada, C., Gardiner, K., Marsh, T., Pace, N. and Altman, S. (1983) The RNA moiety of ribonuclease P is the catalytic subunit of the enzyme. *Cell*, **35**, 849-906.
9. Smith, D. and Pace, N.R. (1993) Multiple magnesium ions in the ribonuclease P reaction mechanism. *Biochemistry*, **32**, 5273-5354.
10. Beebe, J.A., Kurz, J.C. and Fierke, C.A. (1996) Magnesium ions are required by Bacillus subtilis ribonuclease P RNA for both binding and cleaving precursor tRNAAsp. *Biochemistry*, **35**, 10493-10505.
11. Gardiner, K.J., Marsh, T.L. and Pace, N.R. (1985) Ion dependence of the Bacillus subtilis RNase P reaction. *J Biol Chem*, **260**, 5415-5419.
12. Steitz, T.A. and Steitz, J.A. (1993) A general two-metal-ion mechanism for catalytic RNA. *Proc Natl Acad Sci U S A*, **90**, 6498-6502.
13. Zahler, N.H., Sun, L., Christian, E.L. and Harris, M.E. (2005) The pre-tRNA nucleotide base and 2'-hydroxyl at N(-1) contribute to fidelity in tRNA processing by RNase P. *J Mol Biol*, **345**, 969-985.
14. Reiter, N.J., Osterman, A., Torres-Larios, A., Swinger, K.K., Pan, T. and Mondragón, A. (2010) Structure of a bacterial ribonuclease P holoenzyme in complex with tRNA. *Nature*, **468**, 784-789.
15. Koutmou, K.S., Day-Storms, J.J. and Fierke, C.A. (2011) The RNR motif of B. subtilis RNase P protein interacts with both PRNA and pre-tRNA to stabilize an active conformer. *RNA (New York, N.Y.)*, **17**, 1225-1260.
16. Altman, S., Gopalan, V. and Vioque, A. (2000) Varieties of RNase P: a nomenclature problem? *RNA*, **6**, 1689-1694.
17. Wang, M.J., Davis, N.W. and Gegenheimer, P. (1988) Novel mechanisms for maturation of chloroplast transfer RNA precursors. *EMBO J*, **7**, 1567-1574.
18. Thomas, B.C., Li, X. and Gegenheimer, P. (2000) Chloroplast ribonuclease P does not utilize the ribozyme-type pre-tRNA cleavage mechanism. *RNA*, **6**, 545-1098.
19. Rossmanith, W. and Karwan, R.M. (1998) Characterization of human mitochondrial RNase P: novel aspects in tRNA processing. *Biochem Biophys Res Commun*, **247**, 234-241.
20. Holzmann, J., Frank, P., Löffler, E., Bennett, K., Gerner, C. and Rossmanith, W. (2008) RNase P without RNA: identification and functional reconstitution of the human mitochondrial tRNA processing enzyme. *Cell*, **135**, 462-474.
21. Gobert, A., Gutmann, B., Taschner, A., Gössringer, M., Holzmann, J., Hartmann, R., Rossmanith, W. and Giegé, P. (2010) A single Arabidopsis organellar protein has RNase P activity. *Nature structural & molecular biology*, **17**, 740-744.
22. Taschner, A., Weber, C., Buzet, A., Hartmann, R., Hartig, A. and Rossmanith, W. (2012) Nuclear RNase P of Trypanosoma brucei: a single protein in place of the multicomponent RNA-protein complex. *Cell reports*, **2**, 19-25.
23. Gutmann, B., Gobert, A. and Giegé, P. (2012) PRORP proteins support RNase P activity in both organelles and the nucleus in Arabidopsis. *Genes & development*, **26**, 1022-1027.

24. Hartmann, E. and Hartmann, R. (2003) The enigma of ribonuclease P evolution. *Trends in genetics : TIG*, **19**, 561-569.
25. Piccinelli, P., Rosenblad, M. and Samuelsson, T. (2005) Identification and analysis of ribonuclease P and MRP RNA in a broad range of eukaryotes. *Nucleic acids research*, **33**, 4485-4495.
26. Rosenblad, M., López, M., Piccinelli, P. and Samuelsson, T. (2006) Inventory and analysis of the protein subunits of the ribonucleases P and MRP provides further evidence of homology between the yeast and human enzymes. *Nucleic acids research*, **34**, 5145-5156.
27. Goldfarb, K., Borah, S. and Cech, T. (2012) RNase P branches out from RNP to protein: organelle-triggered diversification? *Genes & development*, **26**, 1005-1009.
28. Krehan, M., Heubeck, C., Menzel, N., Seibel, P. and Schön, A. (2012) RNase MRP RNA and RNase P activity in plants are associated with a Pop1p containing complex. *Nucleic acids research*, **40**, 7956-7966.
29. Sugita, C., Komura, Y., Tanaka, K., Kometani, K., Satoh, H. and Sugita, M. (2014) Molecular characterization of three PRORP proteins in the moss Physcomitrella patens: nuclear PRORP protein is not essential for moss viability. *PLoS One*, **9**, e108962.
30. Lai, L., Bernal-Bayard, P., Mohannath, G., Lai, S., Gopalan, V. and Vioque, A. (2011) A functional RNase P protein subunit of bacterial origin in some eukaryotes. *Molecular genetics and genomics : MGG*, **286**, 359-369.
31. Vilardo, E., Nachbagauer, C., Buzet, A., Taschner, A., Holzmann, J. and Rossmanith, W. (2012) A subcomplex of human mitochondrial RNase P is a bifunctional methyltransferase--extensive moonlighting in mitochondrial tRNA biogenesis. *Nucleic acids research*, **40**, 11583-11593.
32. Helm, M., Brulé, H., Friede, D., Giegé, R., Pütz, D. and Florentz, C. (2000) Search for characteristic structural features of mammalian mitochondrial tRNAs. *RNA*, **6**, 1356-1379.
33. Goldfarb, K.C., Borah, S. and Cech, T.R. (2012) RNase P branches out from RNP to protein: organelle-triggered diversification? *Genes Dev*, **26**, 1005-1009.
34. Berg, O.G. and Kurland, C.G. (2000) Why mitochondrial genes are most often found in nuclei. *Mol Biol Evol*, **17**, 951-961.
35. Yarham, J.W., Elson, J.L., Blakely, E.L., McFarland, R. and Taylor, R.W. (2010) Mitochondrial tRNA mutations and disease. *Wiley Interdiscip Rev RNA*, **1**, 304-324.

Chapter 2 [2]

Mitochondrial Ribonuclease P Structure Provides Insight into the Evolution of Catalytic Strategies for Precursor-tRNA 5'-Processing

Abstract

Ribonuclease P (RNase P) catalyzes the maturation of the 5' end of tRNA precursors. Typically these enzymes are ribonucleoproteins with a conserved RNA component responsible for catalysis. However, protein-only RNase P (PRORP) enzymes process precursor-tRNAs in human mitochondria and in all tRNA-utilizing compartments of *Arabidopsis thaliana*. PRORP enzymes are nuclear encoded and conserved among higher eukaryotes. Here we report the crystal structure of PRORP1 from *A. thaliana* at 1.75 Å resolution revealing a prototypical metallonuclease domain and a pentatricopeptide repeat (PPR) domain tethered together by a structural zinc binding domain. The metallonuclease domain is one of the first high resolution structures of a NYN domain which is a member of the PIN domain-like fold super-family, including the flap nuclease family. The structural similarity between PRORP1 and the flap nuclease family suggests that they evolved from a common ancestor. Biochemical data reveal that conserved aspartate residues in PRORP1 are important for catalytic activity and metal binding, and that the PPR domain also enhances activity, likely through an interaction with pre-tRNA. These results provide a foundation for understanding tRNA maturation in organelles. Furthermore, these studies allow for a molecular level comparison of the catalytic strategies employed by the only known naturally evolved protein and RNA-based catalysts that perform the same biological function, pre-tRNA maturation, thereby

[2] Work in this chapter is published: Howard,M.J., Lim,W.H., Fierke,C.A. and Koutmos,M. (2012) Mitochondrial ribonuclease P structure provides insight into the evolution of catalytic strategies for precursor-tRNA 5' processing. *Proc. Natl. Acad. Sci. U.S.A.*, **109**, 16149–54. M.J.H. and M.K. conducted crystallographic studies; M.K. performed crystallographic analyses; M.J.H. and W.H.L. prepared enzymes and substrate; M.J.H. conducted biochemical assays; M.J.H., C.A.F., and M.K. participated in the study design and interpretation. M.J.H., C.A.F., and M.K. participated in writing the manuscript.

providing insight into the differences between the prebiotic RNA world and the present protein-dominated world.

Background

According to the RNA world hypothesis, RNA played dual roles as carrier of genetic information and catalyst in a prebiotic world. However, over eons of evolution, proteins with their expanded twenty amino acid alphabet and greater structural and functional complexity took over many RNA-based functions. Structural insights into this evolutionary transition are limited because of the lack of examples of RNA and protein macromolecules that perform the same biological function in nature. One notable exception is ribonuclease P (RNase P) that catalyzes maturation of the 5' end of tRNA across all domains of life. Until recently, all known RNase P enzymes included a catalytic RNA component. The discovery of a protein-only RNase P (PROteinacous RNase P (PRORP)) from human mitochondria and *Arabidopsis thaliana* has dramatically shifted this paradigm (1-3). These enzymes represent a new class of metallonucleases and are conserved among higher eukaroytes (1,2). *A. thaliana* encodes three PRORP enzymes (PRORP1, 2, and 3) that catalyze pre-tRNA processing (2). PRORP1 localizes to the mitochondria and chloroplast whereas PRORP2 and PRORP3 localize to the nucleus (2) suggesting that protein-based enzymes catalyze pre-tRNA maturation in all organelles (2,3). To gain mechanistic and evolutionary insights into the PRORP enzyme family we crystallized PRORP1 from *A. thaliana*.

This structure clearly demonstrates that there is no structural homology between PRORP1 and any of the proteins associated with either the bacterial or the nuclear human RNase P (4,7) revealing that this protein evolved independently from the ribonuclearprotein RNase P. Furthermore, the combination of structural and biochemical data suggests that the RNA and protein-based catalysts employ distinct strategies to bind and cleave pre-tRNA. In PRORP1, the PPR domain enhances pre-tRNA binding affinity, in contrast to the RNA-tRNA contacts in the ribozyme (4). While both PRORP1 and bacterial RNase P are magnesium-dependent enzymes, the metal ions are coordinated by carboxylate side chains and non-bridging phosphate oxygens / nucleotide carbonyl groups (4), respectively. These studies allow us to begin to compare, at a molecular level,

the catalytic strategies and molecular recognition employed by the protein-only and RNA-based RNase P enzymes.

Results

Global Architecture of PRORP1

The crystal structure of a functional recombinant protein-only RNase P from *A. thaliana* (residues 76-572 with the mitochondrial signal sequence deleted) was solved by single wavelength anomalous dispersion (SAD) and was refined to a resolution of 1.98 Å (R_{work} = 18.7%, R_{free} = 22.0% with good stereochemistry; Table A-1). One molecule is present per asymmetric unit and the final refined model includes residues 95-570 (Figure 1). PRORP1 adopts a conformation that resembles an upside down “V”, where two arms, each ~70 Å in length, fold at an angle of ~56º. Arm1 is comprised of 11 α-helices, whereas arm 2 is composed of a parallel β-sheet flanked by α-helices (Figure 2-1). The two arms are attached to a core domain consisting of an anti-parallel β-sheet. These discrete structural elements represent three domains: PPR domain (residues 95 to 292; red in Figure 2-1C), central domain (residues 328 to 357 and 534 to 570; yellow in Figure 1C) and metallonuclease domain (residues 358 to 533; blue in Figure 2-1C).

The PPR Domain is Important for Activity and Substrate Affinity

PPR motifs are often found in tandem and are composed of a helix-turn-helix fold of approximately 35 amino acids (8). These motifs have been implicated in RNA binding and editing activities and are prevalent among proteins targeted to mitochondria and chloroplasts (9-11). The PPR domain in PRORP1 is comprised of 11 α-helices forming 5.5 consecutive PPR repeats, each consisting of a helix-turn-helix hairpin (Figures 2-1,2-2A). These tandem helical repeats associate to form a right-handed super-helical structure that resembles the arrangement of domains in tetratricopeptide repeat (TPR)-motifs. As a result, the PPR domain forms an inner concave surface facing the putative active site of the metallonuclease domain. A comparative search based on the PPR domain using the Dali server (12) reveals structural similarity with a plethora of proteins (or protein domains) that notably include mitochondrial RNA polymerase (mtRNAP) (13),

Get4 (14), proteosomal subunit Rpn6 (15), and small glutamine-rich tetratricopeptide repeat protein (hSGT) (16) (Figure 2-2B). Except for mtRNAP, which contains the first and only structural data on PPR motifs, all of the homologous domains contain TPR motifs that are involved in protein-protein interactions (8). The PPR domain of mtRNAP is proposed to interact with upstream DNA promoter sequences (13). Similarly, we posit that the PPR domain of PRORP1 facilitates interactions with pre-tRNA. An N-terminal truncation of PRORP1 (Δ245) that removes 8 of the 11 helices in the PPR domain decreases pre-tRNA binding affinity by 34-fold and catalytic activity by ≥ 2,000-fold (Figure 2-3C) with little effect on zinc binding (Table A-2). Since the PPR domain is located far away from the metal-binding active site, we propose that this domain is important for properly orientating the leader of pre-tRNA in the active site rather than playing a direct role in catalysis. The electrostatic surface potential for PRORP1 (calculated using Apbs (17)) (Figure 2-1D) demonstrates that the concave surface facing the putative active site has an overall neutral charge, suggesting that the PPR-nucleic acid interaction is not mainly electrostatic. The only positive patch is found in the base of the PPR domain closest to the active site, including side chains from the inner facing helices and connecting loops. The PPR domain could interact directly with pre-tRNA through contacts between this positive patch and the negatively phosphodiester back-bone, recognition of the tertiary fold of tRNA, and/or interactions with conserved nucleobases of tRNA, as proposed for other PPR domains (18).

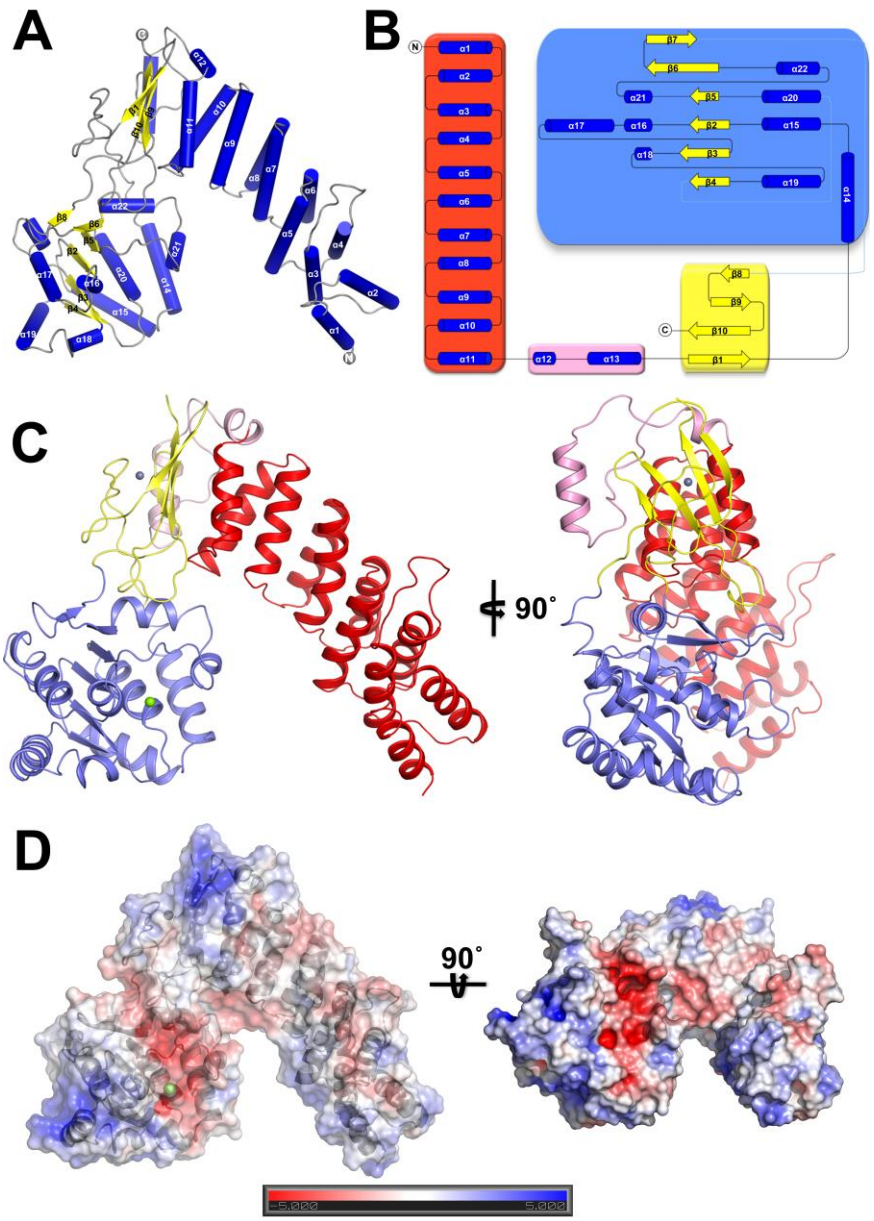

Figure 2-1. Crystal Structure of PRORP1. **(**A) Structure of PRORP1 (helices shown in blue, strands shown in yellow); (B) Topology map of secondary structure elements; (C) Cartoon depiction of the PRORP1 domain arrangements: PPR domain (residues 95 to 292; red), central domain (residues 328 to 357 and 534 to 570; yellow) and metallonuclease domain (residues 358 to 533; blue); and (D) Electrostatic surface potential.

Central Domain

The central domain contains an anti-parallel 4-stranded β-sheet that interacts with the PPR domain and two extended loops that connect it to the metallonuclease domain. The central domain houses a conserved structural zinc binding site (Figure 2-2C, Figure A-1). Zinc is coordinated by four invariant residues: C344, C350, H548 and C565. C344 and C350 are found on the 15 aa-long two-turn loop (between β1 and α14) connecting the metallonuclease and the central domains. H548 and C565 are located in β-strands 9 and 10, respectively (Figure 2-2C). The zinc structural site appears to be important for both stabilizing the structure of the loop-rich central domain and for properly orienting this domain with respect to the metallonuclease domain. The central and metallonuclease domain interface (473 $Å^2$) is mainly stabilized by electrostatic interactions.

The beta sheet of the central domain forms a large hydrophobic interface with helices α9, α10 and α11 of the PPR domain. In addition, 10 hydrogen bonds and two salt bridges (between R335 and D285 and D288) mold the PPR and central domain interface. Furthermore, the PPR domain is linked to the central domain through a 32 residue insertion (shown in pink in Figure 2-1C and Figure A-1) found only in plant species. This positively charged insertion contains a loop-helix-loop that interacts with the PPR/central domain interface forming primarily hydrophobic interactions with the PPR domain (473 $Å^2$) and mainly electrostatic interactions with the central domain (621 $Å^2$), including 10 hydrogen bonds and 4 salt bridges. The central domain may function as an adaptor, orienting the metallonuclease and PPR domains to optimize catalytic activity and molecular recognition.

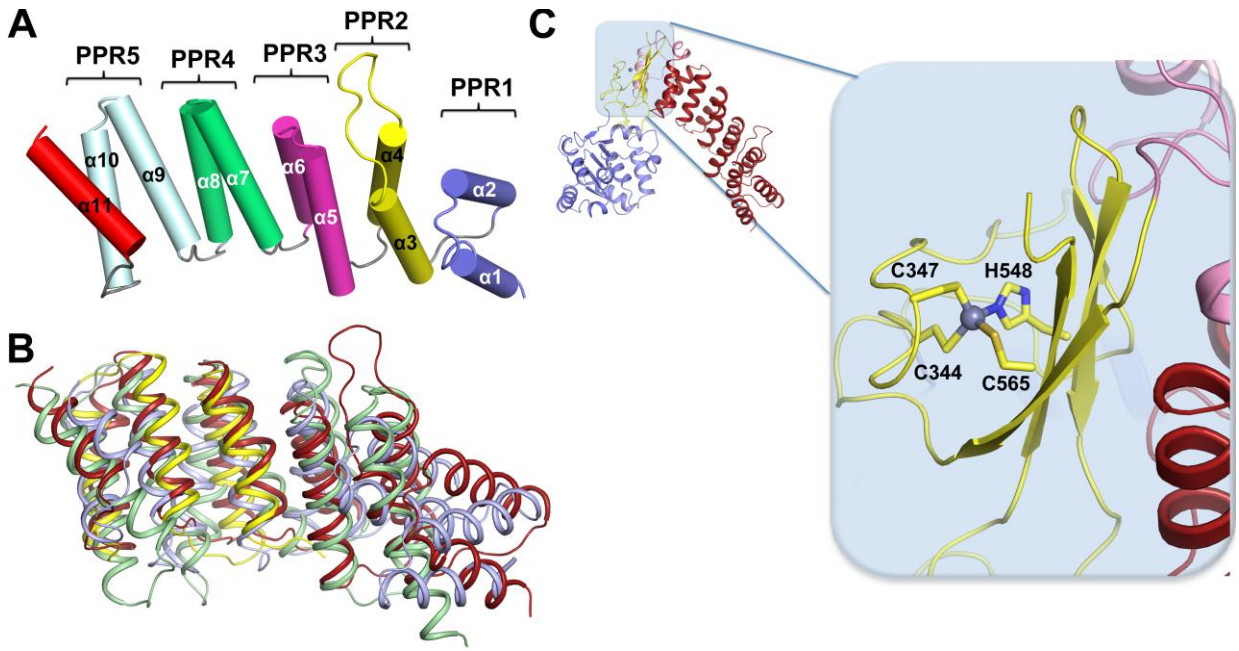

Figure 2-2. PPR Domain Architecture and Structural Zn Binding Site. (A) Tandem repeats of the PPR domain. Domain and profile analysis of PRORP1 using PROSITE predicts three PPR motifs (PPR1, resi 96-130; PPR3, resi 175-209 and PPR4, resi 210-244) based on sequence consensus. The structure reveals two additional helix-turn-helix hairpins that adopt the PPR motif (PPR2, resi 131-174; and PPR5, 245-278) despite their divergence from the canonical PPR sequence. The PPR2 hairpin contains an extended loop, ~11 aa versus the typically observed 3 aa loop, between alpha helices 3 and 4. (B) Structural superposition of PPR/TPR domains: PRORP1 (red; residues 95-293), mtRNAP (yellow; residues 258-331), Get4 (blue; residues 58-236), and the proteasomal subunit Rpn6 (green; residues 38-222); and (C) Close-up of the Zn binding site of PRORP1.

Lastly, the central domain contains two major positively charged patches (Figure 2-1D) that could interact with the tRNA backbone. One of these patches is in close proximity to the zinc site, suggesting that the bound zinc site stabilizes the structure of the central domain such that positively charged residues are oriented to interact with pre-tRNA, similar to the role of structural zinc sites in zinc fingers (19).

Metallonuclease Domain

The structure of the metallonuclease domain of PRORP1 is one of the first high resolution structures of a NYN (Nedd4-BP1, YacP Nucleases) domain, a distinct ribonuclease family member of the PIN (PilT N-Terminal) domain-like fold super-family (20). This structure resembles the nuclease domains of DNA polymerase I and flap

nucleases; the closest metallonuclease domain structural homologues include Taq polymerase (21), and human exonuclease 1 (5) (hExo1; Figure 2-3). However the PRORP1 metallonuclease domain lacks hallmark structural features of flap nucleases, including the helical arc and the helix-two-turn-helix motifs important for nucleic acid binding. The alteration in the substrate binding site is expected given the differences in the structures of the RNA and DNA substrates of PRORP1 and flap nucleases. Nonetheless, these enzymes have a similar architecture around the putative active site.

The flap nuclease family members are proposed to use a two metal-ion catalytic mechanism with the metal ions bound to conserved aspartate residues (5). The metallonuclease domain of PRORP1 contains four invariant aspartate residues (D474, D475, D493, and D399) that are likely important for function based on the structural similarity to hExo1 (Figure 2-3) (3). However, PRORP enzymes lack two of the conserved aspartates in flap nucleases (D173 and D225 in hExo1, highlighted with arrows in Figure 2-3C) that are proposed to chelate a second metal ion. Despite this, structural studies indicate that PRORP1 can bind two metal ions at the active site (Figure 2-3). In metal soaking experiments, a single ion is bound to the active site upon addition of Ca(II) or Sr(II) ions, while two metal ions are observed in the presence of Mn(II). One metal ion bound to PRORP1 (Ca(II), Sr(II) or Mn_1(II); Figure 2-3) forms inner-sphere interactions with D475 and water-mediated contacts with D399, D474, and D493. In the Mn(II)-bound structure, the second metal ion (Mn_2(II)) forms inner-sphere interactions with D475 and D493 and is displaced by 0.5 Å from the position of the second metal ion in hEXo1. The lower metal occupancy (80%) of this site in PRORP1 suggests that Mn_2(II) is more weakly bound. Although structural data cannot prove the function of a metal ion, we propose that the second metal ion activates catalysis by comparison to the flap nucleases. Furthermore, the affinity of the second metal ion may be enhanced by interactions with the pre-tRNA substrate rather than aspartate side chains. Given the similarities between the hExo1 and PRORP1 active sites, we predict that the pre-tRNA scissile phosphate will be located between the two metal ions and form inner-sphere interactions with both.

Mutagenesis experiments confirm the functional importance of invariant aspartate residues in PRORP1 (3). Alanine substitution of each of the four aspartate residues (D474, D475, D493, and D399) in Δ76PRORP1 decreases cleavage activity by >1000-

fold without significantly affecting pre-tRNA binding affinity (Figure 2-3C) indicating that these side chains are mainly important for catalytic activity. The negatively charged residues located in the active site pocket lead to an overall negative electrostatic potential at the active site (Figure 2-1D), perhaps mimicking the negative electrostatic potential at the active site of the bacterial RNA-dependent RNase P.

Metal Activation

Mg(II) had previously been shown to activate PRORP1 catalysis (3). To further analyze the metal dependence, we examined the activation of PRORP1 by other divalent cations in the presence of the magnesium hexahydrate mimic, cobalt(III)hexamine (22), to stabilize the tertiary structure of pre-tRNA. PRORP1 with a stoichiometric zinc ion (Table A-2) cannot catalyze pre-tRNA cleavage, indicating that the bound Zn(II) is a structural cofactor (Figure A-2). No cleavage activity is observed upon addition of Ca(II) (Figure 2-3E). In contrast, both Mg(II) and Mn(II) activate PRORP1-catalyzed phosphodiester bond hydrolysis to form mature tRNA (Figure 2-3E and Figures A-2, A-3). Given the relative abundance of Mg(II) compared to Mn(II) *in vivo (23)*, Mg(II) is likely the PRORP1 cofactor in mitochondria and chloroplasts, similar to other metallonucleases, including bacterial RNase P (24).

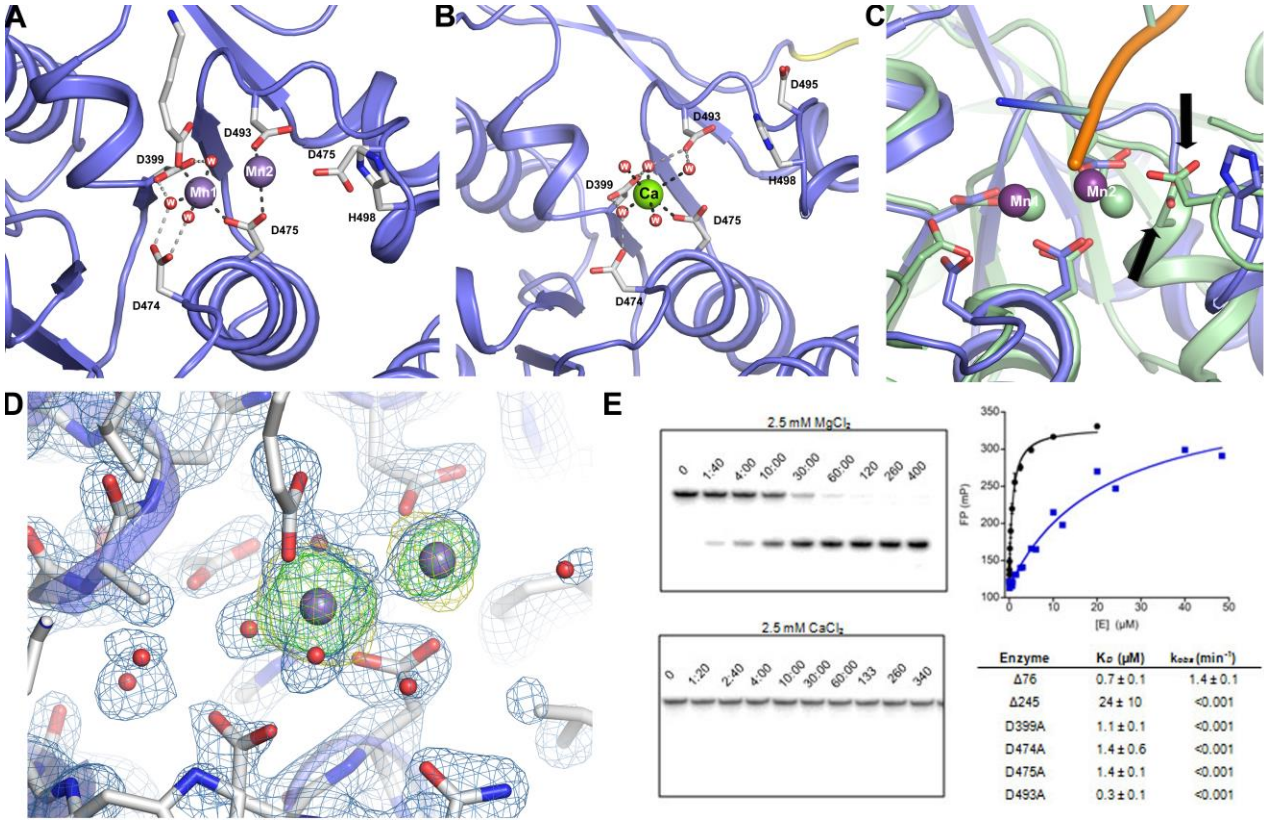

Figure 2-3. Active Site, Metal Dependence, and Pre-tRNA Binding of PRORP1. (A) Close up of the Mn(II) bound PRORP1 active site indicating conserved residues involved in metal binding. (B) Close up of the Ca(II) bound PRORP1 active site. (C) Structural alignment of the active sites of the PRORP1 metallonuclease domain (blue) and hExo1 (green bound to DNA)(5); active site Mn(II) metals shown in purple spheres for PRORP1 and green spheres for hExo1. Red arrows indicate the location of the two aspartates in hExo1 that coordinate the second active site metal ($Mn(II)_2$); there are no equivalent residues in PRORP1 that bind $Mn(II)_2$. (D) Electron density maps of the active site in the Mn(II)-bound PRORP1. The anomalous difference 2Fo-Fc electron density map, contoured at 3σ, is shown in yellow and is superimposed on the PRORP1 structure. This map was calculated from experimental phases derived from data collected at the Mn-edge. The composite omit 2Fo-Fc difference density map for PRORP1 with Mn(II) contoured at 1.5σ is shown in blue. The omit Fo-Fc difference map for the PRORP1 model refined without the active site Mn atoms and inner sphere water molecules, is contoured at 10σ and is shown in green. (E) Representative gels of metal-dependent single turnover cleavage assays (top and bottom left panels). Reactions containing *A. thaliana* mitochondrial 5'-^{32}P-pre-$tRNA^{Cys}$, 500 nM Δ76PRORP1, 2.5 mM $MgCl_2$ or $CaCl_2$ and 250 μM cobalt(III)hexammine were quenched at specified time points, resolved by denaturing PAGE, and analyzed with a phosphorimager. Mg(II) and Mn(II) activate catalysis of phosphodiester bond hydrolysis while Zn(II) and Ca(II) do not (Figure A-2). Fluorescent polarization binding data in 1 mM $CaCl_2$ (top right panel) indicate that the binding affinity for fluorescein-labeled mitochondria pre-$tRNA^{Cys}$ is decreased 34-fold by deletion of 4 PPR motifs (Δ245PRORP1, blue squares; Δ76PRORP1, black circles). Cleavage rate constants and K_D values for mutant PRORP1 proteins are summarized in the bottom right panel. The errors reported for the K_D and k_{obs} values represent the standard deviation from 2 and 4, respectively, independent experiments (Figure A-3).

Discussion

Here we present the first crystal structure of a protein-only RNase P, a member of the novel family of PRORP proteins. The metallonuclease domain of PRORP1 provides insight into the active site architecture, metal dependence, and potential functional roles of active site side chains in the broad family of NYN domain-containing proteins. The prototypical NYN domain is found across all kingdoms of life, often fused to RNA-binding motifs (20). These domains have evolved to play important roles in RNA processing and they are over-represented in eukaryotic organisms. The similarity of this class of RNases with the flap nucleases is striking, suggesting that they both originated from a common structural fold that diverged from a single ancestor. This common ancestor might have provided an early protein alternative to the RNA-based RNase P (25).

The PRORP1 structure is likely typical of proteins with 5 in-tandem PPR motifs. A number of proteins containing PPR domains are implicated in diseases that stem from mitochondria dysfunction. For example, leucine-rich pentatricopeptide repeat cassette (LRPPRC) and pentatricopeptide repeat domain 2 (PTCD2) are two human PPR-containing proteins that are important for the processing of mitochondrial transcripts as mutations lead to a deficient respiratory chain (26,27). PRORP enzymes from *A. thaliana* and *Ostreococcus tauri* are sufficient to catalyze cleavage of mitochondrial pre-tRNAs *in vitro* (2,28) However, human mitochondrial RNase P requires two additional protein components for efficient tRNA maturation, a tRNA methyltransferase termed MRPP1 and its binding partner MRPP2 which has promiscuous alcohol dehydrogenase activity (1). The role of MRPP1 and MRPP2 in pre-tRNA processing remains to be firmly established, but the need for additional components may reflect the non-canonical structure and methyl modification at position 9 of tRNAs encoded by mammalian mitochondria (29). Nonetheless, the structure of PRORP1 provides a foundation for understanding the complexity of human mitochondrial RNase P, serving as a model for the human catalytic subunit of mitochondrial RNase P (MRPP3). The metallonuclease domains of MRPP3 and PRORP1 share all of the conserved active site residues as well as the side chains that bind zinc in the central domain. Moreover, despite the low sequence identity of their N-terminal domains, the structures of these regions are predicted to be homologous (PPR

domains). Thus, in the absence of an MRPP3 structure, PRORP1 provides a roadmap to rationalize how mutations in pre-tRNAs affect substrate recognition by MRPP3 (30).

Comparison with RNA-based RNase P

PRORP and RNA-based RNase P enzymes employ strikingly different structural scaffolds to catalyze the same biological reaction. Apart from the visually similar 'v' topologies, and the overall negatively charged and relatively flat, open and accessible active sites, there are no conserved structural features between PRORP1 and the RNase P ribonucleoprotein complex (4). This result is consistent with bioinformatic analyses indicating that PRORP evolved separately, and not from their ribonucleoprotein counterparts (2). The protein component of the bacterial RNA-based RNase P is essential for catalysis *in vivo* but not *in vitro* at high salt (31). This protein interacts with both the pre-tRNA 5' leader and the ribozyme to enhance substrate and metal ion affinity and to stabilize the RNA active site (31-33). In contrast, the proteinaceous RNase P has the ability to recognize, orient, and bind pre-tRNA and metal ions without any extraneous assistance. The lack of conserved structural features between the bacterial RNase P proteins and PRORP1 further supports their proposed disparate evolution.

Strikingly, these structural studies suggest that PRORP1 uses a two-metal ion mechanism to catalyze 5' end cleavage, as previously suggested for a variety of nucleases, including enzymes composed of either protein or RNA (5),(34). The RNase P ribozyme is similarly a metalloenzyme, requiring at least 2 co-catalytic metal ions (4,24). Nevertheless, differential chemical moieties at the active sites of the RNA- and protein-based enzymes likely lead to divergent mechanistic strategies. For example, the side chains of aspartate (D399) and histidine (H498) in PRORP1 are positioned such that they could catalyze deprotonation of the nucleophilic metal water and protonation of the leaving group, respectively (Figure 2-4B). In contrast, RNA-based RNase P is proposed to rely on metal activation of bound water to generate the hydroxide nucleophile (35) (Figure 2-4A). Additionally, phosphorothioate-substituted pre-tRNA studies suggest that the active site metal(s) of PRORP1 enzymes do not coordinate the *pro-*R_p oxygen of the scissile phosphate bond (6). This is in direct contrast with RNA-based RNase P enzymes, but similar to other proteinaceous RNases, such as RNase H (36). This direct comparison

of the structures of RNA and protein macromolecules that catalyze pre-tRNA cleavage allows insight into the altered catalytic strategies afforded by protein side chains.

Enhanced catalytic activity is one proposed reason for the evolutionary switch from a prebiotic RNA catalyst to a protein catalyst. However, the efficiency (estimated from k_{cat}/K_M for PRORP3 (~6 x 10^4 M^{-1} s^{-1}) (3) and $k_{chem}/K_{1/2}$ for PRORP1 (~ 5 x 10^4 M^{-1} s^{-1})) for catalysis of pre-tRNA cleavage under *in vitro* conditions is slower than catalysis by *B. subtilis* (~100-fold) or *S. cerevisiae* (~30-fold) RNase P under similar conditions (3,37,38). Nonetheless, PRORPs can complement *E. coli* RNase P and the large multi-component yeast nuclear RNase P *in vivo (2,39).* This comparison suggests that factors other than catalytic efficiency, such as enhanced stability or regulation of expression and activity, were the main driving forces for the evolutionary switch from RNA-dependent to protein-only RNase P.

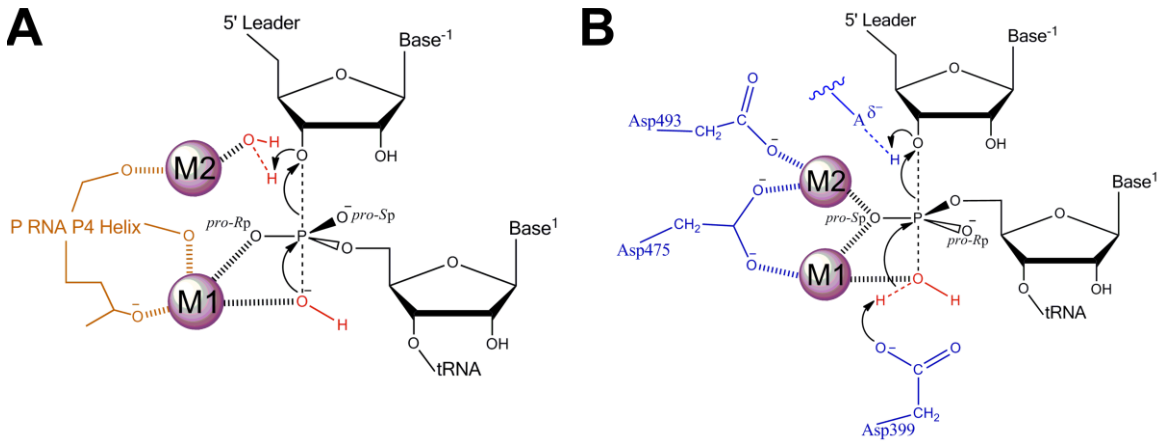

Figure 2-4. Mechanistic comparison of the RNA and protein-based RNase P catalyzed reaction. (A) Proposed mechanism of cleavage catalyzed by RNA-based RNase P (recreated from ref.(4)). The bound metals (M1 and M2) are proposed to be coordinated by non-bridging oxygen phosphates and oxygen atoms of nucleotide bases within the catalytic RNA component. The metal (M1) bound hydroxide is proposed as the catalytic nucleophile. M1 is also proposed to coordinate the *pro-R_p* oxygen of the scissile phosphate bond. M2 is proposed to position a water molecule for leaving group stabilization through protonation of the 3' hydroxyl. (B) Proposed mechanism of cleavage catalyzed by PRORP enzymes. An active site aspartate is proposed to function as a general base, catalyzing deprotonation of a metal (M1) bound water to activate the nucleophilic water. Based on comparison with hExo1 and lack of a phosphorothioate effect on the *pro-R_p oxygen (6)*, the *pro-S_p* oxygen of the scissile phosphodiester is predicted to be coordinated by both active site metal ions to increase electrophilicity and stabilize the transition state. An active site general acid is proposed to protonate and stabilize the leaving group.

Methods

The *PRORP1* gene from *A. thaliana* with the mitochondrial signal sequence deleted (res 76-572) was amplified using PCR and cloned into a pETM-11 vector that adds an N-terminal His_6-tag. The protein was expressed in *E. coli* in the presence or absence of selenomethione (SeMet) and purified using metal affinity, cation exchange and gel filtration chromatography. Crystals of the SeMet-derivatized protein were obtained at 4 °C by the vapor diffusion method from 2:1 mixtures of protein solution with reservoir solution. The reservoir solution contained 18% PEG 3,350 and 0.1 M sodium citrate pH 5.5. Crystals of SeMet Δ76 PRORP1 and wt Δ76 PRORP1 in the presence of Sr and Ca were obtained by adding 0.02 M $SrCl_2$ or $CaCl_2$ into the crystallization solution described above. Crystals of Δ76 PRORP1 in the presence of Mn were obtained through soaking with a solution containing 0.05 M $MnSO_4$. Diffraction data were collected on beamline GM/CA-CAT 23-ID-D at the Advanced Photon Source, Argonne National Laboratory (Argonne, IL). Data were processed with HKL200(40). Phenix AutoSol (41) was used to identify the heavy atom sites and calculate density-modified 1.98 Å experimental maps based on a single-wavelength SAD data set (Se-peak) from one SeMet Δ76 PRORP1 crystal as well as density-modified 2.4 Å experimental maps based on a single-wavelength SAD data set (Mn-peak) from a Mn-soaked Δ76 PRORP1 crystal (Table A-1). Experimental phases were calculated with Phaser, followed by density modification by RESOLVE. COOT (42) was used to manually fix incorrectly modeled residues in all structures, and the final models were built through successive iterative rounds of refinement and manual model building. Refinement was performed using REFMAC5 (43). In the final PRORP1 models residues 76–94 and 571,572 were not modeled. The geometric quality of the models was assessed with MolProbity (44). PyMOL (45) was used to create molecular images.

Appendix A.

This appendix contains supplemental methods

Expression and Purification

DNA encoding the full-length PRORP1 gene (At2g32230) from *Arabidopsis thaliana* was synthesized by Integrated DNA Technologies (IDT). A N-terminal truncation corresponding to residues 76-572 was amplified using PCR and cloned into a pETM-11 vector that adds an N-terminal His_6-tag followed by a TEV protease site. The resulting PRORP1 vector was transformed and expressed in Rosetta(DE3) *E. coli* cells (Novagen). Cells were grown to an $O.D._{600}$ of 0.8 in LB medium and then induced by the addition of 660 µM isopropyl β-D-1-thiogalactopyranoside (IPTG) followed by growth for 16 hrs at 18°C. Harvested cells were lysed using a microfluidizer and centrifuged for 60 min at 20,000 x g at 4°C. The soluble fraction was then applied to a Ni-sepharose column pre-equilibrated in 20 mM 3-(N-morpholino)propanesulfonic acid (Mops) pH 7.8, 150 mM NaCl, 15 mM imidazole, 10% glycerol and 1 mM tris(2-carboxyethyl)phosphine (TCEP).The column was washed with 5 column volumes (CV) of 20 mM MOPS pH 7.8, 150 mM NaCl, 50 mM imidazole 10% glycerol and 1 mM TCEP. Bound proteins were eluted by a gradient from 50 mM to 500 mM imidazole in the same buffer as above over 10 CV. Fractions containing Δ76PRORP1 were pooled and dialyzed against 20 mM MOPS pH 7.8, 150 mM NaCl, 10% glycerol, 1 mM TCEP. Pooled fractions were then loaded onto a SP cation-exchange column and eluted with a NaCl gradient (150 mM to 1000 mM). Fractions of interest were pooled, his_6-tagged tobacco etch virus protease was added and the reaction was dialyzed overnight against 20 mM Mops pH 7.8, 10% glycerol, 150 mM NaCl, and 1 mM TCEP. The sample was then applied to a 2^{nd} Ni-sepharose column. The flow-through was collected, concentrated, and dialyzed into 20 mM Mops pH 7.8, 300 mM NaCl, and 1 mM TCEP. The sample was then loaded onto a Sephacryl-200 gel-filtration column (GE Healthcare) and peak fractions were pooled. Selenomethionine-labeled (SeMet) PRORP1 was expressed and purified in an identical manner with the exception that the cells were grown in minimal media supplemented with 50 mg/liter of SeMet. The Δ245 PRORP1 construct and protein purification were prepared in a similar manner as Δ76 PRORP1.

Mitochondrial pre-tRNA^{Cys} Synthesis and Radio-Labeling

A. thaliana mitochondrial pre-tRNA^{Cys} was created by primer extension from oligonucleotides encoding the T7 promoter and pre-tRNA^{Cys} and cloned into a PUC19 vector. The substrate contains a 53 nt 5' leader, 70 nt body, and 24 nt trailer. Run-off transcription, labeling, and refolding were performed as described in (46,47).

RNase P Cleavage Assays

All cleavage reactions were performed under single-turnover conditions. Standard assay conditions include: 500 nM PRORP1 (as determined by absorbance (Δ76 and mutants: ε_{280} =84630 M^{-1} cm^{-1}; Δ245: ε_{280} =75440 M^{-1} cm^{-1}), 25 pM (30,000 cpm per 70 µL reaction) of 5'-^{32}P labeled *A. thaliana* mitochondrial pre-tRNA^{Cys}, 30 mM Mops pH 7.8, 150 mM NaCl, 1 mM TCEP, and 1 mM $MgCl_2$, 25°C, unless otherwise indicated. The metal reconstitution assays were performed in 250 µM cobalt(III)hexammine (ε_{473} =56.2 $M^{-1}cm^{-1}$) with addition of varied metal species. Reaction time points were quenched by addition of an equal volume of 8 M urea, 100 mM EDTA, and 0.05% (w/v) each of xylene cyanol and bromophenol blue. Quenched reactions were resolved on an 8% denaturing polyacrylamide gels and scanned using a Typhoon imager. Gels were quantitated using Image Quant 5.2 software.

Fluorescent Polarization Binding Assays

The *A. thaliana* mitochondrial pre-tRNA^{Cys} was fluorescently labeled with fluorescein on the 5' terminus as described (48). The binding assays contained 30 mM Mops pH 7.8, 100 mM NaCl, 1 mM TCEP, 1 mM $CaCl_2$, 20 nM 5'fluorescein-pre-tRNA^{Cys} and varying concentration of protein. Reactions were incubated at room temperature for 10 min. Fluorescence polarization data were collected on a Tecan plate reader.

Crystallization and Crystal Harvesting

Stock solutions of 5.5 mg of Δ76 PRORP1 or 5 mg/ml of the SeMet Δ76 PRORP1 variant in 20 mM MOPS pH 7.8, 100 mM NaCl, 1 mM TCEP were used for crystallization trials. Crystals for both the Δ76 PRORP1 and for (1) SeMet Δ76 PRORP1 were obtained

at 4 °C by the vapor diffusion method from 2:1 mixtures of protein solution with reservoir solution in sitting-drop plates. The reservoir solution contained 18% PEG 3,350, and 0.1 M sodium citrate tribasic, pH 5.5. Crystals of (2) SeMet Δ76 PRORP1 in the presence of Sr and (3) wt Δ76 PRORP1 in the presence of Ca were obtained by using the following crystallization solutions: (2) 18% PEG 3,350, 0.1 M sodium citrate, pH 5.5, and 0.02 M $SrCl_2$ and (3) 18% PEG 3,350, 0.1 M sodium citrate, pH 5.5, and 0.02 M $CaCl_2$. Harvested crystals were cryoprotected by soaking in 14% PEG 3,350, 0.08 M sodium citrate tribasic, pH 5.5, w/o 0.015M $SrCl_2$ or $CaCl_2$ and 18% (v/v) glycerol for a few minutes prior to flash cooling in liquid N_2.Manganese soaks were used to incorporate Mn metals in the active site of PRORP1. Specifically, crystals of (4) wt Δ76 PRORP1 were grown by mixing 2:1 mixtures of protein solution with a reservoir solution containing 18% PEG 3,350, 0.1 M sodium citrate, pH 5.5, and 6% w/v 6-aminohexanoic acid. These crystals were transferred in a solution containing 15.3% PEG 3,350, 0.85 M sodium citrate pH 5.5, 5.1% 6-aminohexanoic acid, 12.5 % glycerol and 0.05M $MnSO_4$. After three hours of soaking the crystals were harvested and were flash frozen in liquid N_2. Crystals of (1) SeMet Δ76 PRORP1 were of space group $P2_12_12_1$ (a = 41.8 Å, b = 111.9 Å, c = 139.9 Å) with one molecule in the asymmetric unit (Matthews' coefficient V_M = 2.8 $Å^3$/Da for one molecule per asymmetric unit, 55.6% solvent content). Crystals of (2) SeMet Δ76 PRORP1 with Sr were of space group $P2_12_12_1$ (a = 41.9 Å, b = 112.0 Å, c = 140.0 Å) with one molecule in the asymmetric unit (Matthews' coefficient V_M = 2.9 $Å^3$/Da for one molecule per asymmetric unit, 57.7% solvent content). Crystals of (3) Δ76 PRORP1 with Ca were of space group $P2_12_12_1$ (a = 41.8 Å, b = 111.9 Å, c = 140.1 Å) with one molecule in the asymmetric unit (Matthews' coefficient V_M = 2.9 $Å^3$/Da for one molecule per asymmetric unit, 57.7% solvent content). Crystals of (4) Δ76 PRORP1 with Mn were of space group $P2_12_12_1$ (a = 41.8 Å, b = 112.5 Å, c = 148.8 Å) with one molecule in the asymmetric unit (Matthews' coefficient V_M = 2.9 $Å^3$/Da for one molecule per asymmetric unit, 57.5% solvent content).

Data Collection and Structure Determination

Diffraction data were collected at 100 K on beamline GM/CA-CAT 23-ID-D at the Advanced Photon Source, Argonne National Laboratory (Argonne, IL). Data were

recorded on a Mar300 detector and processed with HKL200 (40). Phenix AutoSol (41) was used to identify the selenium sites and calculate density-modified 1.98 Å experimental maps based on a single-wavelength SAD data set from one SeMet Δ76 PRORP1 crystal (1). Specifically, 14 of 14 selenium sites in addition to one zinc site were located and used for SAD phasing, using phenix.hyss. Subsequently, Phaser**(49)** was used to calculated experimental phases, followed by density modification by RESOLVE**(50)** (figure of merit 0.39 before and 0.64 after density modification). The experimental density map showed clear features of the protein backbone and well-defined side chains. RESOLVE traced and automatically built 449 residues and the side chains for 417 of these residues in the experimental electron density. Phenix AutoSol was also used to locate heavy atoms sites and calculate density-modified 2.4 Å experimental maps based on a single-wavelength SAD data set (Mn-peak) from one Δ76 PRORP1 crystal that was soaked with Mn (5). From the 10 heavy atom sites identified by phenix.hyss, the two heaviest peaks corresponded to the two Mn atoms, while the remaining were “lighter” and mostly corresponded to the position of cysteine or methionine sulfur atoms. Phaser was then used to calculate experimental phases, followed by density modification by RESOLVE that traced and automatically built 373 residues and the side chains for 285 of these residues in the experimental electron density. This structure was not refined further since it only was used to unequivocally locate the position of the active site atoms. COOT (42) was used to manually correct the incorrectly modeled residues and through successive iterative rounds of refinement and manual model building the remaining residues were traced in the electron density to afford the final model. Restrained individual atomic refinement, and restrained isotropic individual B-factor refinement with maximum likelihood targets using the Babinet model for bulk solvent scaling was performed using REFMAC5 (43) of the CCP4 suite (51). The final SeMet Δ76 PRORP1 model, after the removal of Zn, residues with high B-factors, and water molecules was used as a starting model for the refinement of the (2) SeMet Δ76 PRORP1 with Sr to 2 Å, of the (3) Δ76 PRORP1 with Ca to 1.75 Å and of the (4) Δ76 PRORP1 with Mn to 1.95 Å resolution. Initial simulated annealing refinement (torsional and cartesian) was performed for all three structures with phenix.refine followed by iterative rounds of refinement and model building/correcting with Refmac5 and Coot as described above. In the final rounds of

refinement for the (3) Δ76 PRORP1 with Ca 1.75 Å structure, mixed isotropic and anisotropic individual B-factor refinement were used. In all the final Δ76 PRORP1 models residues 76–94 and 571,572 are missing and were not modeled since no visible electron density associated with these residues was found. The geometric quality of the models was assessed with MolProbity (44). APBS (17) (Adaptive Poisson-Boltzmann Solve) was used to create the electrostatic surface potential for Δ76 PRORP1. PyMOL (45) and UCSF Chimera (52) were used to create molecular images.

Table A-1. Data Collection and Refinement Statistics (SAD Phasing)

Protein	SeMet PRORP1 (peak)	SeMet PRORP1 with Sr	PRORP1 with Ca	PRORP1 with Mn	PRORP1 with Mn (peak)
Data Collection					
Space Group	$P2_12_12_1$	$P2_12_12_1$	$P2_12_12_1$	$P2_12_12_1$	$P2_12_12_1$
Cell Dimensions					
a, b, c (Å)	41.8, 111.9, 139.9	41.9, 112.0, 140.0	41.8, 111.9, 140.1	41.8, 112.5, 138.8	41.8, 112.4, 138.6
α, β, γ (°)	90, 90, 90	90, 90, 90	90, 90, 90	90, 90, 90	90, 90, 90
Wavelength (Å)	0.979	0.968	0.979	0.968	1.893
Resolution (Å)	50-1.98 (2.05-1.98)	50-2.00 (2.07-2.00)	50-1.75 (1.81-1.75)	50-1.95 (2.02-1.95)	50-2.4 (2.49-2.40)
R_{sym} (%)	10.3 (62.0)	8.4 (63)	7.5 (54.4)	6.1 (47.3)	6.6 (45.4)
I/σI	17.7 (3.8)	12.6 (2.6)	12.1 (1.5)	16.0 (3.9)	15.2 (2.9)
Completeness (%)	99.5 (96.0)	98.4 (97.9)	98.2 (88.1)	99.9 (100)	87.5 (45.7)
Redundancy	9.8 (9.6)	5.4 (5.4)	(3.9) 3.1	6.2 (6.1)	5.6 (3.5)
Refinement					
Resolution (Å)	87.4-1.98	87.4-2.00	43.9-1.75	87.4-1.95	
No. reflections	46672	44733	65673	48453	
R_{work} / R_{free}	0.187/0.220	0.194/0.233	0.163/0.210	0.194/0.226	
No. atoms					
Protein	3815	3835	3837	3832	
Water	345	236	384	330	
B-factors					
Protein	38.8	43.8	44.0	47.9	
Water	38.9	38.5	45.1	47.8	
R.m.s Deviations					
Bond lengths (Å)	0.012	0.014	0.013	0.011	
Bond angles (°)	1.427	1.552	1.379	1.380	
Ramachandran plot (%)					
Favored/allowed/outliers	97.3/2.7/0.0	97.5/2.3/0.0	99.0/1.0/0.0	97.7/2.3/0.0	
Protein Data Bank code	**4G23**	**4G25**	**4G26**	**4G24**	

	Mg	Ca	Mn	Fe	Ni	Zn
Δ76 Buffer	**0.29**	**5.68**	**0.02**	**0.15**	**0.09**	**0.08**
Δ76 PRORP1	**0.35**	**4.94**	**0.01**	**0.18**	**0.07**	**1.41**
Δ245 Buffer	**<0.5**	**2.90**	**<0.03**	**0.15**	**<0.05**	**0.02**
Δ245 PRORP1	**<0.5**	**2.10**	**<0.03**	**<0.01**	**<0.05**	**0.91**

Table A-2. Inductively coupled plasma mass spectrometry (ICP-MS) data of metals bound to Δ76PRORP1 and Δ245PRORP1. The numbers shown are mol metal/mol protein. After purification, Δ76 and Δ245PRORP1 were dialyzed against 5 mM EDTA, 20 mM Mops pH 7.8, 100 mM NaCl, and 1 mM TCEP at 4°C to remove adventitious metal ions followed by dialysis against 20 mM Mops pH 7.8, 100 mM NaCl, 1 mM TCEP pre-treated with Chelex 100 resin (Bio Rad) and made using chemicals of high purity (Δ76 and Δ245 Buffer). The protein concentration was determined by absorbance (Δ76 and mutants: ε_{280} = 84630 M^{-1} cm^{-1}; Δ245: ε_{280} = 75440 M^{-1} cm^{-1}). All protein samples used for metal-dependent studies were prepared in this manner.

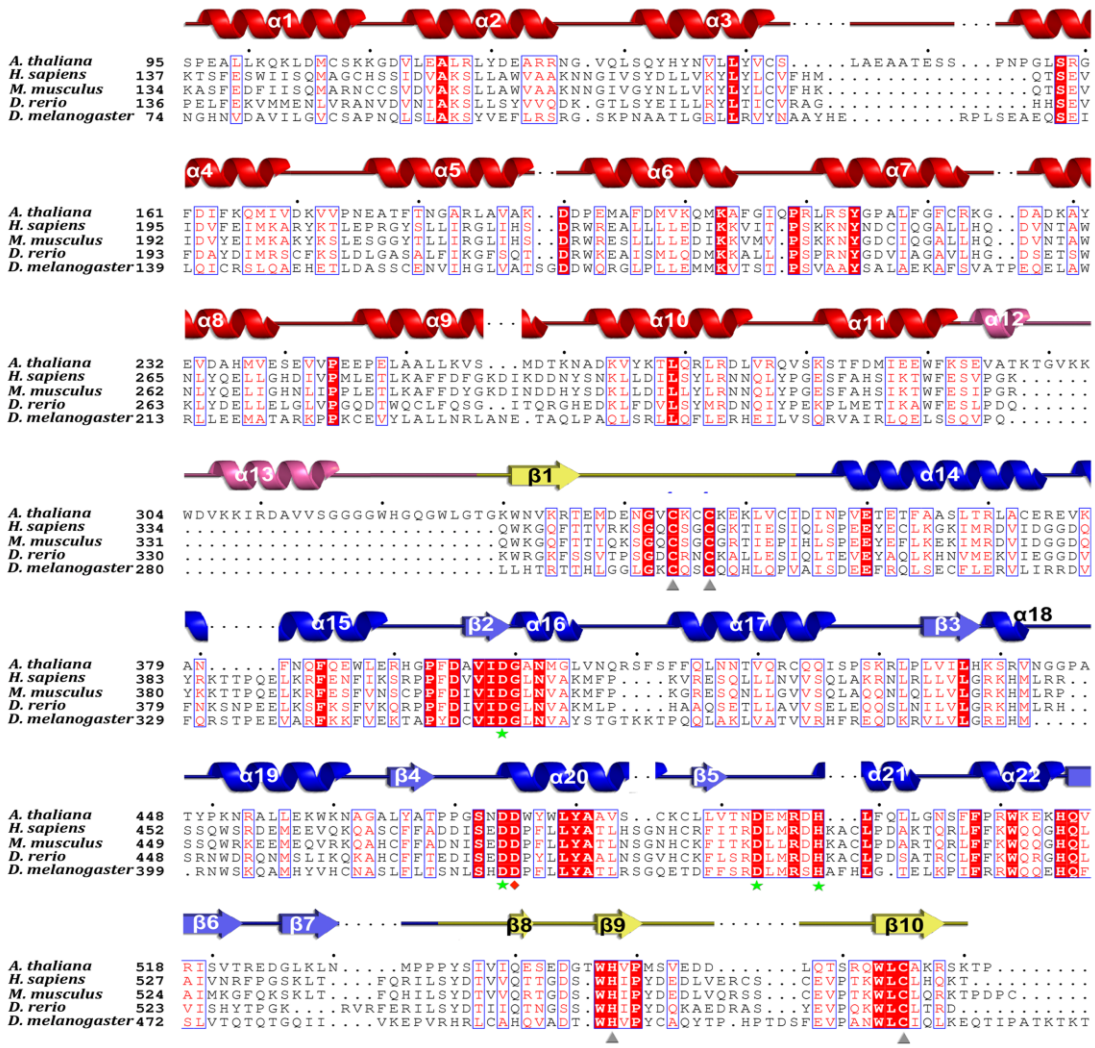

Figure A-1. Representative multiple sequence alignment (five shown) of 20 different species. The secondary structure is predicted from the PRORP1 structure. Boxed regions indicate conservation; red highlighted boxes represent completely conserved and pink lettered boxed regions indicate partial conservation. The CCCH Zn binding site is designated by gray arrows. The green stars and red diamonds indicate residues that were mutated to alanine. The aspartate indicated by the diamond makes an inner sphere contact with the active site metal.

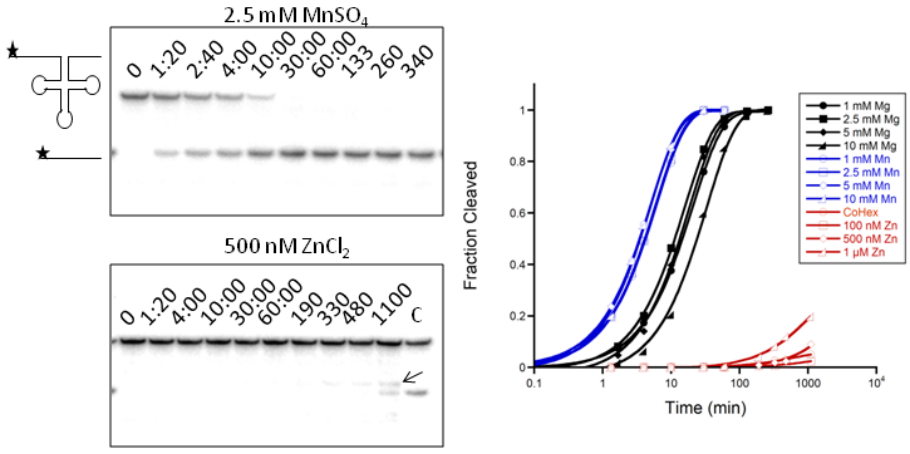

Metal	Concentration (mM)	k_{obs} (min^{-1})
Mg (mM)	1	0.047 ± 0.001
	2.5	0.062 ± 0.002
	5	0.054 ± 0.003
	10	0.030± 0.002
Mn (mM)	1	0.162 ± 0.004
	2.5	0.167 ± 0.002
	5	0.199 ± 0.004
	10	0.198 ± 0.008
Ca (mM)	1	∓
	2.5	∓
	5	∓
	10	∓
Zn (µM)	0	0.001 ± 0.0005
	0.1	0.001 ± 0.0009
	0.5	∓
	1	0.001 ± 0.0002

Figure A-2. Metal activation of PRORP1. (A) Representative gels of divalent metal ion activation of Δ76PRORP1-catalyzed cleavage of 5'-^{32}P labeled *A. thaliana* mitochondrial pre-tRNA^{cys} in cobalt(III)hexammine. The reactions containing 500 nM Δ76PRORP1 were incubated under standard assay conditions for varying times (min) with either 2.5 mM $MnSO_4$ (top) or 500 nM $ZnCl_2$ (bottom). At long incubation times (1100 min) pre-tRNA mis-cleavage was observed in assays containing Zn(II) (indicated by arrow). Lane C is a 1 min time point from a Δ76 PRORP1 control reaction under standard assay conditions (1 mM $MgSO_4$). (B) Reactions were performed under standard assay conditions with 250 µM cobalt(III)hexammine and varied divalent cations, including: $MnSO_4$ (blue data, 1 mM, 2.5 mM, 5 mM, and 10 mM), $MgCl_2$ (black data, 1 mM, 2.5 mM, 5 mM, and 10 mM) and $ZnCl_2$ (red data, 100 nM, 500 nM, and 1 µM). No formation of 5' leader was observed with assays containing calcium (1 mM, 2.5 mM, 5 mM, and 10 mM). The control reaction contains only 250 µM cobalt(III)hexammine (CoHex sample). A single exponential equation is fit to the data. The observed rate constant from these fits is shown in the Table. ∓ Indicates that no significant tRNA formation was observed under these conditions.

References

1. Holzmann, J., Frank, P., E, L., Bennett, K. L., Gerner, C., and Rossmanith, W. (2008) RNase P without RNA: identification and functional reconstitution of the human mitochondrial tRNA processing enzyme. *Cell* **135**, 462-536
2. Gobert, A., Gutmann, B., Taschner, A., Gobringer, M., Holzmann, J., Hartmann, R., Rossmanith, W., and Giegé, P. (2010) A single Arabidopsis organellar protein has RNase P activity. *Nature structural & molecular biology* **17**, 740-744
3. Gutmann, B., Gobert, A., and Giegé, P. (2012) PRORP proteins support RNase P activity in both organelles and the nucleus in Arabidopsis. *Genes & development*
4. Reiter, N., Osterman, A., Torres-Larios, A., Swinger, K., Pan, T., and MondragÃ³n, A. (2010) Structure of a bacterial ribonuclease P holoenzyme in complex with tRNA. *Nature* **468**, 784-793
5. Orans, J., McSweeney, E. A., Iyer, R. R., Hast, M. A., Hellinga, H. W., Modrich, P., and Beese, L. S. (2011) Structures of human exonuclease 1 DNA complexes suggest a unified mechanism for nuclease family. *Cell* **145**, 212-223
6. Thomas, B. C., Li, X., and Gegenheimer, P. (2000) Chloroplast ribonuclease P does not utilize the ribozyme-type pre-tRNA cleavage mechanism. *RNA* **6**, 545-1098
7. Reiner, R., Alfiya-Mor, N., Berrebi-Demma, M., Wesolowski, D., Altman, S., and Jarrous, N. RNA binding properties of conserved protein subunits of human RNase P. *Nucleic acids research* **39**, 5704-5718
8. Small, I. D., and Peeters, N. (2000) The PPR motif - a TPR-related motif prevalent in plant organellar proteins. *Trends in biochemical sciences* **25**, 46-53
9. Mili, S., and Piñol-Roma, S. (2003) LRP130, a pentatricopeptide motif protein with a noncanonical RNA-binding domain, is bound in vivo to mitochondrial and nuclear RNAs. *Molecular and cellular biology* **23**, 4972-5054
10. Meierhoff, K., Felder, S., Nakamura, T., Bechtold, N., and Schuster, G. (2003) HCF152, an Arabidopsis RNA binding pentatricopeptide repeat protein involved in the processing of chloroplast psbB-psbT-psbH-petB-petD RNAs. *The Plant cell* **15**, 1480-1575
11. Schmitz-Linneweber, C., and Small, I. (2008) Pentatricopeptide repeat proteins: a socket set for organelle gene expression. *Trends in plant science* **13**, 663-733
12. Holm, L., and Rosenstrom, P. (2010) Dali server: conservation mapping in 3D. *Nucleic Acids Res* **38**, W545-549
13. Ringel, R., Sologub, M., Morozov, Y., Litonin, D., Cramer, P., and Temiakov, D. (2011) Structure of human mitochondrial RNA polymerase. *Nature* **478**, 269-342
14. Chartron, J., Suloway, C., Zaslaver, M. a., and Clemons, W. (2010) Structural characterization of the Get4/Get5 complex and its interaction with Get3. *Proceedings of the National Academy of Sciences of the United States of America* **107**, 12127-12159
15. Pathare, G. R., Nagy, I., Bohn, S., Unverdorben, P., Hubert, A., Korner, R., Nickell, S., Lasker, K., Sali, A., Tamura, T., Nishioka, T., Forster, F., Baumeister, W., and Bracher, A. (2012) The proteasomal subunit Rpn6 is a molecular clamp holding the core and regulatory subcomplexes together. *Proc Natl Acad Sci U S A* **109**, 149-154
16. Dutta, S., and Tan, Y. J. (2008) Structural and functional characterization of human SGT and its interaction with Vpu of the human immunodeficiency virus type 1. *Biochemistry* **47**, 10123-10131
17. Baker, N. A., Sept, D., Joseph, S., Holst, M. J., and McCammon, J. A. (2001) Electrostatics of nanosystems: application to microtubules and the ribosome. *Proc Natl Acad Sci U S A* **98**, 10037-10041
18. Williams-Carrier, R., Kroeger, T., and Barkan, A. (2008) Sequence-specific binding of a chloroplast pentatricopeptide repeat protein to its native group II intron ligand. *RNA (New York, N.Y.)* **14**, 1930-1971
19. Krishna, S., Majumdar, I., and Grishin, N. (2003) Structural classification of zinc fingers: survey and summary. *Nucleic acids research* **31**, 532-582
20. Anantharaman, V., and Aravind, L. (2006) The NYN domains: novel predicted RNAses with a PIN domain-like fold. *RNA biology* **3**, 18-45
21. Eom, S. H., Wang, J., and Steitz, T. A. (1996) Structure of Taq polymerase with DNA at the polymerase active site. *Nature* **382**, 278-281

22. Ouameur, A., Bourassa, P., and Tajmir-Riahi, H.-A. (2010) Probing tRNA interaction with biogenic polyamines. *RNA (New York, N.Y.)* **16**, 1968-2047
23. Finney, L. A., and O'Halloran, T. V. (2003) Transition metal speciation in the cell: insights from the chemistry of metal ion receptors. *Science (New York, N.Y.)* **300**, 931-937
24. Smith, D., and Pace, N. R. (1993) Multiple magnesium ions in the ribonuclease P reaction mechanism. *Biochemistry* **32**, 5273-5354
25. Goldfarb, K. C., Borah, S., and Cech, T. R. (2012) RNase P branches out from RNP to protein: organelle-triggered diversification? *Genes & development* **26**, 1005-1014
26. Mili, S., and PiÃ±ol-Roma, S. n. (2003) LRP130, a pentatricopeptide motif protein with a noncanonical RNA-binding domain, is bound in vivo to mitochondrial and nuclear RNAs. *Molecular and cellular biology* **23**, 4972-5054
27. Xu, F., Ackerley, C., Maj, M., Addis, J., Levandovskiy, V., Lee, J., Mackay, N., Cameron, J., and Robinson, B. (2008) Disruption of a mitochondrial RNA-binding protein gene results in decreased cytochrome b expression and a marked reduction in ubiquinol-cytochrome c reductase activity in mouse heart mitochondria. *The Biochemical journal* **416**, 15-41
28. Lai, L. B., Bernal-Bayard, P., Mohannath, G., Lai, S. M., Gopalan, V., and Vioque, A. (2011) A functional RNase P protein subunit of bacterial origin in some eukaryotes. *Molecular genetics and genomics : MGG* **286**, 359-428
29. Helm, M., BrulÃ©, H., Friede, D., GiegÃ©, R., PÃ¼tz, D., and Florentz, C. (2000) Search for characteristic structural features of mammalian mitochondrial tRNAs. *RNA (New York, N.Y.)* **6**, 1356-1435
30. Wittenhagen, L. M., and Kelley, S. O. (2003) Impact of disease-related mitochondrial mutations on tRNA structure and function. *Trends in biochemical sciences* **28**, 605-616
31. Guerrier-Takada, C., Gardiner, K., Marsh, T., Pace, N., and Altman, S. (1983) The RNA moiety of ribonuclease P is the catalytic subunit of the enzyme. *Cell* **35**, 849-906
32. Koutmou, K. S., Day-Storms, J. J., and Fierke, C. A. (2011) The RNR motif of B. subtilis RNase P protein interacts with both PRNA and pre-tRNA to stabilize an active conformer. *RNA (New York, N.Y.)* **17**, 1225-1260
33. Buck, A. H., Dalby, A. B., Poole, A. W., Kazantsev, A. V., and Pace, N. R. (2005) Protein activation of a ribozyme: the role of bacterial RNase P protein. *The EMBO journal* **24**, 3360-3368
34. Steitz, T. A., and Steitz, J. A. (1993) A general two-metal-ion mechanism for catalytic RNA. *Proceedings of the National Academy of Sciences of the United States of America* **90**, 6498-7000
35. Cassano, A. G., Anderson, V. E., and Harris, M. E. (2004) Analysis of solvent nucleophile isotope effects: evidence for concerted mechanisms and nucleophilic activation by metal coordination in nonenzymatic and ribozyme-catalyzed phosphodiester hydrolysis. *Biochemistry* **43**, 10547-10606
36. Nowotny, M., Gaidamakov, S. A., Crouch, R. J., and Yang, W. (2005) Crystal structures of RNase H bound to an RNA/DNA hybrid: substrate specificity and metal-dependent catalysis. *Cell* **121**, 1005-1021
37. Hsieh, J., and Fierke, C. A. (2009) Conformational change in the Bacillus subtilis RNase P holoenzyme--pre-tRNA complex enhances substrate affinity and limits cleavage rate. *RNA (New York, N.Y.)* **15**, 1565-1642
38. Hsieh, J., Walker, S. C., Fierke, C. A., and Engelke, D. R. (2009) Pre-tRNA turnover catalyzed by the yeast nuclear RNase P holoenzyme is limited by product release. *RNA (New York, N.Y.)* **15**, 224-258
39. Taschner, A., Weber, C., Buzet, A., Hartmann, Roland K., Hartig, A., and Rossmanith, W. (2012) Nuclear RNase P of Trypanosoma brucei: A Single Protein in Place of the Multicomponent RNA-Protein Complex. *Cell Reports*
40. Otwinowski, Z., and Minor, W. (1997) Processing of x-ray diffraction data collected in oscillation mode. *Methods Enzymol* **276**, 307-326
41. Adams, P. D., Afonine, P. V., Bunkoczi, G., Chen, V. B., Davis, I. W., Echols, N., Headd, J. J., Hung, L. W., Kapral, G. J., Grosse-Kunstleve, R. W., McCoy, A. J., Moriarty, N. W., Oeffner, R., Read, R. J., Richardson, D. C., Richardson, J. S., Terwilliger, T. C., and Zwart, P. H. (2010) PHENIX: a comprehensive Python-based system for macromolecular structure solution. *Acta Crystallogr D Biol Crystallogr* **66**, 213-221
42. Emsley, P., and Cowtan, K. (2004) Coot: model-building tools for molecular graphics. *Acta Crystallogr D Biol Crystallogr* **60**, 2126-2132

43. Murshudov, G. N., Vagin, A. A., and Dodson, E. J. (1997) Refinement of macromolecular structures by the maximum-likelihood method. *Acta Crystallogr D Biol Crystallogr* **53**, 240-255
44. Davis, I. W., Leaver-Fay, A., Chen, V. B., Block, J. N., Kapral, G. J., Wang, X., Murray, L. W., Arendall, W. B., 3rd, Snoeyink, J., Richardson, J. S., and Richardson, D. C. (2007) MolProbity: all-atom contacts and structure validation for proteins and nucleic acids. *Nucleic Acids Res* **35**, W375-383
45. DeLano, W. L. (2002) The PyMOL Molecular Graphics System Schrödinger, LLC, Portland, OR
46. Milligan, J. F., & Uhlenbeck, 0. C. (1989) Synthesis of small RNAs using T7 RNA polymerase. *Methods Enzymol.* **180**, 51-62
47. Beebe, J. A., and Fierke, C. A. (1994) A kinetic mechanism for cleavage of precursor tRNA(Asp) catalyzed by the RNA component of Bacillus subtilis ribonuclease P. *Biochemistry* **33**, 10294-10598
48. Rueda, D., Hsieh, J., Day-Storms, J. J., Fierke, C. A., and Walter, N. G. (2005) The 5' leader of precursor tRNAAsp bound to the Bacillus subtilis RNase P holoenzyme has an extended conformation. *Biochemistry* **44**, 16130-16139
49. McCoy, A. J., Grosse-Kunstleve, R. W., Adams, P. D., Winn, M. D., Storoni, L. C., and Read, R. J. (2007) Phaser crystallographic software. *J Appl Crystallogr* **40**, 658-674
50. Terwilliger, T. C. (2000) Maximum-likelihood density modification. *Acta Crystallogr D Biol Crystallogr* **56**, 965-972
51. (1994) The CCP4 suite: programs for protein crystallography. *Acta Crystallogr D Biol Crystallogr* **50**, 760-763
52. Pettersen, E. F., Goddard, T. D., Huang, C. C., Couch, G. S., Greenblatt, D. M., Meng, E. C., and Ferrin, T. E. (2004) UCSF Chimera--a visualization system for exploratory research and analysis. *J Comput Chem* **25**, 1605-1612

Chapter 3 [3]

Mechanistic Studies Reveal Similar Catalytic Strategies for Phosphodiester Bond Hydrolysis by Protein-only and RNA-dependent Ribonuclease P

Abstract

Ribonuclease P (RNase P) is an endonuclease that catalyzes the essential removal of the 5' end of tRNA precursors. Until recently, all identified RNase P enzymes were a ribonucleoprotein with a conserved catalytic RNA component. However, the discovery of protein-only RNase P (PRORP) shifted this paradigm, affording a unique opportunity to compare mechanistic strategies used by naturally evolved protein and RNA-based enzymes that catalyze the same reaction. Here we investigate the enzymatic mechanism of pre-tRNA hydrolysis catalyzed by the NYN metallonuclease of Arabidopsis thaliana, PRORP1. Multiple and single-turnover kinetic data support a mechanism where a step at or before chemistry is rate-limiting and provide a kinetic framework to interpret the results of metal alteration, mutations, and pH dependence. Catalytic activity has a cooperative dependence on the magnesium concentration (nH = 2) under kcat/Km conditions, suggesting that PRORP1 catalysis is optimal with at least 2 active site metal ions, consistent with the crystal structure. Metal rescue of Asp-to-Ala mutations identified 2 aspartates important for enhancing metal ion affinity. The single-turnover pH dependence of pre-tRNA cleavage revealed a single ionization (pKa ~8.7) important for catalysis, consistent with deprotonation of a metal-bound water nucleophile. The pH and metal dependence mirrors that observed for the RNA-based RNase P, suggesting similar catalytic mechanisms. Thus, despite different macromolecular composition, the RNA and

[3] Work in this chapter has been published: Howard,M.J., Klemm,B.P. and Fierke,C.A. (2015) Mechanistic Studies Reveal Similar Catalytic Strategies for Phosphodiester Bond Hydrolysis by Protein-only and RNA-dependent Ribonuclease P. *J. Biol. Chem.*, **290**, 13454–64. B.P.K. analyzed pH dependence of PRORP1 histidine mutants and the STO Mg^{2+} dependence of PRORP1 and aspartate mutants. M.J.H performed all other experiments and wrote the paper.

protein-based RNase P act as dynamic scaffolds for the binding and positioning of magnesium ions to catalyze phosphodiester bond hydrolysis.

Background

Transfer RNAs (tRNAs) are transcribed as precursors (pre-tRNA) with extra nucleotides flanking the 5' (leader) and 3' (trailer) ends. Removal of these extra sequences is essential for tRNA function, making the enzymes that catalyze pre-tRNA end-maturation essential. Ribonuclease P (RNase P) catalyzes the formation of the mature 5' end of pre-tRNA and has remarkable diversity in subunit and macromolecular composition throughout domains and even within the same species (1). RNA-based RNase P (ribozyme) contains varying numbers of protein subunits ranging from one in bacteria to at least 10 in eukaryotes (2).

Some eukaryotic species, such as *Arabidopsis thaliana*, are seemingly devoid of an RNA-based RNase P and instead encode a protein-only RNase P (PRORP) (3). Mammals, including humans, use both RNA- and protein-based RNase P to catalyze pre-tRNA maturation (4). This redundancy in humans can be partly explained by differential localization; protein-only RNase P (PRORP or MRPP3) functions in the mitochondria while the RNA-based RNase P functions in the nucleus (4, 5). Knockdown of human PRORP results in accumulation of mitochondrial pre-tRNA in HeLa cells and knockout of the homologous PRORP1 in *A. thaliana* is lethal (3, 4, 6). Thus, PRORP enzymes play an essential role in mitochondria.

In *A. thaliana* three PRORPs are encoded within the nuclear genome (PRORP1, 2, and 3). PRORP2 and PRORP3 co-localize to the nucleus, whereas PRORP1 functions within both the mitochondria and chloroplasts (6). PRORP is homologous to the nuclease component of the human mitochondrial RNase P (MRPP3/ human PRORP). The structure of *A. thaliana* PRORP1 revealed 3 domains: a Nedd4-BP1, YacP Nuclease (NYN) metallonuclease domain, a central structural Zn-binding domain, and a pentatricopeptide repeat (PPR) domain involved in pre-tRNA binding (Figure 3-1A) (7). The NYN domain is a novel metallonuclease domain, sharing structural homology to the PIN (PilT N terminus) and flap nuclease families (8). NYN domains have a relatively exposed active site and contain 4 conserved aspartates, as compared to the flap nuclease family that has 6 conserved aspartates (7, 8). Despite having only 4 conserved

potential metal ligands within its active site, the crystal structure visualized the binding of two manganese ions to the NYN domain of PRORP1 in positions similar to those observed in the flap nuclease family (7, 9). These similarities led to the proposal that NYN metallonuclease domains catalyze phosphodiester bond hydrolysis using a classical 2-metal ion mechanism (6, 7, 10). In this mechanism metal I is proposed to activate a coordinated water molecule for nucleophilic attack, both metals are proposed to stabilize the negative charge build up in the transition state, and metal II is proposed to stabilize the developing charge on the 3' oxyanion leaving group (10).

Here, we investigate the catalytic mechanism of PRORP1 by examining the metal and pH dependence of pre-tRNA cleavage. These data provide evidence for a 2-metal ion mechanism and identify a single ionization that is important for catalysis. The pH dependence is consistent with deprotonation of a catalytic metal-bound water and provides no evidence for an amino acid side chain acting as a general acid to protonate the leaving group. Alanine mutations of the conserved aspartate residues that coordinate metal ions significantly reduce single-turnover activity, as previously observed (6, 7). However, addition of high concentrations of Mg^{2+} can partially rescue the activity of the D474A and D475A mutant enzymes, indicating that these residues are important for enhancing metal ion affinity. These findings provide insight into the enzymatic mechanism and metal binding properties of PRORP1 that can be extended to the NYN metallonuclease domains found throughout Eukaryotes. Furthermore, the mechanism of PRORP1 has important similarities to the RNA-dependent RNase P.

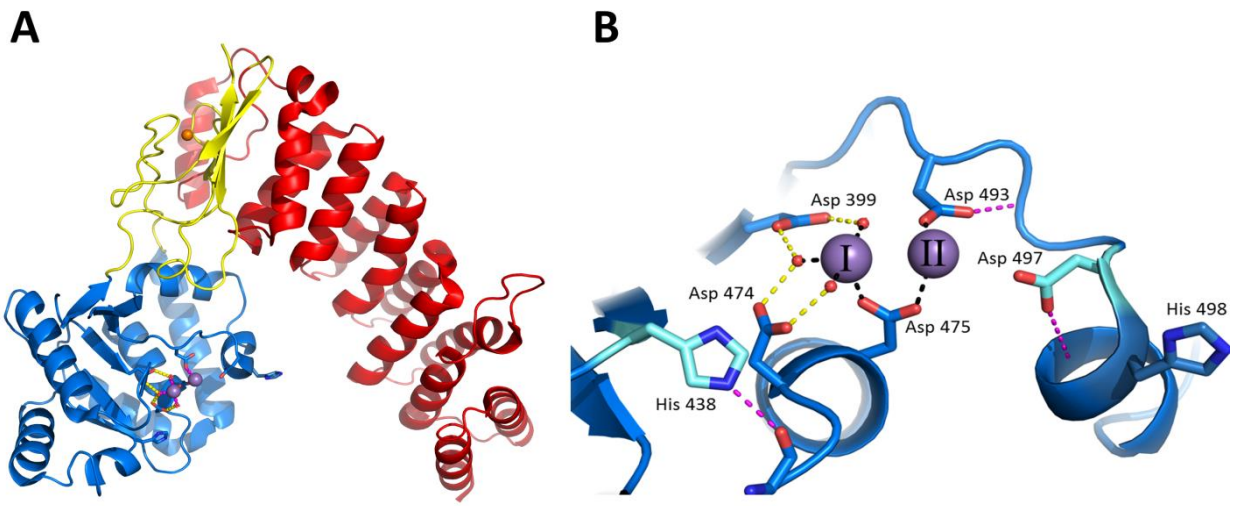

Figure 3-1. Crystal structure and active site of PRORP1. A. A. thaliana PRORP1 (PDB 4G24) contains 3 domains: PPR domain, red; central domain, yellow; and the NYN-metallonuclease domain, blue. B. Active site of PRORP1 with two bound Mn^{2+} ions. Completely conserved residues are represented as blue sticks (D399, D493, D474, D475, and H498). Partially conserved residues are in cyan (H438 and D497). Potential hydrogen bonds are depicted by magenta dashes (with other amino acids) and yellow dashes (with metal-bound waters). Black dashes represent proposed inner-sphere coordination of the metal ions. In the crystal structure metal II has a lower occupancy (~80%) and the metal-bound waters are not visible (7).

Results

Single- and Multiple-turnover kinetics of PRORP1-catalyzed Pre-tRNA Cleavage

We measured the single-turnover (STO) and multiple-turnover (MTO) kinetics of pre-tRNA cleavage catalyzed by PRORP1 to establish a kinetic framework to evaluate the effects of pH, metal ion concentration, and mutations. Cleavage reactions were carried out using two substrates: *A. thaliana* mitochondrial pre-$tRNA^{Cys}$ (*A.t.* pre-tRNA) and *Bacillus subtilis* pre-$tRNA^{Asp}$ (*B.s.* pre-tRNA), a bacterial substrate extensively used to analyze the reactivity of the RNA-based RNase P (Figure 3-2). These substrates were 5'end-labeled with fluorescein and contain a 5 nt leader and a 3' discriminator base. For MTO reactions, we used a recently developed real-time fluorescent polarization (FP) assay to monitor the dependence of PRORP1-catalyzed pre-tRNA cleavage on the substrate concentration (14). Representative MTO data from the FP assay are shown in

Figure 3-3A; the value of k_{cat}/K_M is ~ 1 x 10^5 $M^{-1}s^{-1}$, approximately 35-fold slower than the reaction catalyzed by *B. subtilis* RNA-dependent RNase P (19) and the value of k_{cat} is 0.03 – 0.06 s^{-1} (Table 1). Cleavage of pre-tRNA catalyzed by PRORP1 under STO conditions was too fast to measure using the FP assay. Therefore, these reactions were performed in a stopped-assay format at saturating enzyme concentrations and product formation was analyzed by urea-PAGE (Figure 3-3C), as described in methods. A single exponential was fit to the data (Figure 3-3D). The values of the STO rate constant at saturating enzyme (k_{max}), 0.03 – 0.04 s^{-1}, are comparable to the multiple-turnover parameter at saturating substrate (k_{cat}), suggesting that a step at or before cleavage is rate-limiting for both substrates under these conditions.

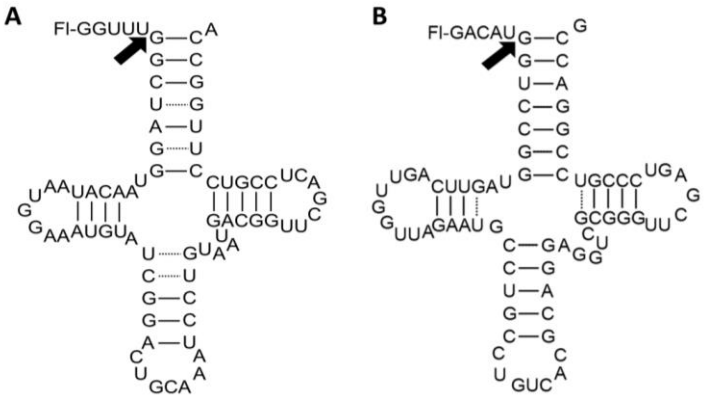

Figure 3-2. Proposed secondary structures of the pre-tRNA substrates used in this study. Both substrates are labeled at the 5' end with fluorescein (Fl) and contain 5 nt leaders and a discriminator base at the 3' end. The cleavage sites are identified with an arrow. A. *Arabidopsis thaliana* mitochondrial pre-$tRNA^{Cys}$ (*A.t* pre-tRNA). B. *Bacillus subtilis* pre-$tRNA^{Asp}$ (*B.s.* pre-tRNA).

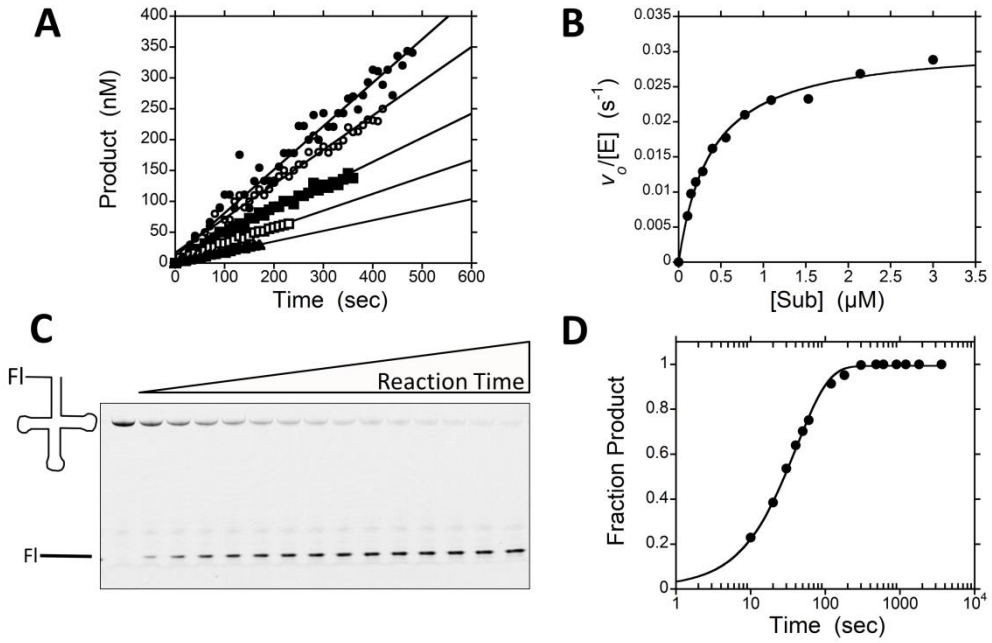

Figure 3-3. Representative multiple- and single-turnover data of PRORP1-catalyzed pre-tRNA cleavage. A. Representative initial rates of product formation using the FP assay under multiple-turnover conditions with varying concentrations of B.s. pre-tRNA (circle, 1 μM; open circle, 0.5 μM; square, 0.3 μM; open square, 0.15 μM; triangle, 0.06 μM) and 20 nM PRORP1 in 30 mM MOPS pH 7.8, 150 mM NaCl, 1 mM TCEP, and 1 mM $MgCl_2$ at 25°C .B. Dependence of the initial velocities, normalized by the PRORP1 concentration, on the substrate concentration. The Michaelis-Menten equation was fit to the data. C. Representative fluorescent scan of a urea 20% poly-acrylamide gel of a single-turnover assay containing 5 μM PRORP1 and 20 nM B.s. pre-tRNA under standard reaction conditions. D. The gel was quantified and the fraction product was calculated at each time point. A nonlinear regression curve of a single exponential fit to the data is shown. Kinetic parameters are summarized in Table 3-1.

Table 3-1. Kinetic parameters for PRORP1-catalyzed *A.t.* pre-tRNA and *B.s.* pre-tRNA cleavage[a].

	Multiple-turnover[b]			*Single-turnover*[c]
Pre-tRNA	K_m (nM)	k_{cat} (s^{-1})	k_{cat}/K_m (M^{-1} s^{-1})	k_{max} (s^{-1})
A.t.	630 ± 60	0.06 ± 0.01	9.8 ± 1.0 x 10^4	0.04 ± 0.003
B.s.	350 ± 50	0.03 ± 0.003	1.0 ± 0.2 x 10^5	0.03 ± 0.003

[a]Reactions were measured at 25°C in 30 mM MOPS pH 7.8, 150 mM NaCl, 1 mM TCEP, and 1 mM $MgCl_2$, as described in the legend of Figure 3. Values reported reflect the mean of two independent experiments with the error reported as the standard deviation.
[b]Measured using the FP assay with 20 nM PRORP and 0.06 – 3 μM pre-tRNA.
[c]Measured using a stopped assay with 5 μM PRORP1 and 20 nM pre-tRNA.

PRORP1 Magnesium Dependence

The crystal structure of PRORP1 in the presence of Mn^{2+} revealed two metal ion binding sites within the active site (Figure 3-1B) (7). Based on this observation and the similarity of the NYN domain of PRORP1 to other nucleases, it has been proposed that PRORP enzymes use a 2-metal ion mechanism for catalyzing phosphodiester bond hydrolysis (6, 7). To test this hypothesis, we measured the magnesium dependence of the steady state kinetics for cleavage of *B.s.* pre-tRNA catalyzed by PRORP1 (Figure 3-4A). The measured k_{cat} values show a hyperbolic dependence on the Mg^{2+} concentration (Figure 3-4B). Fitting Equation 1 to these data yields a Hill coefficient (n^H) of 1.2 ± 0.2, a k_{cat}^{Mg} of 0.06 ± 0.01 s^{-1} and a $K_m^{Mg}(k_{cat})$ of 1.4 ± 0.3 mM (solid line in Figure 3-4B) indicating that no cooperativity is observed. The dashed line in Figure 3-4B shows that a fit with n^H = 2 does not describe the data. The value k_{cat}^{Mg} reflects the maximal turnover number at saturating Mg^{2+} concentrations and $K_m^{Mg}(k_{cat})$ represents the concentration of Mg^{2+} at which the rate is half of k_{cat}^{Mg}. In contrast, the apparent k_{cat}/K_m values show a cooperative dependence on Mg^{2+} concentration with a Hill coefficient (n^H) of 2.0 ± 0.6 resulting in a maximal value for k_{cat}/K_M at saturating Mg^{2+} ($(k_{cat}/K_M)^{Mg}$) of 2.2 ± 0.3 x 10^5 $M^{-1}s^{-1}$ and $K_m^{Mg}{}_{(kcat/Km)}$ of 510 ± 270 µM (Figure 3-4C). To determine if these effects are substrate-specific we also examined the Mg^{2+} dependence of the *A.t.* pre-tRNA at a sub-saturating substrate concentration (250 nM) reflecting k_{cat}/K_m conditions, and a saturating substrate concentration (5 µM), reflecting k_{cat} conditions. The magnesium dependence of the PRORP1-catalyzed cleavage of the *A.t.* pre-tRNA substrate mirrors that observed for the *B.s*. pre-tRNA substrate; a cooperative dependence on Mg^{2+} concentration is observed under k_{cat}/K_m conditions (Figure 3-4E) but disappears under saturating substrate (k_{cat}) conditions (Figure 3-4D). Finally, to test whether the magnesium cooperativity observed under k_{cat}/K_m conditions is due to stabilization of the structure of pre-tRNA, we repeated these activity measurements in the presence of 1 mM $CaCl_2$. Calcium stabilizes tRNA structure (20) but does not activate PRORP1 catalysis (7). However, we still observe an n^H = 2.1 ± 0.2 for the Mg^{2+} dependence of k_{cat}/K_m in the presence of 1 mM $CaCl_2$ (Figure 3-4F). Potential models for the Mg^{2+} dependence under k_{cat}/K_M conditions and k_{cat} conditions are represented in schemes 1 and 2, respectively. Taken together, these magnesium-dependent data indicate that PRORP1 requires at

least 2 Mg^{2+} ions for optimal catalysis and that the Mg^{2+} ions bind cooperatively to PRORP1. Additionally, because Mg^{2+} cooperativity is only observed under k_{cat}/K_M conditions these data suggest that Mg^{2+} binding to PRORP1 is coupled to pre-tRNA binding

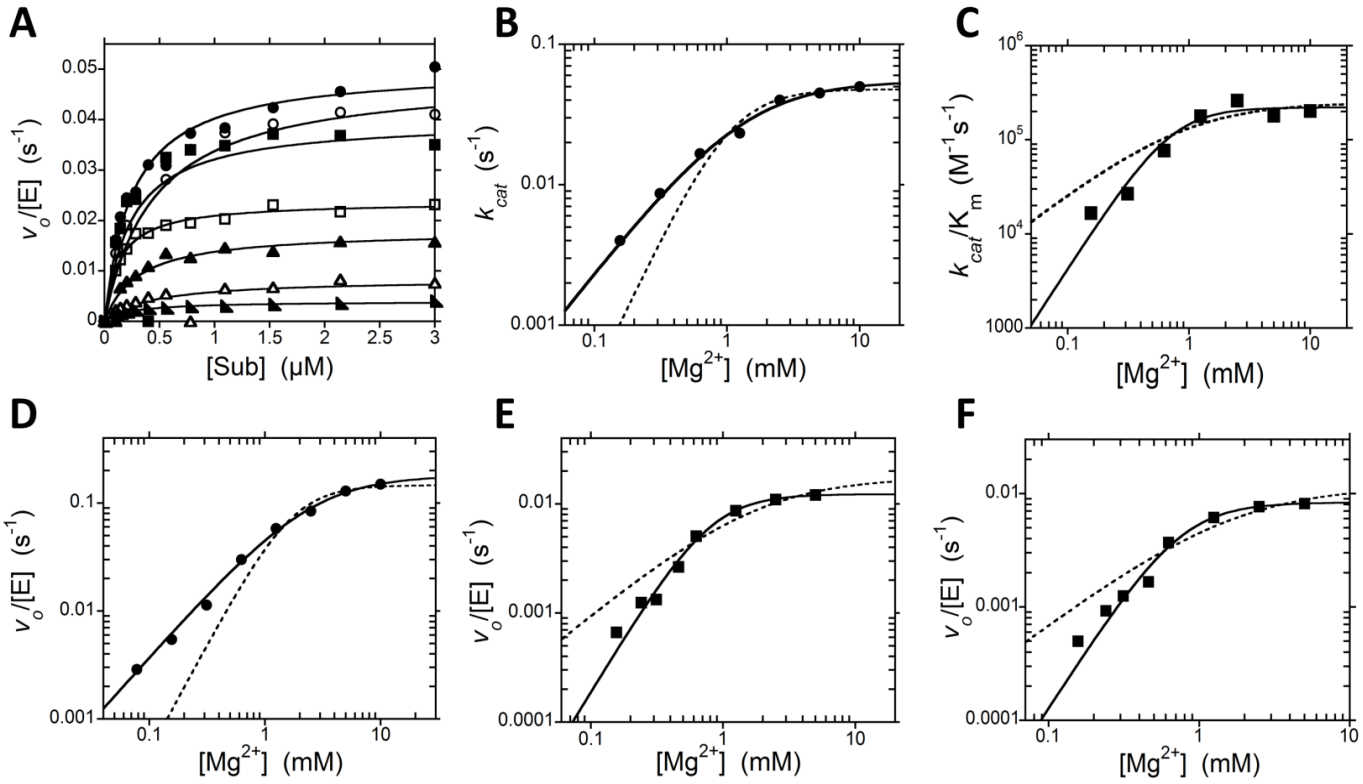

Figure 3-4. Mg^{2+} dependence of multiple-turnover reactions catalyzed by PRORP1. Data in plots A-C were collected with the *B.s* pre-tRNA substrate. A. Dependence of PRORP1-catalyzed cleavage on the concentration of *B.s.* pre-tRNA and varying concentrations of Mg^{2+} (10 mM; circle, 5 mM; open circle, 2.5 mM; square, 1.25 mM; open square, 0.63 mM; triangle, 0.31 mM; open triangle, and 0.16 mM; right triangle). Reactions were performed at 25°C, in MOPS pH 7.8, 1 mM TCEP, with varying concentrations of $MgCl_2$ and NaCl to maintain ionic strength. The Michaelis-Menten equation is fit to the data. The apparent steady state kinetic parameters are plotted in B and C. B. Dependence of k_{cat} on the Mg^{2+} concentration. The solid line shows a fit of Equation 1 to the data yielding: k_{cat}^{Mg} = 0.06 ± 0.01 s^{-1}, $K_m^{Mg}(k_{cat})$ = 1.4 ± 0.3 mM and n^H = 1.2 ± 0.2. The dotted line simulates data with a Hill coefficient of 2. C. Dependence of k_{cat}/K_m on Mg^{2+} concentration. The solid line shows a weighted fit of Equation 1 to the data yielding: k_{cat}/K_M^{Mg} = 2.2 ± 0.3 x 10^5 M^{-1} s^{-1}, $K_m^{Mg}(k_{cat}/K_m)$ of 510 ± 270 μM and n^H = 2.0 ± 0.6. The dotted line simulates data with a Hill coefficient of 1. Data in plots D-F were collected with the *A.t.* pre-tRNA substrate. D. Dependence of the initial velocity on Mg^{2+} at saturating substrate (5 μM). The solid line shows a fit of Equation 1 to the data yielding: k_{cat}^{Mg} = 0.18 ± 0.01 s^{-1}, $K_m^{Mg}(k_{cat})$ = 3.0 ± 0.3 mM, and n^H = 1.2 ± 0.1. The dotted line simulates data with a Hill coefficient of 2. E. Dependence of the initial velocity on the Mg^{2+} concentration using a sub-saturating substrate concentration (250 nM). The solid line shows a fit of Equation 1 to the data yielding a maximal rate constant of 0.01 ± 0.001 s^{-1} (4.7 x 10^4 $M^{-1}s^{-1}$), $K_m^{Mg}(k_{cat}/K_m)$ = 640 ± 100 μM, and n^H = 2.0 ± 0.2. The dotted line simulates data with a Hill coefficient of 1. F. Dependence of the initial velocity on the Mg^{2+} concentration using a sub-saturating substrate concentration (250 nM) in the presence of 1 mM $CaCl_2$. The solid line shows a fit of Equation 1 to the data yielding a maximal rate constant of 0.008 ± 0.001 s^{-1} (3.3 x 10^4 $M^{-1}s^{-1}$), $K_m^{Mg}(k_{cat}/K_m)$ = 560 ± 110 μM and n^H = 2.1 ± 0.2. The dotted line simulates data with a Hill coefficient of 1.

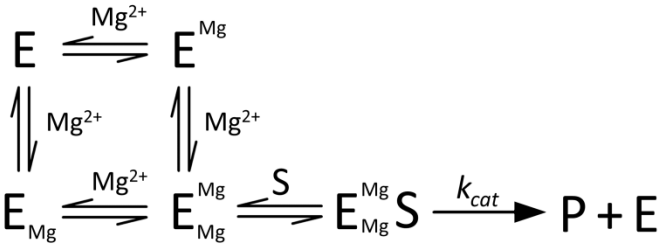

Scheme 1. Mg^{2+} dependence under k_{cat}/K_M conditions

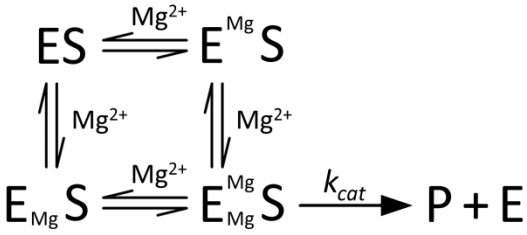

Scheme 2. Mg^{2+} dependence under k_{cat} conditions

Metal Dependence of Aspartate to Alanine Mutants

The PRORP1 crystal structure also revealed amino acid residues that interact with the active site metal ions (7). Two manganese ions are observed bound to the active site interacting with four conserved aspartate residues (D399A, D474A, D475A, and D493A), through both inner and outer sphere interactions (Figure 3-1B). Mutation of any one of these conserved aspartate residues to alanine significantly reduces activity (7); no product formation is observed after a 30 min incubation under standard STO assay conditions (1 mM $MgCl_2$). To evaluate whether the activity of these mutants could be enhanced by higher Mg^{2+} concentrations, we compared the STO cleavage activity at 1 and 20 mM Mg^{2+} (Figure 3-5). The activity of the D474A and D475A increased significantly at the higher magnesium concentration (Figure 3-5). However, no increase in activity was observed with the D399A and D493A mutants (even after incubation at 50 mM Mg^{2+} for 2 hr, data not shown).

We then measured the magnesium dependence of the activity of WT and the D474A and D475A mutants under STO conditions with saturating enzyme (Figure 3-6). For WT, the observed rate constant shows a hyperbolic dependence on Mg^{2+} concentration, yielding a k_{max}^{Mg} = 0.12 ± 0.01 s^{-1}, $K_{1/2}^{Mg}$ = 10 ± 3.3 mM, and $n^{(H)}$ of 1.3 ± 0.3. High concentrations of Mg^{2+} inhibit both wild-type PRORP1 and the aspartate mutants (Figure

3-6, open symbols) and these points were not included in the analysis of the data. For the mutants, the $K_{1/2}^{Mg}$ value is estimated as >90 mM and $k_{max}^{Mg} \geq 0.007$ s^{-1} (D474A) and 0.002 s^{-1} (D475A), indicating that the value of $K_{1/2}^{Mg}$ is increased at least 9-fold and the activity is decreased at least 17-fold as compared to WT (Table 3-2). The metal-dependent parameters measured for WT PRORP1 under STO conditions, ($K_{1/2}^{Mg}$ = 10 ± 3.3 mM and k_{max}^{Mg} = 0.12 ± 0.01 s^{-1}) are larger than the comparable values measured under MTO conditions (K_m^{Mg}(k_{cat}) = 1.4 ± 0.3 mM, k_{cat}^{Mg} = 0.06 ± 0.01 s^{-1}); this could potentially be a result of different assay conditions or a change in the rate-limiting step at high Mg^{2+} concentrations for MTO reactions. Nonetheless, these data indicate that one function of D474 and D475 is to enhance metal ion affinity; however, the decrease in activity suggests that these side chains also increase the reactivity of the metal ions, possibly by correct positioning. This proposal is supported by the observation that the D474A and D475A PRORP1 variants catalyze low amounts of miscleaved product (Figure 3-5).

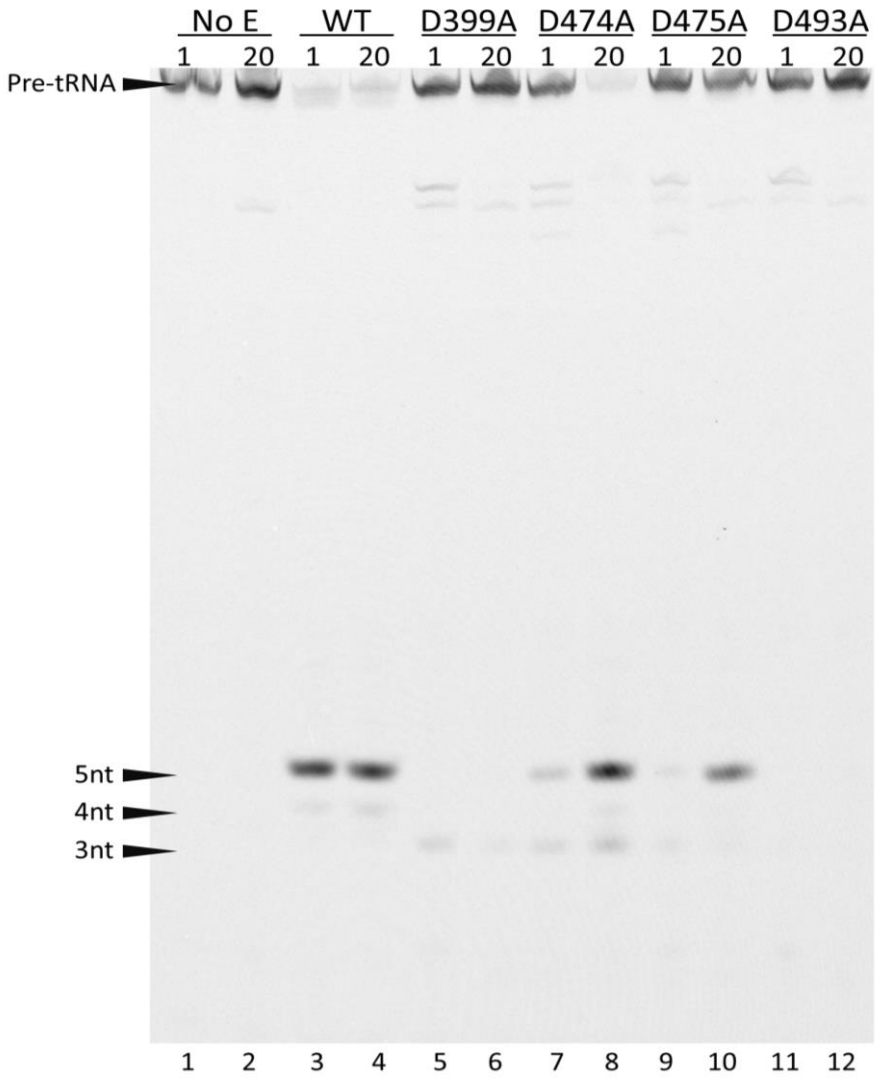

Figure 3-5. The activity of the D474A and D475A mutants increase at high concentrations of Mg^{2+}. 20 nM B.s. pre-tRNA was incubated with 5 μM of each PRORP1 variant at 25 °C with either 1 or 20 mM $MgCl_2$ in 50 mM MTA buffer at pH 8.0, 1 mM TCEP, and NaCl adjusted to maintain ionic strength. Reactions were quenched at 2 hr and resolved on a 22.5% denaturing PAGE. Less intense bands, representing miscleaved products, are observed between the substrate and product bands and below the correct 5 nt product band (4 and 3 nt products).

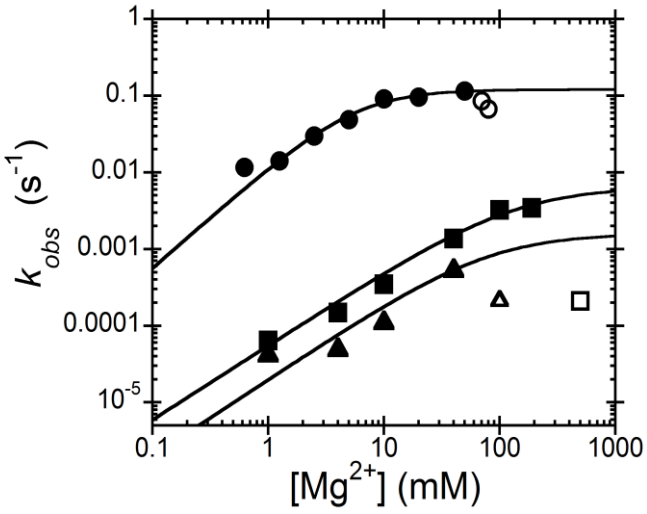

Figure 3-6. Single-turnover magnesium dependence of WT, D474A, and D475A PRORP1-catalyzed cleavage. Reactions were performed with 5 μM PRORP1 (WT, circle; D474A, square; D475A, triangle) and 20 nM *B.s.* pre-tRNA as described in the legend of Figure 5. Inhibition was observed at high concentrations of $Mg^{2+}$and these data were not included in the fit (shown as open symbols). Equation 1 was fit to the data, resulting in a k_{max}^{Mg} = 0.12 ± 0.01 s^{-1}, $K_{1/2}^{Mg}$ = 10 ± 3.3 mM, and $n^{(H)}$ of 1.3 ± 0.3 for WT. The $K_{1/2}^{Mg}$ and k_{max}^{Mg} values for the D474A and D475A mutants were estimated as >90 mM and ≥ 0.007 and ≥ 0.002 s^{-1}, respectively. Data are summarized in Table 3-2.

Table 3-2. Single-turnover magnesium dependence of PRORP1 metal ligand mutants.

Enzyme	Interaction with active site metals[a]	Mg Rescue	$K_{1/2}^{Mg}$ (mM)[b]	Fold	k_{max}^{Mg} (s^{-1})	Fold
WT	--	--	10 ± 3.3	1	0.12 ± 0.01	1
D399A	Outer sphere with metal I	No	--	--	--	--
D474A	Outer sphere with metal I	Yes	>90	>9	≥0.007	≥17
D475A	Inner sphere, bidentate	Yes	>90	>9	≥0.002	≥60
D493A	Inner sphere with metal II	No	--	--	--	--

[a]Interactions of Asp side chains with bound metal ions are predicted from the crystal structure (see Figure 3-1; (7)).
[b]The $K_{1/2}^{Mg}$ values were determined as described in the legend of Figure 3-6.

pH Dependence

To provide further insight into the mechanism of PRORP-catalyzed phosphodiester bond hydrolysis, we measured the pH dependence of STO cleavage with both *A.t*. and *B.s.* pre-tRNA substrates. The k_{obs} for both substrates show a similar dependence on pH: a log-linear increase with increasing pH, which becomes pH-independent under alkaline conditions (Figure 3-7A). These data are well-described by a single ionization that increases activity with pK_a values of 7.9 ± 0.1 (*A.t.* pre-tRNA) and 8.7 ± 0.4 (*B.s.* pre-tRNA), suggesting that deprotonation of a single group enhances activity. The lack of an alkaline limb suggests that no protein side chain acts as a general acid.

In addition to the conserved aspartate residues, the active site of PRORP1 contains two histidine side chains that are located ~ 6 angstroms from the metal binding sites (Figure 3-1B). H498 is invariant, while H438 is conserved in plants. To examine whether either of these histidine side chains play a role in PRORP1 catalysis or pH dependence, we mutated H498 and H438 to alanine. Under the standard STO assay conditions, the H498A and H438A mutations reduce the observed rate constant to 5.0 ± 0.2 x 10^{-4} and 0.02 ± 0.001 s^{-1} representing a 80- and 2-fold decrease, respectively, as compared to WT (0.04 s^{-1}, Table 3-1). However, the more conservative mutation of H498 to glutamine (H498Q) decreases the STO rate constant only 4-fold compared to WT. Furthermore, a single ionization is observed in the pH dependence of the STO cleavage rate constants for both the H498Q and H438A mutants, with pK_a values of 8.2 ± 0.1 and 7.8 ± 0.1, respectively. These mutations decrease the value of k_{max}^{pH} to 0.03 ± 0.002 and 0.04 ± 0.003 s^{-1}, respectively, representing a ~3 fold decrease for both as compared to WT (Figure 3-7B). These modest alterations in the activity and pK_a values for the H438A and H498Q mutants are not consistent with a function as a general acid/base (GAB) catalyst; mutagenesis of a GAB group typically decreases activity by ~10^3-10^4 in hydrolytic reactions (21, 22).

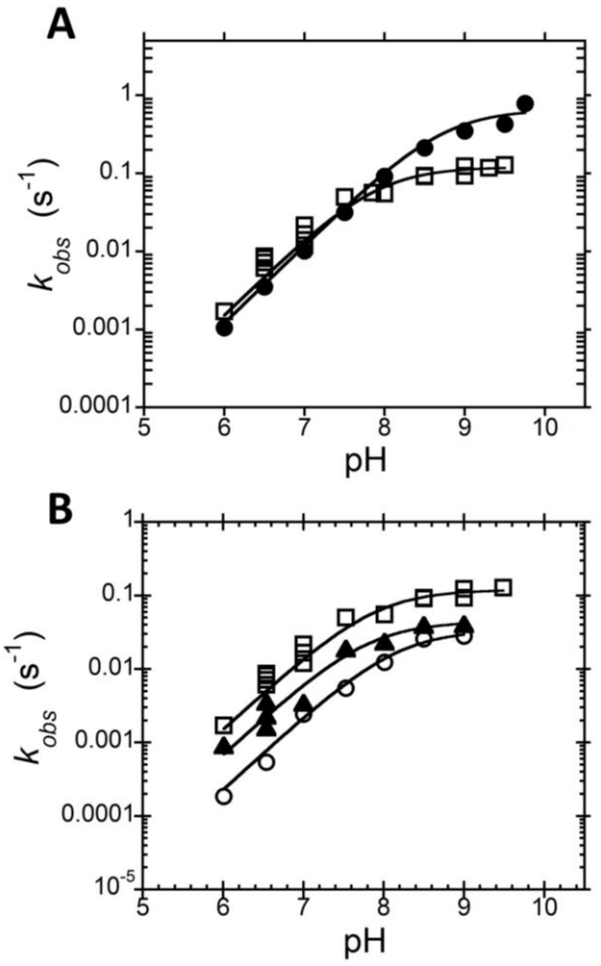

Figure 3-7. pH dependence of PRORP1-catalyzed cleavage of pre-tRNA under single turnover conditions. Single turnover reactions were carried out as described in the legend of Figure 3-3 in a 3-component buffer system (MTA) with NaCl varied to maintain ionic strength, 5 μM enzyme, 20 nM substrate, 1 mM TCEP, 1 mM $MgCl_2$ at 25°C. A. pH profile for cleavage of A.t. pre-tRNA (open squares) and B.s. pre-tRNA (circles) under STO conditions. Equation 2 was fit to the data with resulting pK_a values of 7.9 ± 0.1 and 8.7 ± 0.4 and k_{max}^{pH} values of 0.12 ± 0.01 and 0.65 ± 0.08 s^{-1} for A.t. pre-tRNA and B.s. pre-tRNA, respectively. B. pH profile for H498Q (triangles) and H438A (open circles) catalyzed cleavage of A.t pre-tRNA. WT (open squares) data is shown for comparison. Equation 2 was fit to the data, with resulting pK_a values of 8.2 ± 0.1 and, 7.8 ± 0.1 and k_{max}^{pH} values of 0.03 ± 0.002 and 0.04 ± 0.003 s^{-1} for H498Q and H438A, respectively.

To determine if the side chains of H498 and H438 enhance pre-tRNA binding, we measured the affinity of the variants for *A.t.* pre-tRNA using an anisotropy assay (Figure 3-8). No significant change in binding affinity was observed for these histidine mutants in comparison to WT, with dissociation constants of ~700 nM. However, the endpoint anisotropy, reflecting the anisotropy of the ES complex, for the H498 mutants varied significantly from the values measured for the WT and H438A enzymes. This result may indicate that the fluorescein and potentially the 5' leader adopt a different position and/or conformation when bound to the His498 mutants as compared to WT.

To examine whether the observed ionization reflects deprotonation of a metal-bound water, we measured the dependence of the activity on the identity of the metal ion. PRORP1 is activated by Mg^{2+}, Mn^{2+}, Co^{2+} and Ni^{2+} (but not Ca^{2+}, Zn^{2+}, or Cd^{2+} (7, 23)). We measured the rate constant for single turnover cleavage (k_{max}) at pH 6.5 with saturating concentrations of PRORP1 and metal (Co^{2+}, Ni^{2+}, Mn^{2+}, or Mg^{2+}). At pH 6.5, PRORP1 catalysis is within a log-linear region of the pH profile (Figure 3-7). Furthermore, this pH is below the pK_a values of the hydrated metals used (Co^{2+} = 9.65, Ni^{2+} = 10.0 Mn^{2+} = 10.46, and Mg = 11.4) (24, 25). Therefore, if the observed ionization reflects metal-water deprotonation, the value of k_{max} should correlate with the concentration of the metal-hydroxide, as indicated by the pK_a value. Thus, the k_{max} values are predicted to follow the order: Co^{2+} >Ni^{2+} >Mn^{2+} >Mg^{2+}. The measured k_{max} values for PRORP1 are 0.417, 0.042, 0.004, and 0.021 s^{-1} for Co^{2+}, Ni^{2+}, Mn^{2+}, and Mg^{2+}, respectively, representing a trend of Co^{2+} >Ni^{2+} >Mg^{2+} >Mn^{2+}. The faster reactivity observed in reactions with Mg^{2+} vs Mn^{2+} could be a result of PRORP1 evolving to specifically use Mg^{2+} ions, thus others factors such as differences in coordination geometries and preferred ligands of the metals used may explain this deviation (26). Excluding the Mg^{2+} data, log k_{max} decreases linearly with the value of the pK_a of the hydrated metal (R = 0.998) consistent with the observed ionization in catalysis arising from a metal-bound water.

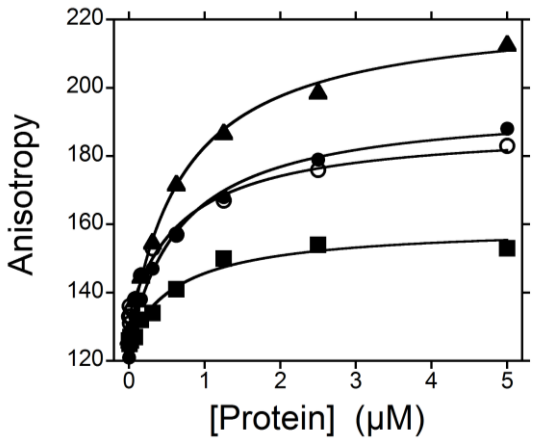

Figure 3-8. Alanine mutations at H498 and H438 do not affect the PRORP1 binding affinity for *A.t.* pre-tRNA. The binding affinity for *A.t.* pre-tRNA of PRORP1 variants (WT, circles; H498A, squares; H498Q, triangles; and H438A, open circles) was measured by changes in the anisotropy of the fluorescein labeled pre-tRNA substrate (20 nM) as the protein concentration varied in a 96-well plate format. Assays were performed in 20 mM MOPS pH 7.8, 300 mM NaCl, 1 mM TCEP, and 1 mM $CaCl_2$ at 25 °C. The dissociation constants (K_d) for *A.t.* pre-tRNA were determined by fitting Equation 3 to the data, resulting in values of 700 ± 80, 680 ± 150, 710 ± 60, and 700 ± 120 nM for WT, H498A, H498Q, and H438A, respectively.

Discussion

A Minimal Kinetic Mechanism Reveals Product Release is Not Rate-limiting at Neutral pH

We have determined kinetic parameters for PRORP1-catalyzed pre-tRNA cleavage for a cognate *A. thaliana* substrate and a bacterial pre-tRNA substrate. Despite being from different organisms and domains of life, these substrates show similar kinetic parameters (Table 3-1). This is not surprising given that both of these tRNAs have conserved secondary and tertiary features (27). Furthermore, the similarity between the STO (k_{max}) and MTO (k_{cat}) values suggests that a step observable under STO conditions is rate-limiting (*e.g.* a step at or before cleavage) and rules out product release as the rate-limiting step under MTO conditions. Consistent with this proposal, we do not observe

burst kinetics in the steady state turnover with the substrates used in this study (Figure 3-3A). This is in contrast to other RNase P enzymes that have been kinetically characterized. For instance, bacterial and yeast nuclear RNase P (RNA-based enzymes) are both limited by product dissociation and display burst kinetics under MTO conditions (28, 29). The standard assay condition (pH 7.8) is within the log-linear region of the pH dependence for PRORP1-catalyzed hydrolysis of *B.s.* pre-tRNA, suggesting that the cleavage step is rate-limiting.

Evidence for a 2-metal Ion Mechanism

Crystal structures of metallonucleases with metals bound in the active site have fuelled mechanistic proposals for one, two, and even three metal ion mechanisms (30, 31). In fact, structures of PRORP1 in the presence of different divalent metal ions have revealed one (calcium) to two-metal ions (manganese) bound within the active site. The metal dependence of PRORP1-catalyzed phosphodiester bond hydrolysis has a cooperativity of 2 for Mg^{2+} under k_{cat}/K_m conditions for both substrates, indicating that at least 2 metal ions activate catalysis. Addition of calcium does not abrogate the cooperativity, providing evidence that this effect is not due to stabilization of the pre-tRNA structure. Given these observations, we propose a model where the binding of one Mg^{2+} ion at the active site enhances the affinity of the second metal ion leading to the cooperativity observed at low pre-tRNA concentrations (Scheme 1). Furthermore, the loss of cooperativity at saturating pre-tRNA concentration is most easily explained by enhancement of the affinity of one of the two metal ions by substrate. One model consistent with the data is that under k_{cat} conditions an inactive ES complex with one tightly bound Mg^{2+} ion forms ($E^{Mg}S$) (Scheme 2). The enhanced metal binding affinity to the ES complex could be the result of either an indirect effect or the direct coordination of Mg^{2+} to a phosphodiester oxygen from the substrate. Similarly, the bacteriophage T5 exonuclease (T5 FEN), a member of the homologous flap nuclease family, shows no cooperativity for Mg^{2+} under k_{cat} conditions but a cooperativity of 2 is observed under k_{cat}/K_m conditions within the same Mg^{2+} concentration range tested for PRORP1 (31).

D474 and D475 Enhance the Active Site Metal Ion Affinity

Metal dependence measurements of aspartate to alanine mutations identified 2 side chains that enhance metal ion affinity by at least 9-fold. These mutations also decrease activity a maximum of 17 and 60-fold for the D474A and D475A mutants, respectively. These residues both lie on the end of an active site helix (Figure 3-1B). Based on the crystal structure, D475 makes an inner sphere bidentate interaction with both active site metal ions (Figure 3-1B). A bidentate Asp ligand is very common among metallonucleases where it has proposed to orient the active site metal ions for optimal catalysis (32). However, in PRORP1 other groups besides D475 must also help orient the metal ions, potentially including interactions with the substrate, since this mutant has significant activity at high concentrations of Mg^{2+}. The activity of D399A and D493A mutants could not be rescued by high Mg^{2+} concentrations, suggesting that they serve other roles in addition to metal binding. For instance, D399 makes a hydrogen bond with a metal-bound-water that is positioned approximately between the two active site metals (Figure 3-1B), suggesting that D399 could position a metal-bound water for nucleophilic attack. In the other nonrescuable aspartate mutant, D493A, the Asp side chain forms a hydrogen bond with the backbone amide of methionine 495 (Figure 3-1B), thus mutation of D493 may deleteriously affect the active site architecture.

pH Dependence Reveals a Single Ionization Important for Catalysis

The pH dependence of PRORP1-catalyzed cleavage of pre-tRNA is consistent with ionization of a single group that enhances catalysis. However, for the *A.t.* pre-tRNA the value of both k_{max}^{pH} and pK_a is decreased compared to the *B.s.* substrate. There are two models that could account for this. In the first model, the plateau in activity at high pH could result from a change in the rate-limiting step, from chemistry at low pH to a pH independent step, such as a conformational change, at high pH. In this case, the observed pK_a does not reflect the thermodynamic ionization, but rather a kinetic pK_a due to a change in the rate-limiting step over the pH range tested. This mechanism leads to an underestimation of the pK_a value, as previously observed in the pH dependence of *B.s.* RNase P where the pK_a reflects a change in the rate-limiting step (33). Alternatively, the difference in pK_a values observed with the *A.t.* and *B.s.* pre-tRNAs could arise from

differences in local active site environments in the pre-tRNA•PRORP complex, potentially arising from differences in nucleotide composition and/or the conformation of the bound pre-tRNA.

The pH dependent data for cleavage of *B.s.* pre-tRNA indicate that ionization of a functional group with a pK_a of 8.7 or higher is important for catalytic activity. The crystal structure demonstrates that the active site of PRORP1 contains two His residues but no conserved lysine or arginine side chains within 8 Å of the metal binding sites. Mutagenesis data demonstrate that the ionization does not reflect one of the His side chains (His498 and His438). Therefore, the most likely ionizable functional group within the active site vicinity with a pK_a of 8.7 or higher is a metal-bound water molecule, as predicted from $[Mg(H_2O)_6]^{2+}$ pK_a = 11.4 (24). This proposal is also consistent with the finding that the k_{max} value is dependent on the pK_a of the hydrated metal ion used in the reaction. We therefore propose that the observed ionization in PRORP1 is deprotonation of a metal-bound water to form the attacking hydroxide nucleophile. Bacterial RNase P and T5 FEN have a similar pH dependence to PRORP1 with a single deprotonation important for catalysis of phosphodiester bond cleavage, proposed to be deprotonation of a metal-bound water (34, 35).

Convergence of Enzyme Mechanism

A comparison of the proposed enzymatic mechanisms of PRORP and RNA-dependent RNase P reveals that both enzymes require catalytic metal ions, although the metal ligands vary (Figure 3-9). The metal ions in PRORP1 are coordinated by conserved aspartate residues, whereas the RNA-based RNase P mainly uses non-bridging phosphodiester oxygens for metal ion coordination. Furthermore, the data suggest that one of the scissile phosphate oxygens of pre-tRNA interacts with bound metal ion(s). In PRORP, the *pro-*S_p oxygen of pre-tRNA is hypothesized to interact with the active site metal ions (23, 36), although this needs to be confirmed experimentally, while the *pro-*R_p substrate oxygen coordinates a metal ion in RNA-based RNase P (37, 38). Modeling of bound substrate suggests that coordination of the *pro-*S_p or *pro-*R_p oxygen affects the position of the metal ion relative to the scissile phosphate, leading to an alteration in the pre-tRNA binding mode. Other protein-based phosphoryl-transfer enzymes also contact

the *pro-S_p* oxygen of the scissile phosphate, including RNase H, EcoRv, and DNA transposases (39-41). The Hammerhead ribozyme and Spliceosome are proposed to contact the *pro-R_p* oxygen at the cleavage site, whereas the *Tetrahymena* ribozyme contacts the *pro-S_p* oxygen (42-44).

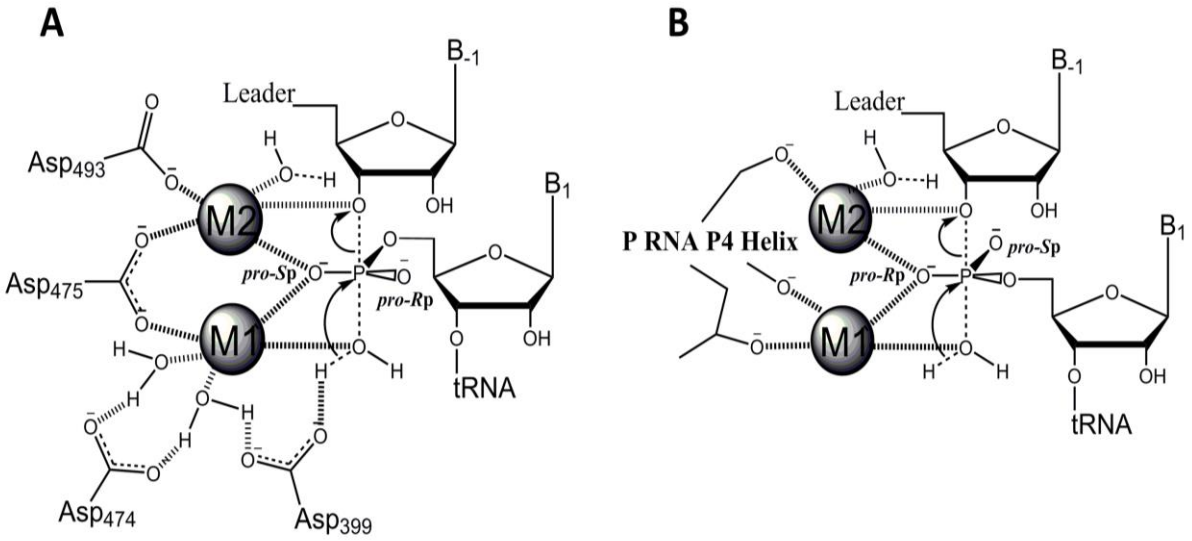

Figure 3-9. Proposed enzymatic mechanisms for protein-only (A) and RNA-based (B) RNase P enzymes. Both protein and RNA-based RNase P enzymes use at least 2-metal ions for phosphodiester bond hydrolysis. The metal ions in PRORP1 are positioned through conserved aspartate residues whereas the RNA-based RNase P coordinates metal ions mainly using non-bridging phosphate oxygens. Metal ion 1 (M1 is proposed to coordinate the nucleophilic water molecule and aid in transition state stabilization by interaction with a non-bridging phosphate oxygen. Metal ion 2 (M2) is also proposed to stabilize the transition state and potentially coordinates the 3' oxyanion leaving group to facilitate bond cleavage.

The RNA-based RNase P reaction has been proposed to catalyze cleavage using a metal-bound hydroxide nucleophile (34). Similarly, the pH dependence of PRORP1 suggests a similar mechanism for the protein catalyzed reaction. A possible alternate mechanism is activation of a metal-bound nucleophile by a general base, as suggested for EcoRV and RNase H (45, 46). However, 2 ionizations (slope = 2) and pK_a values of ~6.0 - 7.0 are observed in pH profiles of these enzymes (45-47), which is significantly different than the pH dependence observed with PRORP1. Thus, it is unlikely that PRORP1 uses a general base mechanism for activation of the nucleophile. In both cases, the metal ions are proposed to stabilize the negative charge build up in the transition state and facilitate bond cleavage by stabilizing the 3' oxyanion leaving group. The absence of an alkaline limb on the pH profile for PRORP1 and RNA-based RNase P (48) suggests that an amino acid or nucleotide with a pK_a < 10 does not serve as a general acid. Rather the proton donor for the 3' oxyanion leaving group is most likely a water molecule. The functional convergence of enzymes is not uncommon (49), however the functional and mechanistic convergence of two different enzymatic macromolecules (RNA and protein) is remarkable. This observation suggests that the protein and RNA macromolecules act as dynamic scaffolds that achieve large rate enhancements mainly through the binding and positioning of hydrated magnesium ions.

Methods

Enzyme Preparation

A truncation of PRORP1 lacking the N-terminal 76 amino acids, encompassing the mitochondrial localization sequence, was used in this study. PRORP1 WT and mutants were purified as previously described (7). Enzyme concentration was determined by absorbance using an extinction coefficient at 280 nm of 84,630 M^{-1} cm^{-1}. Purified enzymes were aliquoted, flash-frozen, and stored at -80 °C in 20 mM MOPS pH 7.8, 100 mM NaCl, and 1 mM TCEP.

Pre-tRNA Preparation

The *A. thaliana (A.t.)* pre-tRNA was produced by run-off transcription from a linearized plasmid containing a T7 promoter, a 5:1 (leader nt length : discriminator base) mitochondrial pre-tRNA^{Cys} gene, and a 3'-BstNI restriction site. The *Bacillus subtilis (B.s.)* pre-tRNA^{Asp} was transcribed from a PCR product containing a T7 promoter, with a 5 nt leader and a discriminator base (1 nt trailer) using a plasmid encoding *B.s.* pre-tRNA^{Asp} with a 5 nucleotide leader and GCCA trailer as the template (11). Transcription reactions were performed in the presence of guanosine-5'-O-monophosphorothioate (GMPS) and the 5' phosphorothioate was reacted with 5-(iodoacetamido)fluorescein (5-IAF) to fluorescently label the 5' end (12). Substrates were purified on 12% urea-page gels, crush-soaked to elute, then washed and concentrated. The concentration of pre-tRNA substrates was calculated by absorbance using extinction coefficients of 674,390 M^{-1} cm^{-1} and 685,000 M^{-1} cm^{-1} at 260 nm for *A.t.* and *B.s*. pre-tRNA, respectively. Labeling efficiency was assessed by fluorescein absorbance at 492 nm using an extinction coefficient of 78,000 M^{-1} cm^{-1}. Samples were stored at -20 or -80 °C in 10 mM Tris pH 7.4. Proposed tRNA secondary structures were generated with tRNAscan-SE 1.21 (13).

Enzyme Assays

Standard reaction conditions are 30 mM MOPS pH 7.8, 150 mM NaCl, 1 mM TCEP, and 1 mM $MgCl_2$ at 25 °C. Pre-tRNA substrates were denatured by heating at 95 °C for 1 min in milli-Q H_2O and then refolded by incubating at 25 °C for 15 min, adding reaction buffer, and incubating at 25 °C for at least 15 min before use. For single-turnover reactions, the enzyme and pre-tRNA concentrations were 5 µM and 20 nM, respectively, unless otherwise noted. Single-turnover reactions were initiated by addition of enzyme (5 µM) and quenched at specified times with an equal volume of 100 mM EDTA, 6 M Urea, 0.1 % bromophenol blue, 0.1 % xylene cyanol, 2 µg/µl yeast tRNA. The labeled 5' leader product was separated from pre-tRNA by electrophoresis on 20 or 22.5% urea-PAGE. Gels were visualized using a Typhoon 9410 scanner and the fraction product quantified using ImageQuant 5.2 software. The observed single-turnover rate constant was calculated from a fit of a first order exponential equation to the data using KaleidaGraph

fitting software. The k_{obs} was not significantly dependent on the PRORP1 concentration (2 and 5 μM), confirming that the enzyme was saturating (k_{max} conditions).

Multiple-turnover reactions were performed in black Costar half-area 96-well plates using a fluorescent polarization (FP) assay (as described in (14)). Standard reaction conditions were used with an enzyme concentration of 20 nM. The concentration of fluorescently labeled pre-tRNA was held constant at 40 nM in the reactions while the concentration of unlabeled pre-tRNA substrate was varied. The ratio of labeled to unlabeled substrate did not alter the measured initial rates. Initial rates were calculated from the linear decrease in fluorescence anisotropy (ex. = 488 nm, em. = 535 nm). The steady state kinetic parameters were calculated from a fit of the Michaelis-Menten (15) equation to the concentration dependence of the initial rates using Kaleidagraph.

Metal Dependence

The metal dependence of cleavage of *B.s.* pre-tRNA was measured under multiple-turnover conditions using the FP assay. The pre-tRNA concentration dependence of the initial velocity was measured at 7 $MgCl_2$ concentrations with the ionic strength held constant by adjusting the NaCl concentration (μ = 200 taking only the NaCl and $MgCl_2$ concentrations into account). The metal dependence of PRORP-catalyzed cleavage of *A.t* pre-tRNA^{Cys} was measured at two substrate concentrations, 250 nM and 5 μM, mimicking k_{cat}/K_m and k_{cat} conditions, respectively. Metal dependence reactions were similarly performed in the presence of 1 mM $CaCl_2$. Equation 1 was fit to the Mg^{2+} dependence of the apparent steady state kinetic parameters where k represents the apparent k_{cat} or k_{cat}/K_M, k^{Mg} represents the maximal rate constant (k_{cat}^{Mg} or $(k_{cat}/K_M)^{Mg}$) at saturating Mg^{2+}, and K_M^{Mg} is the concentration of Mg^{2+} at which k^{Mg} is half maximal.

$$k = \frac{k^{Mg}[Mg^{2+}]^n}{[Mg^{2+}]^n + K_M{}^{Mg}} \qquad (1)$$

Metal Dependence of Mutants

5 μM WT, D399A, D474A, D475A, or D493A PRORP were incubated with 20 nM *B.s.* fluorescein-pre-tRNA^{Asp} in 50 mM MTA buffer (see pH dependence for description of

MTA) pH 8.0, with 1 - 20 mM $MgCl_2$, and 1 mM TCEP. For WT, the NaCl concentration was adjusted to correct for ionic strength while 100 mM NaCl was used to assay the mutant enzymes. These single-turnover reactions were quenched at 2 hr with an equal volume of 100 mM EDTA, 6 M urea, 0.1 % bromophenol blue, 0.1 % xylene cyanol, and 2 µg/µl yeast tRNA. The fraction product was determined using a 22.5% urea-PAGE.

pH Dependence

Reactions were performed under single-turnover conditions (5 µM PRORP and 20 nM pre-tRNA) in a 3-component buffer system (MTA buffer): 50 mM MES (pK_a 6.15), Tris (pK_a 8), and 2-amino-2-methyl-1-propanol (AMP, pK_a 9.7) (16, 17). Reactions also included 1 mM TCEP, 1 mM $MgCl_2$ and NaCl to maintain ionic strength (µ = 240 ± 10 mM). The pH range assayed was 6.0 – 9.75. Doubling the concentration of PRORP to 10 µM at pH 6.5 and 8.0 increased the observed rate constant <20% indicating that the enzyme concentration was saturating. The rate constants measured in MTA buffer were within 20% of assays performed in 50 mM PIPES, pH 6.95; Tris, pH 8.0; and CHES, pH 9.5. Reactions performed with *A.t.* pre-tRNA at and above pH 8.5, displayed biphasic kinetics, possibly due to misfolded substrate (18). The observed rate constant for the first phase (largest amplitude) was used in the pH profile. Reactions at pH 9.5 and 9.75 for cleavage of *B.s.* pre-tRNA were performed using a quench-flow apparatus. A single ionization model (Equation 2) was fit to the pH dependence of the single-turnover reaction where k_{max} is the observed rate constant at a given pH, k_{max}^{pH} is the pH-independent rate constant, and the pK_a is the pH when the activity is half-maximal.

$$k_{max} = \frac{k_{max}^{pH}}{1 + 10^{(\mathrm{p}K_a - \mathrm{pH})}} \qquad (2)$$

STO reactions performed in the presence of various divalent ions contained 8 µM PRORP1, 50 mM MTA buffer at pH 6.5, 10 mM divalent metal, 1 mM TCEP, 250 µM hexamminecobalt(III) chloride, 165 mM NaCl, and 30 nM *B.s.* pre-tRNA. k_{max} was measured under various metal concentrations (1, 5, 10, and 20 mM) to ensure metal saturation and lack of inhibition.

Anisotropy Binding Assays

Binding assays were performed as previously described (7). Briefly, the concentration of fluorescein labeled pre-tRNA was maintained at 20 nM, while the concentration of PRORP was varied (0.005 - 5 µM). Binding experiments were performed in 20 mM MOPS pH 7.8, 300 mM NaCl, 1 mM TCEP, and 1 mM $CaCl_2$ in a 96-well plate format. Fluorescence anisotropy was measured at an excitation wavelength of 488 nm and an emission wavelength of 535 nm (14). PRORP1 is not active in $CaCl_2$ (7). Equation 3 was fit to the dependence of the anisotropy on the protein concentration where A is the observed anisotropy, A_o is the initial anisotropy, ΔA is the total change in anisotropy, P is the concentration of PRORP, and K_d is the apparent dissociation constant.

$$A = A_o + \frac{\Delta A\,[P]}{[P] + K_d} \qquad (3)$$

References

1. Howard, M. J., Liu, X., Lim, W. H., Klemm, B. P., Fierke, C. A., Koutmos, M., and Engelke, D. R. (2013) RNase P enzymes: divergent scaffolds for a conserved biological reaction. *RNA Biol.* **10**, 909–14
2. Walker, S. C., and Engelke, D. R. (2006) Ribonuclease P: the evolution of an ancient RNA enzyme. *Crit. Rev. Biochem. Mol. Biol.* **41**, 77–102
3. Gutmann, B., Gobert, A., and Giegé, P. (2012) PRORP proteins support RNase P activity in both organelles and the nucleus in Arabidopsis. *Genes Dev.* **26**, 1022–7
4. Holzmann, J., Frank, P., Löffler, E., Bennett, K. L., Gerner, C., and Rossmanith, W. (2008) RNase P without RNA: identification and functional reconstitution of the human mitochondrial tRNA processing enzyme. *Cell* **135**, 462–74
5. Rossmanith, W. (2012) Of P and Z: mitochondrial tRNA processing enzymes. *Biochim. Biophys. Acta* **1819**, 1017–26
6. Gobert, A., Gutmann, B., Taschner, A., Gössringer, M., Holzmann, J., Hartmann, R. K., Rossmanith, W., and Giegé, P. (2010) A single Arabidopsis organellar protein has RNase P activity. *Nat. Struct. Mol. Biol.* **17**, 740–4
7. Howard, M. J., Lim, W. H., Fierke, C. A., and Koutmos, M. (2012) Mitochondrial ribonuclease P structure provides insight into the evolution of catalytic strategies for precursor-tRNA 5' processing. *Proc. Natl. Acad. Sci. U.S.A.* **109**, 16149–54
8. Anantharaman, V., and Aravind, L. (2006) The NYN domains: novel predicted RNAses with a PIN domain-like fold. *RNA Biol.* **3**, 18–27
9. Orans, J., McSweeney, E. A., Iyer, R. R., Hast, M. A., Hellinga, H. W., Modrich, P., and Beese, L. S. (2011) Structures of human exonuclease 1 DNA complexes suggest a unified mechanism for nuclease family. *Cell* **145**, 212–23
10. Steitz, T. A., and Steitz, J. A. (1993) A general two-metal-ion mechanism for catalytic RNA. *Proc. Natl. Acad. Sci. U.S.A.* **90**, 6498–502
11. Milligan, J. F., and Uhlenbeck, O. C. (1989) Synthesis of small RNAs using T7 RNA polymerase. *Meth. Enzymol.* **180**, 51–62
12. Rueda, D., Hsieh, J., Day-Storms, J. J., Fierke, C. A., and Walter, N. G. (2005) The 5' leader of precursor $tRNA^{Asp}$ bound to the Bacillus subtilis RNase P holoenzyme has an extended conformation. *Biochemistry* **44**, 16130–9
13. Schattner, P., Brooks, A. N., and Lowe, T. M. (2005) The tRNAscan-SE, snoscan and snoGPS web servers for the detection of tRNAs and snoRNAs. *Nucleic Acids Res.* **33**, W686-9
14. Liu, X., Chen, Y., and Fierke, C. A. (2014) A real-time fluorescence polarization activity assay to screen for inhibitors of bacterial ribonuclease P. *Nucleic Acids Res.* **42**, e159, 10.1093/nar/gku850
15. Johnson, K. A., and Goody, R. S. (2011) The original Michaelis constant: translation of the 1913 Michaelis–Menten paper. *Biochemistry* **50**, 8264-9
16. Jaenicke, L. (1974) *Buffers for pH and metal ion control*, Perrin, D. D., and Dempsey, B., Chapman and Hall, London
17. Perrotta, A. T., Shih, I., and Been, M. D. (1999) Imidazole rescue of a cytosine mutation in a self cleaving ribozyme. *Science* **286**, 123–126
18. Bhaskaran, H., Taniguchi, T., Suzuki, T., Suzuki, T., and Perona, J. J. (2014) Structural Dynamics of a Mitochondrial tRNA Possessing Weak Thermodynamic Stability. *Biochemistry* **53**, 1456-65
19. Kurz, J. C., Niranjanakumari, S., and Fierke, C. A. (1998) Protein component of Bacillus subtilis RNase P specifically enhances the affinity for precursor-$tRNA^{Asp}$. *Biochemistry* **37**, 2393–400
20. Frank, D. N., and Pace, N. R. (1997) In vitro selection for altered divalent metal specificity in the RNase P RNA. *Proc. Natl. Acad. Sci. U.S.A.* **94**, 14355-06
21. Thompson, J. E., and Raines, R. T. (1994) Value of General Acid-Base Catalysis to Ribonuclease A. *J. Am. Chem. Soc.* **116**, 5467–8
22. O'Brien, P. J., and Ellenberger, T. (2003) Human alkyladenine DNA glycosylase uses acid-base catalysis for selective excision of damaged purines. *Biochemistry* **42**, 12418–29
23. Pavlova, L. V., Gössringer, M., Weber, C., Buzet, A., Rossmanith, W., and Hartmann, R. K. (2012) tRNA processing by protein-only versus RNA-based RNase P: kinetic analysis reveals mechanistic differences. *Chembiochem* **13**, 2270–6

24. Dean, J. A. (1985) *Lange's Handbook of Chemistry*, 13th Ed., McGraw-Hill, Chicago, IL
25. Sillen, L. G., Martell, A. E. (1971) Stability constants of metal-ion complexes. *Spec. Publ. Chem. Soc*., 25, London
26. Dahm, S., Derrick, WB, and Uhlenbeck, OC (1993) Evidence for the role of solvated metal hydroxide in the hammerhead cleavage mechanism. *Biochemistry*
27. Westhof, E., and Auffinger, P. (2012) Transfer RNA Structure. In: *eLS*. John Wiley and Sons Ltd
28. Beebe, J. A., and Fierke, C. A. (1994) A kinetic mechanism for cleavage of precursor $tRNA^{Asp}$ catalyzed by the RNA component of Bacillus subtilis ribonuclease P. *Biochemistry* **33**, 10294–304
29. Hsieh, J., Walker, S. C., Fierke, C. A., and Engelke, D. R. (2009) Pre-tRNA turnover catalyzed by the yeast nuclear RNase P holoenzyme is limited by product release. *RNA* **15**, 224–34
30. Dupureur, C. M. (2010) One is enough: insights into the two-metal ion nuclease mechanism from global analysis and computational studies. *Metallomics* **2**, 609–20
31. Syson, K., Tomlinson, C., Chapados, B. R., Sayers, J. R., Tainer, J. A., Williams, N. H., and Grasby, J. A. (2008) Three metal ions participate in the reaction catalyzed by T5 flap endonuclease. *J. Biol. Chem.* **283**, 28741–6
32. Yang, W., Lee, J. Y., and Nowotny, M. (2006) Making and breaking nucleic acids: two-Mg^{2+}-ion catalysis and substrate specificity. *Mol. Cell* **22**, 5–13
33. Hsieh, J., and Fierke, C. A. (2009) Conformational change in the Bacillus subtilis RNase P holoenzyme--pre-tRNA complex enhances substrate affinity and limits cleavage rate. *RNA* **15**, 1565–77
34. Cassano, A. G., Anderson, V. E., and Harris, M. E. (2004) Analysis of solvent nucleophile isotope effects: evidence for concerted mechanisms and nucleophilic activation by metal coordination in nonenzymatic and ribozyme-catalyzed phosphodiester hydrolysis. *Biochemistry* **43**, 10547–59
35. Tock, M. R., Frary, E., Sayers, J. R., and Grasby, J. A. (2003) Dynamic evidence for metal ion catalysis in the reaction mediated by a flap endonuclease. *EMBO J.* **22**, 995–1004
36. Thomas, B. C., Li, X., and Gegenheimer, P. (2000) Chloroplast ribonuclease P does not utilize the ribozyme-type pre-tRNA cleavage mechanism. *RNA* **6**, 545-53
37. Chen, Y., Li, X., and Gegenheimer, P. (1997) Ribonuclease P catalysis requires Mg^{2+} coordinated to the pro-RP oxygen of the scissile bond. *Biochemistry* **36**, 2425–38
38. Warnecke, J. M., Fürste, J. P., Hardt, W. D., Erdmann, V. A., and Hartmann, R. K. (1996) Ribonuclease P (RNase P) RNA is converted to a Cd^{2+}-ribozyme by a single Rp-phosphorothioate modification in the precursor tRNA at the RNase P cleavage site. *Proc. Natl. Acad. Sci. U.S.A.* **93**, 8924–8
39. Nowotny, M., Gaidamakov, S. A., Crouch, R. J., and Yang, W. (2005) Crystal structures of RNase H bound to an RNA/DNA hybrid: substrate specificity and metal-dependent catalysis. Cell **121**, 1005–16
40. Kostrewa, D, and Winkler, FK (1995) Mg2+ Binding to the Active Site of EcoRV Endonuclease: A Crystallographic Study of Complexes with Substrate and Product DNA at 2-. ANG. Resolution. Biochemistry **34**, 683-696
41. Kennedy, AK, Haniford, DB, and Mizuuchi, K (2000) Single active site catalysis of the successive phosphoryl transfer steps by DNA transposases: insights from phosphorothioate stereoselectivity. Cell **101**, 295-305
42. Dahm, S., and Uhlenbeck, OC (1991) Role of divalent metal ions in the hammerhead RNA cleavage reaction. Biochemistry **30**, 9464-9469
43. Fica, S. M., Tuttle, N., Novak, T., Li, N.-S. S., Lu, J., Koodathingal, P., Dai, Q., Staley, J. P., and Piccirilli, J. A. (2013) RNA catalyses nuclear pre-mRNA splicing. Nature **503**, 229–34
43. Shan, S, Kravchuk, AV, Piccirilli, JA, and Herschlag, D (2001) Defining the catalytic metal ion interactions in the Tetrahymena ribozyme reaction. Biochemistry **40**, 5161-5171
45. Stanford, N. P., Halford, S. E., and Baldwin, G. S. (1999) DNA cleavage by the EcoRV restriction endonuclease: pH dependence and proton transfers in catalysis. J. Mol. Biol. **288**, 105–16
46. Bastock, J. A., Webb, M., and Grasby, J. A. (2007) The pH-dependence of the Escherichia coli RNase HII-catalysed reaction suggests that an active site carboxylate group participates directly in catalysis. J. Mol. Biol. **368**, 421–33
47. Campbell, F. E., Cassano, A. G., Anderson, V. E., and Harris, M. E. (2002) Pre-steady-state and stopped-flow fluorescence analysis of Escherichia coli ribonuclease III: insights into mechanism and conformational changes associated with binding and catalysis. *J. Mol. Biol.* **317**, 21–40

48. Kurz, J. C., and Fierke, C. A. (2002) The affinity of magnesium binding sites in the subtilis RNase P x pre-tRNA complex is enhanced by the protein subunit. *Biochemistry* **41**, 9545–58
49. Doolittle, R. F. (1994) Convergent evolution: the need to be explicit. *Trends Biochem. Sci.* **19**, 15–8

Chapter 4 [4]

Kinetic Characterization of Plant Protein-only RNase P Isozymes Reveals Overlapping Substrate Specificities and Varying Cleavage Fidelities

Abstract

Ribonuclease P (RNase P) catalyzes the cleavage of leader sequences from precursor-tRNA (pre-tRNA). Typically these enzymes are ribonucleic protein complexes that are found in all domains of life, including the nucleus of most eukaryotes. In contrast, RNase Ps in human mitochondria and most genome-containing eukaryotic organelles do not contain an RNA component, but instead use protein-only RNase P (PRORP). Land plants are unique because they are seemingly devoid of RNA-based RNase P, instead using three PRORPs localized to different cellular compartments to catalyze 5' pre-tRNA maturation. To provide insight into the evolution and function of PRORP enzymes we surveyed substrate specificities, equilibrium binding affinities, and cleavage fidelities of the three *Arabidopsis* PRORP isozymes with four pre-tRNA substrates. The catalytic efficiencies range from 10^4 - 10^5 M^{-1} s^{-1}, with no apparent preference for the compartmental origin of pre-tRNA. Additionally, PRORPs bind pre-tRNA with comparable affinities, suggesting similar binding modes. However, the PRORP isozymes have varying degrees of cleavage fidelity, which is dependent on the pre-tRNA species and the presence of a 3'-discriminator base. We provide an in-depth comparison of *Arabidopsis* PRORP isozymes that allow insight into a new class of RNA processing enzymes, and

[4] This chapter has been submitted as an article for publication. The authors include: Michael J. Howard, Agnes Karasik, Bradley P. Klemm, Christine Mei, Aranganathan Shanmuganathan, Carol A. Fierke, and Markos Koutmos. M.J.H. designed the experiments, prepared the substrates, performed assays with PRORP1, analyzed the data, made the figures and wrote the paper. B.P.K. prepared PRORP3 constructs and assayed PRORP3 under MTO and STO conditions. A.K. performed MTO and STO assays with PRORP2. C.M. purified PRORP3 and assayed the PRORPs with the model substrates. A.S. purified PRORP2.

forms a basis for understanding the more complicated three protein-component human mitochondrial RNase P.

Background

Transfer RNAs (tRNAs) are transcribed as precursors (pre-tRNA), with extra nucleotides flanking their 5' and 3' ends. Removal of these extraneous sequences is critical for tRNA function, thus the enzymes responsible for tRNA maturation are essential. RNase P is the endonuclease responsible for catalyzing the 5' end maturation of pre-tRNA, and is found in all domains of life (1). RNase P enzymes are extremely diverse with regards to their macromolecular composition (2). In bacteria, archaea, and the nuclei of most eukaryotes, pre-tRNA cleavage is catalyzed by a conserved RNA-based RNase P (ribozyme) that associates with a number of different protein cofactors (1-10, depending on the Domain of origin). In contrast, a protein-only form of RNase P (PRORP) is present in the organelles of most eukaryotic organisms (3). PRORPs were first discovered in human mitochondria, where they process mitochondrial encoded pre-tRNAs (4). Human mitochondrial RNase P requires three protein subunits for efficient catalysis: a nuclease (MRPP3/human PRORP), a tRNA methyltransferase (TRMT10C/MRPP1), and a dehydrogenase (SDR5C1/MRPP2). SDR5C1 and TRMT10C form a complex and are proposed to play a scaffolding role in pre-tRNA maturation catalyzed by human PRORP (5,6). In contrast to the mammalian enzyme, the PRORPs found in plants, some protists and algae do not require additional proteins for efficient catalysis, offering a simpler model system to understand the function of this new class of nucleases (3,7,8).

While the majority of eukaryotes retain an RNA-based RNase P in their nucleus, bioinformatic studies have long suggested that land plants may lack a catalytic RNA component for RNase P activity (9). Consistent with this, the prototypical land plant *Arabidopsis thaliana* possesses three nuclear encoded PRORP enzymes (PRORP1, 2, and 3) (10,11). PRORP1 is essential and found in mitochondria and chloroplasts (3,10), while PRORP2 and 3 are localized to the nucleus where they play essential but redundant roles; knockout of either PRORP2 or 3 shows no macroscopic phenotype, but knockout of both is lethal (3,10,12). Thus, PRORP enzymes have replaced the ancient RNA-based RNase P in *A. thaliana,* processing RNA transcripts in the chloroplast, mitochondria, and

nucleus. However, the molecular interactions that confer substrate specificity of these important enzymes remain largely unknown.

Similar to *Arabidopsis*, the moss, *Physcomitrella patens,* also contains three PRORP enzymes and no apparent catalytic RNA component for the ribonucleic protein version of RNase P (13). In contrast to *Arabidopsis*, *P. patens* localizes two PRORP enzymes to the mitochondria and chloroplast and one to the nucleus (13). Furthermore, knockout of the nuclear PRORP in *P. patens* is not lethal suggesting an unidentified RNase P activity in the nucleus or dual localization of one or both of the organellar PRORPs (13). *In vitro* cleavage assays reveal that the two organellar PRORPs in *P. patens* have overlapping but not identical substrate specificities. This observation suggests that the two nuclear PRORPs in *Arabidopsis* could also have varying substrate specificities.

PRORP enzymes contain three domains: an N-terminal pentatricopeptide repeat (PPR) domain, a central Zn-binding domain, and a Nedd4-BP1, YacP nuclease (NYN) domain (Figure 4-1). (14) The PPR domain contains five PPR or PPR-like motifs, which are helix-turn-helix motifs found in tandem. This domain has been proposed to interact with pre-tRNA and enhance binding affinity (15,16). The largest sequence variation among the PRORPs is found in the PPR domains and thus differences in substrate recognition may lie within this region (14). The central domain binds a structurally important Zn^{2+} ion and links the PPR and metallonuclease domains. The NYN-metallonuclease domain catalyzes phosphodiester bond hydrolysis and contains four conserved aspartates important for binding catalytic metal ions and catalysis (14,17). Both the protein and RNA-based RNase P enzymes are proposed to use a two-metal ion mechanism (17,18). The sequence identity among the *A. thaliana* PRORPs is highest in the metallonuclease domain. PRORP2 and 3 are most similar (80% identity and 88% similarity); the percent identity and similarity between PRORP1 and 2 is 48% and 65% and between PRORP1 and 3 is 49% and 65%, respectively.

Given that *A. thaliana* encodes three PRORPs, it is possible that they have developed distinct but overlapping substrate specificities. To test this hypothesis and provide insight into how this new class of enzyme functions, we assayed the three *A. thaliana* PRORP enzymes with four pre-tRNAs of different organellar origin (chloroplast, mitochondria, and nucleus). Multiple turnover assays reveal comparable catalytic efficiencies among the

PRORPs, suggesting similar, but not identical, substrate selectivity. Furthermore, PRORP binding affinities for the same pre-tRNA are comparable. Despite these similarities, PRORP cleavage fidelity varies with the pre-tRNAs examined due to the presence of the discriminator base.

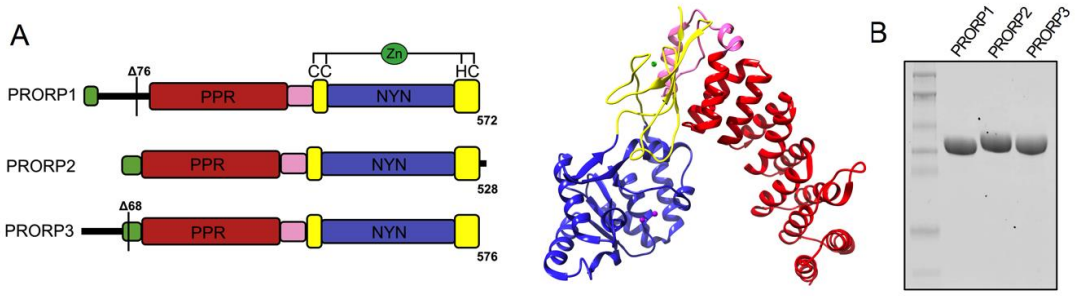

Figure 4-1. A. *A. thaliana* encodes three PRORP enzymes, PRORP1, 2 and 3. N-terminal truncations of PRORP1 (Δ76) and PRORP3 (Δ68) were used in this study. PRORP enzymes contain three domains: the PPR (red), the central-Zn binding (yellow), and NYN (blue) domains. The N-terminal green region represents the proposed localization sequences: PRORP1 1-48, (using the TargetP 1.1 algorithm (35)); PRORP2 and 3 contain canonical bipartate nuclear localization signals (H/R-RSR-R/H-X_9-K-K-K-K) (36). The pink represents a plant specific insert in the gene sequence. The right panel shows the crystal structure of PRORP1 (PDB 4G24). B. SDS-PAGE analysis of purified proteins used in this study.

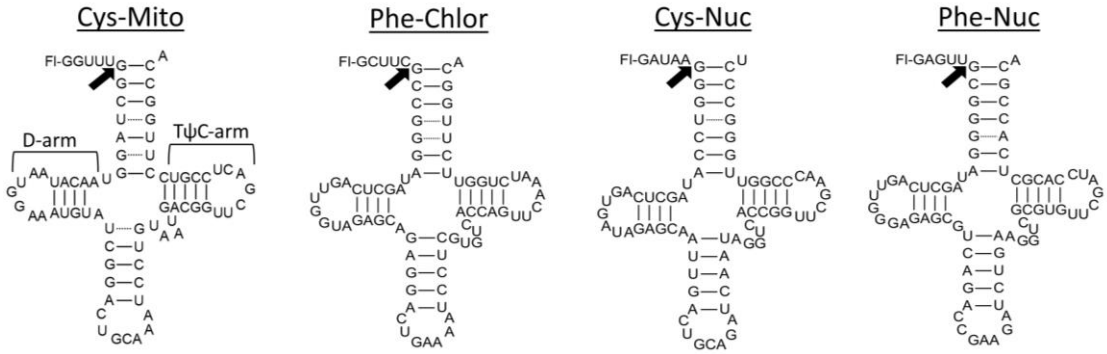

Figure 4-2. Predicted secondary structures of *A. thaliana* pre-tRNA substrates used in this study. All substrates prepared through *in vitro* transcription. Cys-Mito and Phe-Chlor substrates are derived from the organellar genomes (Cys-mitochondrial and Phe-Chloroplast), and Cys-nuclear and Phe-nuclear are from the nuclear genome. The pre-tRNAs contain 5 nt leaders labeled with fluorescein at the 5' end and a discriminator base at the 3' end.

Results

PRORPs Catalyze Cleavage of Most Pre-tRNA Substrates with Uniform Efficiency

To determine if the three *A. thaliana* PRORP enzymes have differing substrate specificities we recombinantly expressed and purified the proteins from *E. coli* (Figure 4-1B). We then assessed the ability of PRORP1, 2 and 3 to catalyze cleavage of four *A. thaliana* pre-tRNAs. The pre-tRNAs that we assayed are: two nuclear encoded pre-tRNAs (Cys-Nuc and Phe-Nuc) and two organellar encoded pre-tRNAs (Cys-Mito and Phe-Chlor) (Figure 4-2). We used a real-time fluorescent anisotropy (FA) assay to monitor the steady-state (or multiple-turnover (MTO)) activity of PRORP-catalyzed pre-tRNA hydrolysis (Figure 4-3A) (19). The resulting steady state kinetic parameters are reported in Table 4-1. To compare substrate specificities we plotted the k_{cat}/K_M values for each substrate and respective PRORP (Figure 4-3B). The k_{cat}/K_M value is a useful parameter for analyzing substrate specificities because it represents the catalytic efficiency for a given enzyme and substrate. For each substrate, PRORP1 is slightly more catalytically

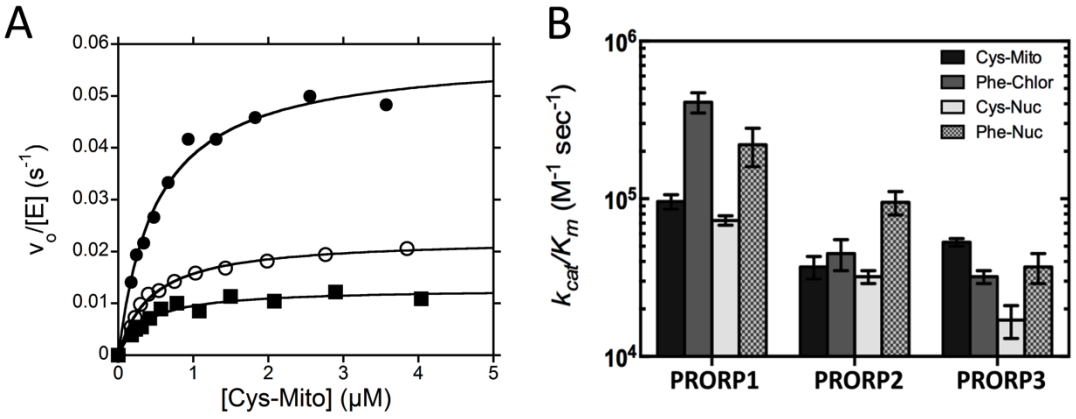

Figure 4-3. Multiple-turnover cleavage of pre-tRNA catalyzed by PRORPs. A. The substrate dependence of the initial velocity for cleavage of Cys-Mito pre-tRNA catalyzed by PRORP1 (Closed circle), PRORP2 (closed square), and PRORP3 (open circle). Reactions were performed under standard reaction conditions. B. Bar graph comparing the catalytic efficiencies (k_{cat}/K_M) of the three PRORP enzymes with the four pre-tRNA substrates.

efficient than PRORP2 and 3. The most significant differences in k_{cat}/K_M are observed with the Phe-Chlor and the Cys-Nuc pre-tRNA substrates. The Cys-Nuc substrate showed the lowest k_{cat}/K_M value with PRORP3 (1.7 x 10^4 M^{-1} s^{-1}), mainly due to a low turnover number (k_{cat}). PRORP1 showed the most selectivity for the Phe-Chlor substrate (k_{cat}/K_M = 4.1 x 10^5 M^{-1} s^{-1}) relative to PRORP2 and 3, representing a 9- and 13-fold difference, respectively. This overall ~10-fold increase in reactivity is due to both an increase in $k_{cat,}$ the rate constant at saturating concentrations of substrate, and a decrease in K_M for Phe-Chlor relative to PRORP2 and PRORP3.

Table 4-1. Kinetic parameters for pre-tRNA cleavage catalyzed by *A. thaliana* PRORP1, 2 and 3

		Single-turnover[a]	*Multiple-turnover*[b]		
Enzyme	Pre-tRNA	k_{obs} (s^{-1})[c]	k_{cat} (s^{-1})	K_M (nM)	k_{cat}/K_M ($M^{-1}s^{-1}$)
PRORP1	Cys-Mito	0.037 ± 0.002	0.062 ± 0.005	670 ± 230	9.6 ±1.0 x 10^4
	Phe-Chlor	0.035 ± 0.002	0.042 ± 0.005	140 ± 50	4.1 ± 0.6 x 10^5
	Cys-Nuc	0.037 ± 0.003	0.040 ± 0.002	550 ± 50	7.3 ± 0.5 x 10^4
	Phe-Nuc	0.078 ± 0.003	0.035 ± 0.003	160 ± 50	2.2 ± 0.6 x 10^5
PRORP2	Cys-Mito	0.013 ± 0.003	0.013 ± 0.002	340 ± 60	3.7 ± 0.6 x 10^4
	Phe-Chlor	0.018 ± 0.003	0.015 ± 0.002	340 ± 100	4.5 ± 1.0 x 10^4
	Cys-Nuc	0.027 ± 0.002	0.030 ± 0.002	940 ± 130	3.2 ± 0.3 x 10^4
	Phe-Nuc	0.035 ± 0.002	0.023 ± 0.002	250 ± 50	9.5 ± 1.6 x 10^4
PRORP3	Cys-Mito	0.023 ± 0.002	0.022 ± 0.002	430 ± 30	5.3 ± 0.3 x 10^4
	Phe-Chlor	0.023 ± 0.002	0.013 ± 0.002	440 ± 50	3.2 ± 0.3 x 10^4
	Cys-Nuc	0.030 ± 0.002	0.008 ± 0.002	420 ±100	1.7 ± 0.4 x 10^4
	Phe-Nuc	0.072 ± 0.003	0.062 ± 0.023	2000 ± 850	3.7 ± 0.8 x 10^4

[a]Reactions contained 5 µM indicated PRORP, 30 nM indicated pre-tRNA, 30 mM Mops pH 7.8, 150 mM NaCl, 1 mM TCEP, and 1 mM $MgCl_2$ at 25ºC.
[b]As described in Figure 3.
[c] Because both correct and incorrect cleavage products are catalyzed with some substrates (See figure 4-5 and Table 4-3), k_{max} represents the single-exponential fit to the time course of total product (C_o + M_{-1}) formation.

PRORPs Bind Individual Pre-tRNAs Similarly, Regardless of Pre-tRNA Origin

To establish if differentially localized PRORPs use binding affinity to discriminate between substrates encoded in the nucleus, chloroplast and mitochondria, we measured the dissociation constants (K_D) of PRORP1, 2, and 3 for the Cys-Mito, Phe-Chlor, Cys-Nuc, and Phe-Nuc pre-tRNA substrates described above using an FA binding assay (Figure 4-4A) (19). Comparison of the dissociation constants reveals that for a given substrate all three PRORPs have comparable binding affinities (< 4-fold different). However, while the K_D values were generally consistent for a given substrate, the affinity of the PRORPs for the different pre-tRNAs vary by as much as 100-fold (ranging from 60 nM to 6000 nM) (Figure 4-4B and Table 4-2). All three PRORPs bound Cys-Nuc pre-tRNA with the weakest affinity, with K_D values 5-fold larger than those measured for the other substrates.

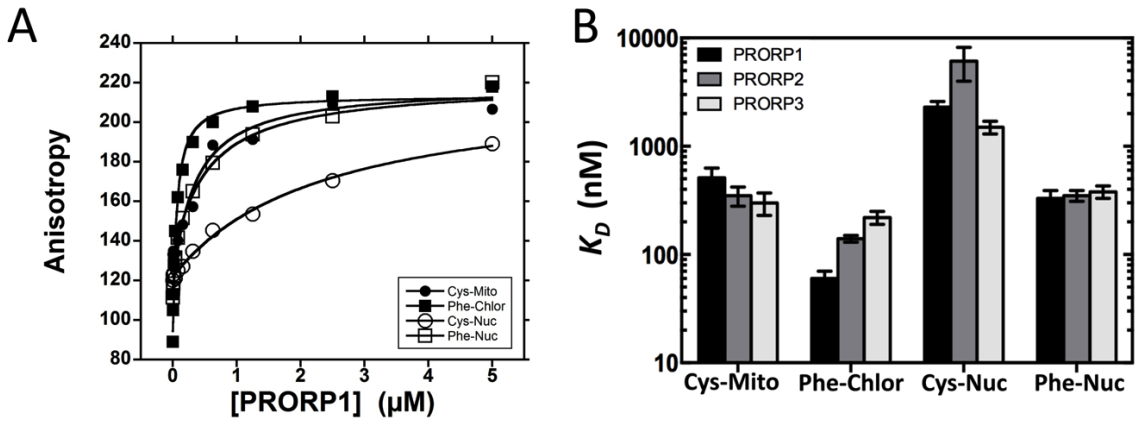

Figure 4-4. PRORP binding affinity for pre-tRNA substrates. A. Representative fluorescence anisotropy binding isotherms for varying concentration of PRORP1 and 20 nM fluorescein labeled pre-tRNA in 20 mM MOPS pH 7.8, 300 mM NaCl, 1 mM TCEP, and 1 mM $CaCl_2$. B. Bar graphs comparing the binding affinities (K_Ds) among the PRORP enzymes for four pre-tRNAs.

Table 4-2. Dissociation constants (K_D in nM) for PRORP1, 2, and 3 binding to pre-tRNAs[a]

	Pre-tRNA			
Enzyme	Cys-Mito	Phe-Chlor	Cys-Nuc	Phe-Nuc
PRORP1	510 ± 120	60 ± 10	2300 ± 300	330 ± 60
PRORP2	350 ± 70	140 ± 10	6100 ± 2100	350 ± 40
PRORP3	300 ± 70	220 ± 30	1500 ± 200	380 ± 50

[a]As measured in figure 4.

Product Release is not the Rate-limiting Step for MTO Catalysis by PRORP

The k_{cat}, K_M, and k_{cat}/K_M values measured in our MTO studies include all of the steps in the PRORP kinetic mechanism. To begin dissecting the contribution of discrete steps in the mechanism (e.g. substrate cleavage, product release, etc) to the progression of the reaction, we measured the STO kinetics of PRORP1, 2, and 3 for catalysis of pre-tRNA cleavage using the four substrates described above. In contrast to the steady-state values measured in MTO assays, the STO rate constants measured here report only the steps in the kinetic mechanism prior to, and including, substrate cleavage. In these assays, excess (5 μM) PRORP is added to limiting concentrations of 5'-fluorescein labeled substrate (30 nM) to initiate the reaction, and the reaction is quenched at discrete time points. The pre-tRNA reactants and products are subsequently visualized on a denaturing PAGE gel. For all three PRORPs the observed STO rate constants (k_{obs}) range between 0.02- 0.07 s^{-1} (Table 4-1) regardless of the substrate assayed. The observed rate constant for total product formation (C_o + M_{-1}) is reported for pre-tRNA substrates that are significantly miscleaved (see following section).

For *B. subtilis* RNase P, significant differences in the STO and MTO rate constants previously revealed that product-release is the rate-limiting step in the reaction (20,21). However, here the MTO k_{cat} values are similar to (within 2-fold) the STO k_{obs} values indicating that the rate-limiting step at saturating PRORP is a step prior to product dissociation. The only exception was the modest difference between the k_{obs} and k_{cat} values for PRORP3 catalyzing cleavage of Cys-Nuc pre-tRNA (k_{obs} 3.6-fold faster than k_{cat}) which suggests that product release may be partially rate limiting for k_{cat}.

PRORPs Have Varying Cleavage Fidelities

Gel analysis of the STO assays indicated two distinct product bands in all reactions with the Phe-Nuc substrate, and for PRORP2 and 3 catalyzed cleavage of the Cys-Mito and Cys-Nuc substrates. These products represent the correct (5 nucleotide long, C_o) and incorrect (4 nucleotide, M_{-1}) cleavage products (Figure 4-5A). To analyze this miscleavage, we propose a model of parallel reactions where product formation proceeds through two distinct enzyme-substrate ($E\text{-}S_c$ and $E\text{-}S_m$) complexes (Figure 4-5C). This model has previously been used to explain miscleavage catalyzed by bacterial RNase P (22,23). In this model, k_c represents the rate constant for the formation of the correct product and k_m represents the rate constant for the miscleaved product, assuming saturating concentrations of enzyme. These rate constants represent the cleavage at a particular site and can be used to compare the fidelity of the different PRORP enzymes (Table 4-3). This analysis reveals that the k_m for PRORP3 miscleavage of the Phe-Nuc substrate is 3.7-fold higher than the correct cleavage (k_c), which represents the lowest fidelity among the PRORPs. Furthermore, the nuclear localized PRORP2 and PRORP3 significantly miscleaved the Cys-Mito and Cys-Nuc substrates whereas the organellar PRORP1 did not, suggesting differences in cleavage site selection between the nuclear and organellar PRORPs (Table 4-3 and Figure 4-6).

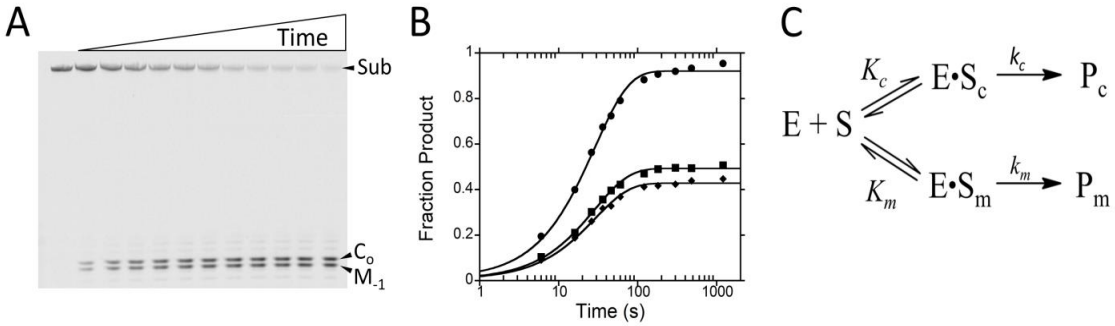

Figure 4-5. Phe-Nuc STO miscleavage kinetics. A. Representative urea-PAGE of STO cleavage of the Phe-Nuc pre-tRNA catalyzed by PRORP2 under standard reaction conditions. Reactions were quenched at specific time points and resolved on a 22.5% urea-PAGE. C_o indicates the correct 5 nt product and M_{-1} represents the miscleaved 4 nt product. B. A plot of the timecourse for product formation. Circle symbols represent the total product formation ((C_o + M_{-1})/(C_o + M_{-1} + Substrate)), squares represent correct product formation (C_o / (C_o + M_{-1} + Substrate)), and diamonds represents incorrect cleavage (M_{-1} / (C_o + M_{-1} + Substrate)). A single-exponential was fit to the timecourses resulting in values for $k_{obs,t}$, $k_{obs,c}$, and $k_{obs,m}$. C. Scheme for miscleavage. K_c and K_m represent the equilibrium constants for respective complex formation, k_c and k_m represent the rate constants for correct cleavage and for miscleavage, respectively. Kinetic parameters for miscleavage are summarized in Table 4-3.

Table 4-3. Single-turnover miscleavage kinetics catalyzed by PRORP1, 2, and 3[a]

Phe-Nuc Pre-tRNA

Enzyme	$k_{obs,c}$ (s^{-1})[b]	A_c[c]	$k_{obs,m}$ (s^{-1})[d]	A_m[e]	k_c (s^{-1})[f]	k_m (s^{-1})[f]	k_c/k_m
PRORP1	0.067	0.70	0.083	0.30	0.047	0.025	1.9
PRORP2	0.035	0.49	0.035	0.41	0.017	0.014	1.2
PRORP3	0.048	0.25	0.050	0.69	0.012	0.045	0.3

Cys-Nuc Pre-tRNA

Enzyme	$k_{obs,c}$ (s^{-1})	A_c	$k_{obs,m}$ (s^{-1})	A_m	k_c (s^{-1})	k_m (s^{-1})	k_c/k_m
PRORP2	0.027	0.77	0.025	0.1	0.021	0.003	7
PRORP3	0.025	0.82	0.020	0.12	0.021	0.002	10.5

Cys-Mito Pre-tRNA

Enzyme	$k_{obs,c}$ (s^{-1})	A_c	$k_{obs,m}$ (s^{-1})	A_m	k_c (s^{-1})	k_m (s^{-1})	k_c/k_m
PRORP2	0.014	0.77	0.009	0.12	0.011	0.001	11
PRORP3	0.023	0.58	0.022	0.36	0.013	0.008	1.6

[a]As measured in figure 4-5.
[b]The observed rate constant for correct product formation (C_o)
[c]Corresponding amplitude of $k_{obs,c}$
[d]The observed rate constant for miscleavage (M_{-1})
[e]Corresponding amplitude of $k_{obs,m}$
[f]Rate constants calculated as described in methods

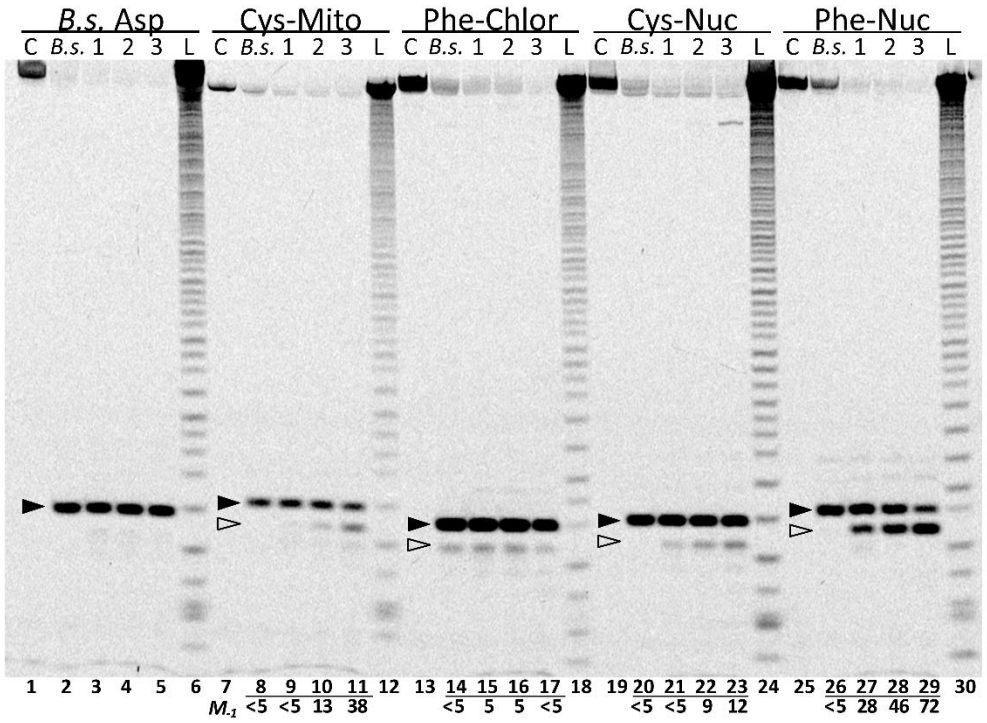

Figure 4-6. PAGE analysis of RNase P reaction products. 30 nM pre-tRNA substrate was incubated with 5 μM PRORP for 30 mins under standard assay conditions. The pre-tRNA substrate in each reaction is indicated above the wells. C:No enzyme control, B.s.:*B. subtilis* RNase P, 1:PRORP1, 2:PRORP2, 3:PRORP3, L:alkaline hydrolysis ladder. The normalized percent miscleaved (% M_{-1}) is represented below the lane number at the bottom of the gel. Closed arrows indicate the correct cleavage product (5 nts) and open arrows indicates miscleaved product (4 nts).

3’ Discriminator Base can Contribute to PRORP Cleavage Fidelity

We sought to discover the feature(s) of the Phe-Nuc substrate that contribute to significant miscleavage by all three PRORP enzymes. We hypothesized that the adenine discriminator base and the uridine base in the N_{-1} position of the leader (Figure 4-2) could base pair, which would extend the acceptor stem helix creating a 4 nt leader and perhaps explain the observed miscleavage. Indeed the three pre-tRNA substrates that can form an extra base pair (U:A) between the discriminator base and the N_{-1} leader position (Phe-Nuc, Cys-Mito, and Cys-Nuc) exhibit miscleavage, albeit to varying extents, depending on the PRORP (Figure 4-6). To further investigate the observed miscleavage, assay products were separated by high resolution urea-page and compared to reactions performed with *B. subtilis* RNase P and *B. subtilis* pre-tRNA^{Asp} (Figure 4-6). All enzymes cleave *B. subtilis* pre-tRNA^{Asp} correctly leaving a 5 nt product, indicating that the miscleavage observed with other substrates is not a result of nuclease contamination. Similarly, *B. subtilis* RNase P cleaves all four *A. thaliana* pre-tRNAs correctly, only a distinct 5 nt product band (< 5% miscleaved product) is observed. In contrast, the PRORP enzymes showed variable cleavage fidelities, with PRORP3 displaying the lowest cleavage fidelity among the PRORPs (Figure 4-6).

To further test our hypothesis that formation of an extra base pair may account for miscleavage we assessed the ability of PRORPs to correctly cleave three different Phe-Nuc pre-tRNAs variants possessing 5 nucleotide-long 5’ leaders and various 3’ ends: with (5:1) or without a 3’ discriminator base (5:0), and with an extended 20 nt 3’ trailer sequence (5:20). Products from STO reactions catalyzed by PRORP1, 2 and 3 with these pre-tRNA Phe-Nuc variants were resolved on a high-resolution denaturing PAGE gel (Figure 4-7A). Removal of the discriminator base (5:0) from Phe-Nuc pre-tRNA eliminated the miscleavage catalyzed by all of the PRORP enzymes, whereas addition of a longer trailer sequence had no significant effect on miscleavage (Figure 4-7A). Similarly, removal of the discriminator base from the Cys-Mito pre-tRNA, to delete a potential A-U basepair with N_{-1}, significantly reduced miscleavage catalyzed by PRORP3 (Figure 4-7B). Taken together these data provide evidence that the presence of a base pair with the N_{-1} in the leader and the discriminator base can engender miscleavage, possibly by allowing the pre-tRNA to adopt an alternative structure. However, the potential to form this base

pair does not always lead to miscleavage; the Cys-Mito and Phe-Chlor substrates, which contain a potential base pair between the N_{-1} and the discriminator base, are not significantly miscleaved by PRORP1 or 2. We posit that other determinants including sequence context, stability of the pre-tRNA structure, and differences in PRORP substrate recognition also influence cleavage fidelity.

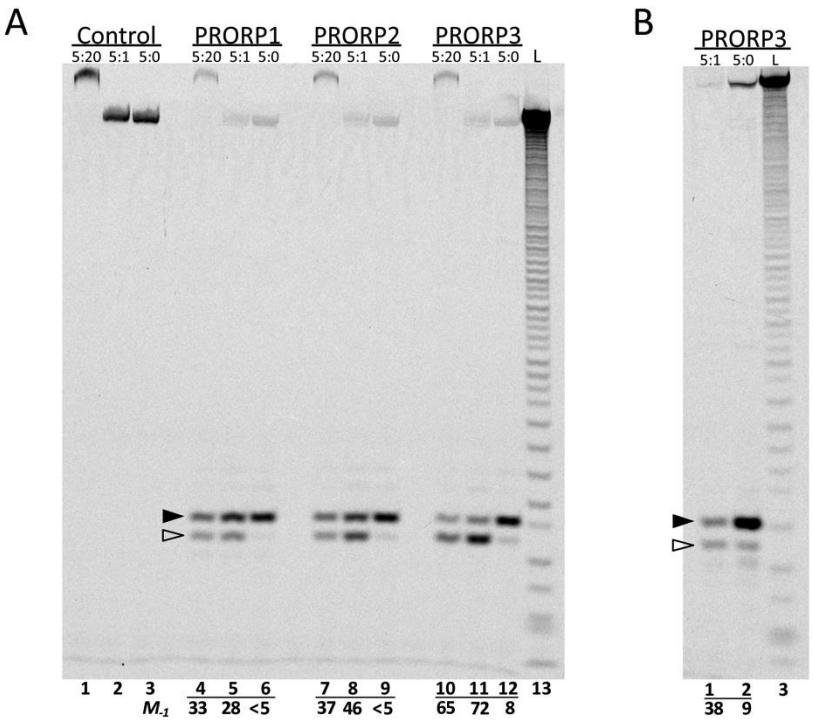

Figure 4-7. Miscleavage is alleviated by removal of the discriminator base. A. 30 nM pre-tRNA Phe-Nuc substrates (5:20, 5:1, and 5:0) were incubated with 5 μM PRORP1, 2, and 3 for 30 mins under standard reaction conditions. Products were resolved on a 20% gel. B. Miscleavage of pre-tRNA Cys-mito catalyzed by PRORP3 is reduced by removal of the discriminator base. Reactions were performed as described in A. Closed arrows indicate the correct cleavage product (5 nts) and open arrows indicates miscleaved product (4 nts).

PRORP Reactivity with Model Substrates

PRORPs must recognize and cleave substrates with a wide variety of sequences, but similar structures. Most proteins that interact with multiple tRNAs (e.g. RNA-based RNase P, EfTu) recognize various secondary structural features (24,25). To explore the structural features that are important for pre-tRNA maturation catalyzed by PRORP we created two truncated versions of the pre-tRNA Cys-Mito substrate: an RNA lacking an anticodon arm (ΔAC), and an RNA that connects the acceptor arm and TψC-arm to form a stem-loop (SL) (Figure 4-8). The 5' ends of □AC and SL were labeled with fluorescein, and the cleavage of the two model substrates catalyzed by PRORP1, 2, 3 was assessed under STO conditions (Table 4-3). All of the RNase P enzymes catalyze the removal of the 5' leader from the ΔAC substrate. This result is consistent with a previous observation that PRORP enzymes can cleave t-element RNA, tRNA-like structures that lack an anticodon stem-loop (3,10). PRORP3, and to a lesser extent PRORP2, catalyze miscleavage of the ΔAC RNA in a manner similar to the full-length pre-tRNA Cys-Mito substrate (gel not shown), suggesting that the anticodon helix does not influence the miscleavage of Cys-Mito pre-tRNA.

The stem-loop RNA was cleaved >30-fold slower than full-length Cys-Mito by all three PRORP enzymes. This suggests that in contrast to the anticodon stem-loop, the D- and TψC- arms are critical for either substrate binding or cleavage by PRORP. Interestingly, the STO rate constants for PRORP2 and 3 catalyzed cleavage of the SL model substrate are at least 12-fold faster than with PRORP1 (Table 4-4), suggesting a divergence in substrate recognition between the nuclear and organellar PRORPs.

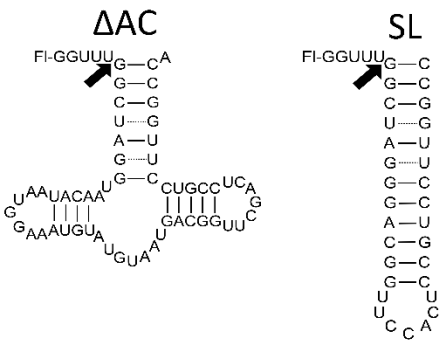

Figure 4-8. Model substrates. Predicted secondary structures of two model substrates, the ΔAC and SL, derived from the mitochondrial pre-tRNA^{Cys} sequence. The SL substrate connects the acceptor stem helix and TψC -arm.

Table 4-4. Single-turnover observed rate constants (k_{obs}) for cleavage of model substrates

	RNA		
Enzyme	Cys-Mito (s^{-1})[a]	Cys-Mito ΔAC (s^{-1})[b]	Cys-Mito SL (s^{-1})[c]
PRORP1	0.037 ± 0.002	0.023 ± 0.005	$< 3.3 \times 10^{-5}$
PRORP2	0.013 ± 0.003	0.012 ± 0.003	$4.2 \pm 0.5 \times 10^{-4}$
PRORP3[d]	0.023 ± 0.002	0.012 ± 0.002	$3.5 \pm 0.2 \times 10^{-4}$

[a]values from Table 1 shown for comparison
[b]Measured under standard reaction conditions using gel-based assay.
[c]Measured under standard assay conditions except with 10 μM enzyme using gel-based assay.
[d]k_{obs} calculated from total product (C_o + M_{-1}) formation.

Discussion

Here we provide a detailed kinetic comparison of *A. thaliana* PRORP enzymes, revealing more similarities than differences. In general, the three *A. thaliana* PRORPs catalyze 5' end cleavage with similar catalytic efficiencies (10^4 -10^5 M^{-1} s^{-1}), display comparable STO activities, and bind the same pre-tRNA substrate with approximately the same affinity. Despite these similarities, we uncovered evidence indicating that there is a sub-set of pre-tRNAs that are more efficiently processed by particular PRORP isozymes. For example, PRORP1 has a ~10-fold higher k_{cat}/K_M value for cleaving Phe-Chlor pre-tRNA compared to PRORP2 and 3. Nucleotide variation in the D- and TψC –loops may contribute to preferential cleavage and recognition by PRORP1. However, more detailed studies will need to be performed to determine the molecular interactions that confer this enhanced reactivity.

While PRORPs bind and cleave substrates with similar K_D values and cleavage rate-constants, they exhibit unexpected differences in cleavage fidelity. For instance, PRORP3 catalyzes the miscleavage of Cys-Mito, Cys-Nuc, and Phe-Nuc pre-tRNA to a greater extent than PRORP1 and PRORP2 (Figure 4-6). Removal of the discriminator base from Cys-Mito and Phe-Nuc pre-tRNAs results in increased fidelity for all three enzymes, suggesting that the discriminator base engenders miscleavage. Base-pairing between the discriminator nucleotide and the N_{-1} nucleotide of the leader, extending the acceptor stem by one base pair, could account for the observed miscleavages. The greater fidelity observed with PRORP1 could originate from specific interactions with the leader and/or interactions with the discriminator base. These data suggest a difference in substrate recognition among the PRORPs with regards to cleavage site selection. However, the question still remains whether PRORP-catalyzed pre-tRNA miscleavage occurs *in vivo.* Cleavage fidelity *in vivo* could be enhanced by RNA binding proteins that decrease incorrect base pairing or that stabilize RNA structure.

While all three PRORP enzymes catalyze miscleavage of the Phe-Nuc pre-tRNA (Figure 4-6), *B. subtilis* RNase P produces only the correctly cleaved product from the same substrate. This observation suggests that PRORP enzymes use different criteria to recognize the substrate cleavage site than bacterial RNase P. Bacterial RNase P recognizes the TψC-loop, nucleotides within the leader sequence, and the CCA of the 3'

end of pre-tRNA, though all are not required for accurate cleavage (23,26). The interactions that PRORP enzymes make with pre-tRNA substrates are still not well characterized. However, it has been proposed that PRORP enzymes recognize the elbow region of tRNA, similar to bacterial RNase P (15,16). Interactions that could increase fidelity of bacterial RNase P compared to PRORP in cleavage of the Phe-Nuc substrate are the base pairing with the RNA component with the N_{-1} uridine and the 3' end of pre-tRNA, leading to splaying of the 3' and 5' ends in the bound complex (26,27).

Based on the kinetic characterization performed here, PRORP2 and 3 are more similar to one another than to PRORP1. This is consistent with their higher sequence similarity and knockout data that suggest a redundant function for PRORP2 and 3 within the nucleus (10). Furthermore, the fidelity of PRORP2 is more similar to PRORP3 and, interestingly, both enzymes share higher STO activity toward the SL substrate than PRORP1 (k_{obs} >12-fold). This suggests that the nuclear PRORPs have some distinct but subtle differences in substrate recognition as compared to the organellar PRORP1. The overlapping substrate specificities of *Arabidopsis* PRORP enzymes suggest that they are in the early stages of diversification, which may be a result of relatively recent gene duplication events (3,28). Although all three PRORP enzymes catalyze pre-tRNA maturation comparably, it is still possible that these enzymes have distinct substrate preferences that were not identified with the substrate set used. It is interesting to note that the nuclease involved in 3' pre-tRNA maturation, tRNase Z, encodes four enzyme variants in *Arabidopsis* (29). These enzymes are differentially localized but only the chloroplast-localized tRNase Z knockout is lethal, suggesting several isozymes have a redundant function, similar to PRORP2 and 3. Furthermore, all recombinant tRNase Z enzymes catalyze 3' end processing of pre-tRNAs *in vitro*, similar to *Arabidopsis* PRORPs. The abundance of tRNase Z enzymes in *Arabidopsis* is attributed to differential cellular compartmental localization, differential expression, and/or tissue specific expression (29). Our data suggest that this is also the case with PRORP enzymes.

Methods

Enzyme and Substrate Preparation

PRORP constructs (Δ76PRORP1, full-length PRORP2, and Δ68PRORP3) were cloned, expressed and purified from *E. coli* as previously described (14). The concentrations of PRORP1, 2 and 3 were determined by absorbance using extinction coefficients in the native state at 280 nm of 84,630 M^{-1} cm^{-1}, 91,300 $M^{-1}cm^{-1}$, and 84,700 $M^{-1}cm^{-1}$, respectively. Purified enzymes were aliquoted, flash-frozen, and stored at -80 °C in 20 mM MOPS pH 7.8, 100 mM NaCl, and 1 mM TCEP. Pre-tRNA substrates were created by *in vitro* transcription with T7 polymerase (19,20). The DNA template for transcription was created by PCR amplification of DNA purchased from Life Technolgies GeneArt. To generate fluoroscein labeled pre-tRNA substrates, transcription reactions were performed in the presence of guanine monophosphothiolate and the 5' phosphorothioate was reacted with 5-(iodoacetamido)fluorescein to label the 5' end, as previously described (21). The pre-tRNA substrates were purified by denaturing PAGE (12%). The proposed tRNA secondary structures were generated with tRNAscan-SE 1.21 (22).

Multiple Turnover Assays

Multiple-turnover (MTO) reactions were performed in a 96-well plate format using a fluorescent anisotropy (FA) assay (as described in (23)). Standard reaction conditions, 30 mM MOPS pH 7.8, 150 mM NaCl, 1 mM TCEP, and 1 mM $MgCl_2$, were used with an enzyme concentration of 20 nM (PRORP1 and PRORP3) and 80 nM for PRORP2. The concentration of fluorescently labeled pre-tRNA was held constant at 40 nM in the reactions while the concentration of unlabeled pre-tRNA substrate was varied. The ratio of labeled to unlabeled substrate did not alter the measured initial rates (data not shown). Black Corning half-area 96-well plates were used with a final reaction volume of 40 µL per well. Initial rates were calculated from the linear decrease in anisotropy (23). The steady state kinetic parameters were calculated from a fit of the Michaelis-Menten equation (1) to the concentration-dependence of the initial rates using KaleidaGraph

(Synergy Software). The reported kinetic parameters and standard error were determined by fitting the concentration-dependence of the initial rates to equation 1.

$$(1)\quad \frac{v_o}{[\mathrm{E}]} = \frac{k_{\mathrm{cat}}[\mathrm{S}]}{K_{\mathrm{M}} + [\mathrm{S}]}$$

Anisotropy Binding Assays

Binding assays were performed as described previously (14). Briefly, the concentration of fluorescein labeled pre-tRNA was maintained at 20 nM, while the concentration of PRORP was varied (0.005 – 5 µM). Binding experiments were performed in 20 mM MOPS pH 7.8, 300 mM NaCl, 1 mM TCEP, and 1 mM $CaCl_2$ in a 96-well plate format. PRORP1 can bind but not cleave substrates in $CaCl_2$ (14). Fluorescence anisotropy was measured at an excitation wavelength of 488 nm and an emission wavelength of 535 nm. Equation 2 was fit to the dependence of the anisotropy on the protein concentration where A is the observed anisotropy, A_o is the initial anisotropy, ΔA is the total change in anisotropy, P is the concentration of PRORP, and K_D is the apparent dissociation constant.

$$(2)\quad \mathrm{A} = \mathrm{A_o} + \frac{\Delta\mathrm{A}\,[\mathrm{P}]}{[\mathrm{P}] + K_{\mathrm{D}}}$$

Single-Turnover Assays

For single-turnover reactions (STO), the enzyme and pre-tRNA concentrations were 5 µM and 30 nM, respectively, unless otherwise noted. Reactions were performed in standard conditions (see MTO) and initiated by addition of enzyme and quenched at specified time points (0 – 1200 sec) with an equal volume of 100 mM EDTA, 6 M urea, 0.1 % bromophenol blue, 0.1 % xylene cyanol, 2 µg/µl yeast tRNA. The fluorescently labeled 5' leader product was separated from pre-tRNA by electrophoresis on 20 or 22.5% denaturing PAGE gel. Gels were visualized using a Typhoon 9410 scanner and the fraction product quantified using ImageQuant 5.2 software. The observed single-turnover rate constant was calculated from a fit of a first order exponential equation to the data using KaleidaGraph fitting software (equation 3), where A is the end point, B is the amplitude, *k* is the observed rate constant, and t is time. The STO assays with *Bacillus subtilis* RNase P were performed at 25ºC with 1.8 µM bacterial RNase P, 50 mM Tris pH 7.4, 100 mM KCl, 75 mM NaCl, 10 mM DTT, and 3 mM $MgCl_2$. The *B. subtilis* RNase P

was prepared as described (24). STO miscleavage kinetics catalyzed by the PRORPs were analyzed as described in (25,26). Briefly, the observed rate constants for both correct and miscleaved product are obtained from a single-exponential fit to the data (equation 3). The resulting amplitude (A_c or A_m) for each respective fit is multiplied by the observed rate constant ($k_{obs,c}$ or $k_{obs,m}$) to obtain k_c and k_m (equations 4 and 5).

$$(3) \quad Fraction\ Product = \mathrm{A} - \mathrm{B}(\mathrm{e}^{-kt})$$

$$(4) \quad k_{\mathrm{c}} = k_{\mathrm{obs,c}}\ (A_{\mathrm{c}})$$

$$(5) \quad k_{\mathrm{m}} = k_{\mathrm{obs,m}}\ (A_{\mathrm{m}})$$

References

1. Walker, S.C. and Engelke, D.R. (2006) Ribonuclease P: the evolution of an ancient RNA enzyme. *Crit Rev Biochem Mol Biol*, **41**, 77-102.
2. Howard, M.J., Liu, X., Lim, W.H., Klemm, B.P., Fierke, C.A., Koutmos, M. and Engelke, D.R. (2013) RNase P enzymes: divergent scaffolds for a conserved biological reaction. *RNA Biol*, **10**, 909-914.
3. Gobert, A., Gutmann, B., Taschner, A., Gössringer, M., Holzmann, J., Hartmann, R.K., Rossmanith, W. and Giegé, P. (2010) A single Arabidopsis organellar protein has RNase P activity. *Nat Struct Mol Biol*, **17**, 740-744.
4. Holzmann, J., Frank, P., Löffler, E., Bennett, K.L., Gerner, C. and Rossmanith, W. (2008) RNase P without RNA: identification and functional reconstitution of the human mitochondrial tRNA processing enzyme. *Cell*, **135**, 462-474.
5. Vilardo, E., Nachbagauer, C., Buzet, A., Taschner, A., Holzmann, J. and Rossmanith, W. (2012) A subcomplex of human mitochondrial RNase P is a bifunctional methyltransferase--extensive moonlighting in mitochondrial tRNA biogenesis. *Nucleic Acids Res*, **40**, 11583-11593.
6. Vilardo, E. and Rossmanith, W. (2015) Molecular insights into HSD10 disease: impact of SDR5C1 mutations on the human mitochondrial RNase P complex. *Nucleic Acids Res*.
7. Taschner, A., Weber, C., Buzet, A., Hartmann, R.K., Hartig, A. and Rossmanith, W. (2012) Nuclear RNase P of Trypanosoma brucei: a single protein in place of the multicomponent RNA-protein complex. *Cell Rep*, **2**, 19-25.
8. Lai, L.B., Bernal-Bayard, P., Mohannath, G., Lai, S.M., Gopalan, V. and Vioque, A. (2011) A functional RNase P protein subunit of bacterial origin in some eukaryotes. *Mol Genet Genomics*, **286**, 359-369.
9. Hartmann, E. and Hartmann, R.K. (2003) The enigma of ribonuclease P evolution. *Trends Genet*, **19**, 561-569.
10. Gutmann, B., Gobert, A. and Giegé, P. (2012) PRORP proteins support RNase P activity in both organelles and the nucleus in Arabidopsis. *Genes Dev*, **26**, 1022-1027.
11. Goldfarb, K.C., Borah, S. and Cech, T.R. (2012) RNase P branches out from RNP to protein: organelle-triggered diversification? *Genes Dev*, **26**, 1005-1009.
12. Zhou, W., Karcher, D., Fischer, A., Maximova, E., Walther, D. and Bock, R. (2015) Multiple RNA Processing Defects and Impaired Chloroplast Function in Plants Deficient in the Organellar Protein-Only RNase P Enzyme. *PLoS One*, **10**, e0120533.
13. Sugita, C., Komura, Y., Tanaka, K., Kometani, K., Satoh, H. and Sugita, M. (2014) Molecular characterization of three PRORP proteins in the moss Physcomitrella patens: nuclear PRORP protein is not essential for moss viability. *PLoS One*, **9**, e108962.
14. Howard, M.J., Lim, W.H., Fierke, C.A. and Koutmos, M. (2012) Mitochondrial ribonuclease P structure provides insight into the evolution of catalytic strategies for precursor-tRNA 5' processing. *Proc Natl Acad Sci U S A*, **109**, 16149-16154.
15. Gobert, A., Pinker, F., Fuchsbauer, O., Gutmann, B., Boutin, R., Roblin, P., Sauter, C. and Giegé, P. (2013) Structural insights into protein-only RNase P complexed with tRNA. *Nat Commun*, **4**, 1353.
16. Imai, T., Nakamura, T., Maeda, T., Nakayama, K., Gao, X., Nakashima, T., Kakuta, Y. and Kimura, M. (2014) Pentatricopeptide repeat motifs in the processing enzyme PRORP1 in Arabidopsis thaliana play a crucial role in recognition of nucleotide bases at TψC loop in precursor tRNAs. *Biochem Biophys Res Commun*, **450**, 1541-1546.
17. Howard, M.J., Klemm, B.P. and Fierke, C.A. (2015) Mechanistic Studies Reveal Similar Catalytic Strategies for Phosphodiester Bond Hydrolysis by Protein-only and RNA-dependent Ribonuclease P. *J Biol Chem*.
18. Steitz, T.A. and Steitz, J.A. (1993) A general two-metal-ion mechanism for catalytic RNA. *Proc Natl Acad Sci U S A*, **90**, 6498-6502.
19. Liu, X., Chen, Y. and Fierke, C.A. (2014) A real-time fluorescence polarization activity assay to screen for inhibitors of bacterial ribonuclease P. *Nucleic Acids Res*, **42**, e159.

20. Beebe, J.A. and Fierke, C.A. (1994) A kinetic mechanism for cleavage of precursor tRNA(Asp) catalyzed by the RNA component of Bacillus subtilis ribonuclease P. *Biochemistry*, **33**, 10294-10598.
21. Hsieh, J., Walker, S.C., Fierke, C.A. and Engelke, D.R. (2009) Pre-tRNA turnover catalyzed by the yeast nuclear RNase P holoenzyme is limited by product release. *RNA*, **15**, 224-234.
22. Loria, A. and Pan, T. (1998) Recognition of the 5' leader and the acceptor stem of a pre-tRNA substrate by the ribozyme from Bacillus subtilis RNase P. *Biochemistry*, **37**, 10126-10133.
23. Zahler, N.H., Sun, L., Christian, E.L. and Harris, M.E. (2005) The pre-tRNA nucleotide base and 2'-hydroxyl at N(-1) contribute to fidelity in tRNA processing by RNase P. *J Mol Biol*, **345**, 969-985.
24. Kikovska, E., Brännvall, M., Kufel, J. and Kirsebom, L.A. (2005) Substrate discrimination in RNase P RNA-mediated cleavage: importance of the structural environment of the RNase P cleavage site. *Nucleic Acids Res*, **33**, 2012-2021.
25. LaRiviere, F.J., Wolfson, A.D. and Uhlenbeck, O.C. (2001) Uniform binding of aminoacyl-tRNAs to elongation factor Tu by thermodynamic compensation. *Science*, **294**, 165-168.
26. Reiter, N.J., Osterman, A., Torres-Larios, A., Swinger, K.K., Pan, T. and Mondragón, A. (2010) Structure of a bacterial ribonuclease P holoenzyme in complex with tRNA. *Nature*, **468**, 784-789.
27. Zahler, N.H., Christian, E.L. and Harris, M.E. (2003) Recognition of the 5' leader of pre-tRNA substrates by the active site of ribonuclease P. *RNA*, **9**, 734-745.
28. Lynch, M. and Conery, J.S. (2000) The evolutionary fate and consequences of duplicate genes. *Science*, **290**, 1151-1155.
29. Canino, G., Bocian, E., Barbezier, N., Echeverría, M., Forner, J., Binder, S. and Marchfelder, A. (2009) Arabidopsis encodes four tRNase Z enzymes. *Plant Physiol*, **150**, 1494-1502.
30. Emanuelsson, O., Brunak, S., von Heijne, G. and Nielsen, H. (2007) Locating proteins in the cell using TargetP, SignalP and related tools. *Nat Protoc*, **2**, 953-971.
31. Lange, A., Mills, R.E., Lange, C.J., Stewart, M., Devine, S.E. and Corbett, A.H. (2007) Classical nuclear localization signals: definition, function, and interaction with importin alpha. *J Biol Chem*, **282**, 5101-5105.

Chapter 5
Conclusions and Future Directions

Overview

The goal of this work has been to understand the molecular function of a novel form of RNase P (PRORP). This work revealed the crystal structure of PRORP1, which provides insight into the functions of the various domains and the overall architecture of PRORP enzymes. Mechanistic work revealed that the catalytic mechanism of PRORP is similar to the RNA-based mechanism. Lastly, this work demonstrates that PRORP enzymes in plants have overlapping substrate specificities but varying degrees of cleavage fidelity. This work describes the molecular function of a new family of RNA processing enzymes.

Conclusions

Crystal Structure of PRORP1

We solved the first crystal structure of a protein-only RNase P. The structure revealed that PRORP enzymes are composed of three domains (PPR, central Zn-binding, and NYN domains). Crystal structures of these domains were non-existent or just recently published, thus the structure provided valuable insight into their potential roles. Truncations and mutations identified active site residues within the NYN domain and revealed that the PPR domain enhances substrate affinity. PRORP enzymes can catalyze pre-tRNA cleavage using Mg^{2+}, Mn^{2+}, Co^{2+}, and Ni^{2+} cofactors. In conclusion, evolution pieced together three novel domains to create a protein-only RNase P.

Catalytic Mechanism of PRORP1

RNA-based RNase P is proposed to use a two-metal ion mechanism to catalyze phosphodiester bond hydrolysis. To determine if PRORP uses a similar catalytic

mechanism we performed metal and pH dependence studies using Wt and mutant enzymes. Surprisingly, these data mirrored the RNA-based RNase P behavior, suggesting that PRORP shares a similar catalytic mechanism to the RNA-based enzymes. Thus, NYN domains likely use a two-metal ion mechanism to catalyze phosphodiester bond hydrolysis with no amino acid side chains acting as a general acid or base. Taken together these data suggest the mechanistic convergence of two different macromolecules and highlight the importance of metal cofactors in catalysis.

Substrate Specificities of Plant PRORPs

For some reason the protein-only RNase P replaced the RNA-based RNase P. In plants, PRORPs replaced the RNA-based RNase P within the chloroplast, mitochondria, and the nucleus. However, in animals the nuclear RNase P has been retained. Why have PRORPs overtaken the nuclear RNA-based RNase P in plants but not within animals? One possible explanation may be that the nuclear PRORPs in plants have evolved additional functions and/or differing specificities, giving them a selective advantage. To test this hypothesis we examined the substrate specificities of the plant PRORPs to catalyze pre-tRNAs encoded in different organelles and with model RNA substrates. The plant PRORPs share similar catalytic efficiencies and bind pre-tRNA with uniform binding affinities. Despite these similarities, there are some substrates that show selectivity for a given PRORP but the reason for this selectivity remains unknown. Furthermore, model substrates react faster with nuclear PRORPs, suggesting some differences in specificity. However, plant PRORPs show more similarities than differences, suggesting, in plants, that the replacement of the nuclear RNA-based RNase P with PRORP did not require substantial changes in specificity or function.

Future Directions

While the work described within these chapters answered many questions about the function of PRORP, many important questions still remain. First, the molecular recognition strategies utilized by PRORP are largely undefined. Specifically, how the PPR domain interacts with pre-tRNA substrates is unknown. Second, a more detailed enzymatic mechanism of PRORP catalyzed pre-tRNA hydrolysis is required for a more detailed

comparison between protein and RNA-based RNase P enzymes. Third, the work described within these chapters focuses on the single-component PRORP found in plants and some protists. However, the human mitochondrial RNase P is composed of three protein components. Understanding the function of the other two components (TRMT10C/SDR5C1) in the pre-tRNA cleavage reaction is the next challenge. Lastly, the NYN domain found within PRORP is found in seven other proteins in humans. Many of these proteins are uncharacterized and contain RNA binding motifs, suggesting that they function as RNases. The biological function of one of these proteins, Regnase-1, has been studied in detail because of its important role in the immune response. However, the molecular function of Regnase-1 remains enigmatic (see Appendix C). I describe progress with regards to answering these outstanding questions and discuss approaches to take in the future.

PRORP Substrate Recognition

The sites of interaction between the pre-tRNA substrate and PRORP1 remain largely unknown. Crystallography, crosslinking, mutagenesis, and analyzing the binding and cleavage of pre-tRNA substrate variants are methods that will provide insight into PRORP1 substrate recognition. Truncation of the PPR domain in PRORP1 reduces binding affinity for pre-tRNA by ~30 fold (Figure 2-2). However, the residues within the PPR domain involved in pre-tRNA binding are unknown. Furthermore, where these residues interact with pre-tRNA is unclear. Site-directed mutagenesis and crosslinking can begin to answer this question and indeed my colleague Bradley Klemm has started this analysis. Interestingly, land plants contain approximately 500 genes that encode for PPR motifs, making it one of the largest gene families in plants (1). There are seven PPR containing proteins encoded within the human genome to date, all of which are proposed to function in the regulation of mitochondrial gene expression (2). The majority of these proteins are predicted to localize to the chloroplast and/or mitochondria where they are proposed to be involved in RNA regulation. Thus, understanding the molecular recognition strategies utilized by the PPR motifs in PRORP will provide great insight into understanding how this large family of proteins recognizes RNA targets.

Transition State Structure of PRORP1

To provide further insight into the cleavage mechanism of the NYN domain of PRORP1 solvent ^{18}O nucleophile KIE experiments could be performed to test the hypothesis that metal-bound hydroxide is the nucleophile in the reaction. This experiment was key to demonstrating a metal-hydroxide nucleophile for RNA-based RNase P (3). Reactions could be performed in 50% $H_2{}^{18}O$ under steady-state conditions where preliminary data indicates cleavage is the rate-limiting step. The mature tRNA product could be gel purified and processed for mass spectrometric analysis. The ratio of $^{18}O/^{16}O$ products relative to the solvent ratio can be used to determine the ^{18}O nucleophile isotope effect ($^{18}k_{nuc}$). Control experiments, including RNA-based RNase P, could be run in parallel. Normal isotope effects ($^{18}k_{nuc}$ >1) indicate nucleophilic attack in the rate-limiting step. A comparison of $^{18}k_{nuc}$ to previously measured isotope effects for model reactions, such as hydrolytic reactions with *p*-nitrophenyl-thymidine-5'-phosphate (T5PNP) in the presence and absence of Mg^{2+} (4), can implicate an inner-sphere interaction of the water nucleophile with Mg^{2+} by quantifying the “stiffness” of the bonding environment.

Single-atom modifications at the scissile phosphate and ribose hydroxyls can also be used to further elucidate the mechanism of catalysis of PRORP1. To test the hypothesis that the pro-S_P oxygen is coordinated to active site metal ions in PRORP, a substrate could be generated with the R_P- or S_P-phosphorothiate at the scissile phosphate. An inner sphere contact could be verified by addition of the more thiophilic Mn^{2+} or Cd^{2+}, which should enhance catalytic activity with the phosphorothioate-substituted substrate. The role of the 2’ hydroxyl at N_{-1} could be examined by substitution with 2’-H, 2’-NH_2, or 2’-OMe and the effects on STO cleavage could be examined. Changes in activity correlating with the hydrogen bonding ability of the substituents will support the role of the 2’ hydroxyl in leaving group stabilization.

Human Mitochondrial RNase P

Mammalian mitochondrial tRNAs often lack the conserved nucleotides involved in stabilizing the tertiary L-shape structure. Thus, they are often referred to as non-canonical tRNAs (10). Based on this observation it has been proposed that mammalian mitochondrial RNase P has recruited the TRMT10C/SDR5C1 complex to aid in substrate

recognition (11). In this model, PRORP recognizes pre-tRNA bound by the TRMT10C/SDR5C1 complex. Furthermore, this model suggests that the pre-tRNA bound by the TRMT10C/SDR5C1 complex adopts a conformation that is efficiently recognized and cleaved by PRORP. Transient kinetic studies analyzing binding and pre-tRNA cleavage via stopped-flow spectroscopy with fluorescein labeled pre-tRNA preincubated with and without the TRMT10C/SDR5C1 complex at varying concentrations of PRORP can be compared to kinetic models using Kintec Explorer or Berkely Madonna to help decipher the role of the complex in pre-tRNA maturation. Furthermore, PRORP alone may catalyze pre-tRNA cleavage of a subset of mitochondrial pre-tRNA substrates. Thus, examining reactivity with all of the predicted pre-tRNA substrates within the human mitochondria genome should also provide insight into the role of TRMT10C/SDR5C1 in RNase P catalysis.

References

1. Small, I.D. and Peeters, N. (2000) The PPR motif - a TPR-related motif prevalent in plant organellar proteins. *Trends in biochemical sciences*, **25**, 46-53.
2. Rackham, O. and Filipovska, A. (2012) The role of mammalian PPR domain proteins in the regulation of mitochondrial gene expression. *Biochimica et biophysica acta*, **1819**, 1008-1016.
3. Cassano, A.G., Anderson, V.E. and Harris, M.E. (2004) Analysis of solvent nucleophile isotope effects: evidence for concerted mechanisms and nucleophilic activation by metal coordination in nonenzymatic and ribozyme-catalyzed phosphodiester hydrolysis. *Biochemistry*, **43**, 10547-10559.
4. Cassano, A.G., Anderson, V.E. and Harris, M.E. (2002) Evidence for direct attack by hydroxide in phosphodiester hydrolysis. *J Am Chem Soc*, **124**, 10964-10965.
5. Klumpp, K., Hang, J.Q., Rajendran, S., Yang, Y., Derosier, A., In, P.W.K., Overton, H., Kevin E. B., P., Cammack, N. and Martin, J.A. (2003) Two-metal ion mechanism of RNA cleavage by HIV RNase H and mechanism-based design of selective HIV RNase H inhibitors. *Nucleic acids research*, **31**, 6852-6859.
6. Davies, J.F., 2nd, Hostomska, Z., Hostomsky, Z., Jordan, S.R. and Matthews, D.A. (1991) Crystal structure of the ribonuclease H domain of HIV-1 reverse transcriptase. *Science*, **252**, 88-95.
7. Pingoud, A. and Jeltsch, A. (2001) Structure and function of type II restriction endonucleases. *Nucleic acids research*, **29**, 3705-3727.
8. Rueda, D., Hsieh, J., Day-Storms, J.J., Fierke, C.A. and Walter, N.G. (2005) The 5' Leader of Precursor tRNA(Asp) Bound to the Bacillus subtilis RNase P Holoenzyme Has an Extended Conformation. *Biochemistry*, **44**, 16130-16139.
9. Howard, M.H., Klemm, B.P. and Fierke, C.A. (2015) Mechanistic Studies Reveal Similar Catalytic Strategies for Phosphodiester Bond Hydrolysis by Protein-only and RNA-dependent Ribonuclease P. *Journal of Biological Chemistry*, **290**, 13454-13464.
10. Suzuki, T., Nagao, A. and Suzuki, T. (2011) Human mitochondrial tRNAs: biogenesis, function, structural aspects, and diseases. *Annual review of genetics*, **45**, 299-329.
11. Reinhard, L., Sridhara, S. and Hallberg, B.M. (2015) Structure of the nuclease subunit of human mitochondrial RNase P. *Nucleic Acids Res*, **43**, 5664-5672.

Appendix B

PRORP1 Molecular Recognition

To determine the regions of pre-tRNA important for PRORP1 recognition, the leader and trailer lengths of Cys-Mito and Phe-Nuc pre-tRNAs were varied and the effects on single-turnover cleavage was examined (Figure B-1 and Table B-1). Variation of the leader and trailer lengths showed no significant correlation with activity and some pre-tRNA substrates displayed biphasic STO behavior (Figure B-1, bottom panel). A possible explanation for the biphasic kinetics is that these pre-tRNAs exist in two different substrate populations that react differently with PRORP1. To test this proposal, I assayed

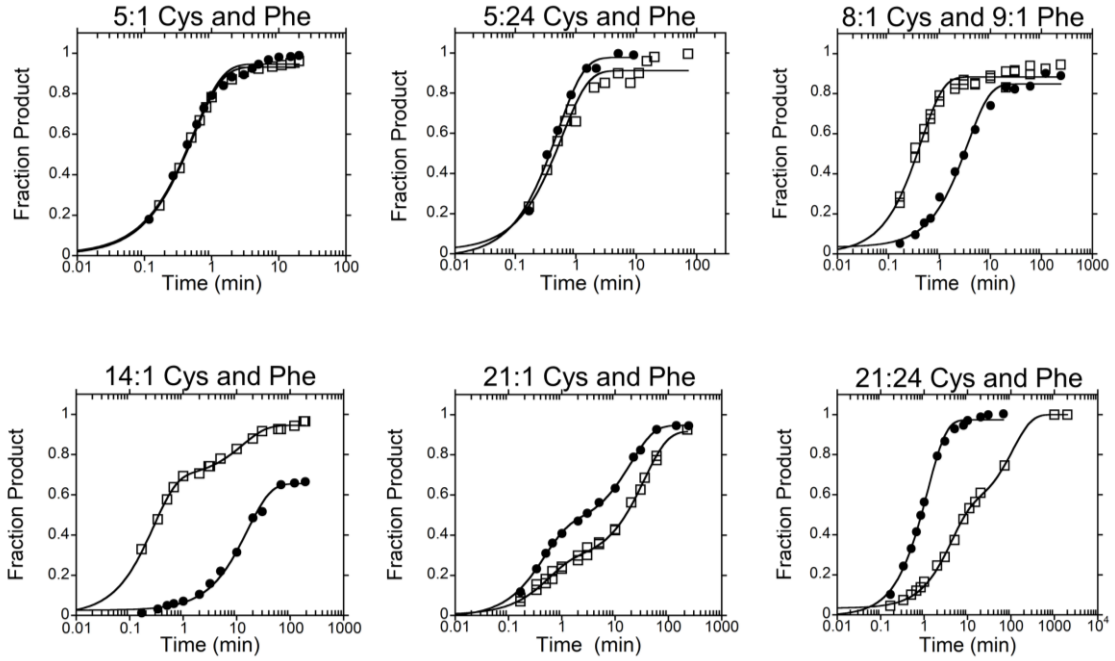

Figure B-1. PRORP1 single-turnover assays with Cys-Mito and Phe-Chlor variants. 5 µM PRORP1 was incubated with 20 nM indicated Fl-labeled pre-tRNAs under standard reaction conditions, quenched at specified time points, and products analyzed by urea-PAGE. The substrates used are mitochondrial pre-tRNA^{Cys} and chloroplastic pre-tRNA^{Phe} with indicated varying leader and trailer lengths (leader:trailer). Longer leader (>=14nt) pre-tRNAs display biphasic behavior and are fit to a double exponential equation (all data in the bottom panel except 21:24 Cys are fit to a double exponential, all other are fit to a single exponential. Data are summarized in table B-1.

the *B. subtilis* RNase P with the 21:1 Cys-Mito, a substrate which displayed biphasic behavior with PRORP1 (Figure B-1). *B. subtilis* RNase P STO activity with pre-tRNA Cys-Mito also displayed biphasic behavior, suggesting that two substrate populations exist that have different single-turnover reactivity (Figure B-2). It is likely that the extra leader sequence destabilizes the tRNA structure through alternative base pairing, creating a tRNA-like structure that is in equilibrium with the reactive pre-tRNA conformation. Given the complexity with these substrates, I moved to using the *B. subtilis* pre-tRNA^{Asp} substrate (*B.s.* pre-tRNA), which has been studied extensively with the ribozyme catalyzed reaction, to examine the leader length dependence on PRORP1 recognition.

Table B-1. Single-turnover rate constants for pre-tRNA^{Cys} and pre-tRNA^{Phe} variants [a]

	Cys-Mito		Phe-Chlor	
Pre-	$k_{obs,1}$ (min^{-1})	$k_{obs,2}$ (min^{-}	$k_{obs,1}$ (min^{-}	$k_{obs,2}$ (min^{-1})
5:1	1.9	-	1.8	-
9:1	0.28	-	2.3	-
14:1	0.06	-	3.6	0.07
21:1	2.2	0.05	1.8	0.05
21:24	1.0	-	1.8	0.03
5:24	2.0	-	1.7	-

[a]as measured in Figure B-1
[b]21:1 Cys-Mito and 14:1, 21:1, and 21:24 Phe-Chloro displayed biphasic kinetics and are fit to a double exponential equation ($k_{obs,1}$ and $k_{obs,2}$).

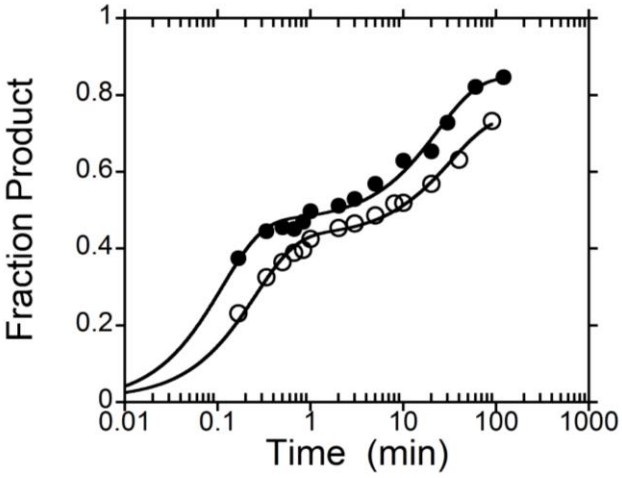

Figure B-2. Single-turnover activity of PRORP1 and *B. subtilis* RNase P with 21:1 Cys-Mito. Reactions were performed as described in figure 1 with the concentration of *B. subtilis* RNase P at 1.8 µM. The data were fit to a double exponential resulting in a $k_{obs,1}$ of 3.9 min^{-1}, $k_{obs,2}$ of 0.03 min^{-1} and amplitudes of 0.42 and 0.31, respectively, for the PRORP1 catalyzed reaction. The resulting parameters for *B. subtilis* catalyzed reaction are $k_{obs,1}$ = 8.9 min^{-1}, $k_{obs,2}$ = 0.04 min^{-1} and amplitudes of 0.47 and 0.37, respectively.

The STO activity of *B.s.* pre-tRNA with varying leader lengths (Figure B-3) was generally uniform (Figure B3 and Table B-2), with the exception of the 2 nt leader which has an ~8-fold increased STO rate constant compared to 14:1 *B.s.* pre-tRNA. Furthermore, variation of the leader length on *B.s.* pre-tRNA has no significant effect on PRORP1 binding affinity (Figure B-4). These data indicate that PRORP1 can efficiently bind and catalyze 1 nt leader substrates, suggesting that PRORP1 does not significantly contact the leader sequence past the -1 nt. The direct binding assay was performed with pre-tRNAs labeled with fluorescein on the 5' end. To exclude artifacts caused by the attached fluorescein, I performed competition binding experiments with the respective unlabeled pre-tRNAs (Figure B-4B). In these experiments an ES complex was formed with 1 µM PRORP1 and 5 nM 5:1 *B.s.* pre-tRNA in the presence of Ca^{2+}. Unlabeled pre-tRNAs were then added to compete off the labeled pre-tRNA, which leads to a decrease in anisotropy. The data were fit to a hyperbolic function and the apparent K_D (K_D^{app}) is reported in (Table B-3). The K_D^{app} value does not represent the K_D for unlabeled pre-tRNA, because it does not take into account the fraction of bound Fl-pre-tRNA. However, the competition experiments revealed the same trend as observed in the labeled binding experiment,

suggesting that the fluorescein has little effect on the binding trend (Table B-4). These experiments also revealed that PRORP1 binds to mature tRNA with approximately a 30-fold reduced binding affinity, suggesting that the 1 nt leader confers ~30-fold binding affinity.

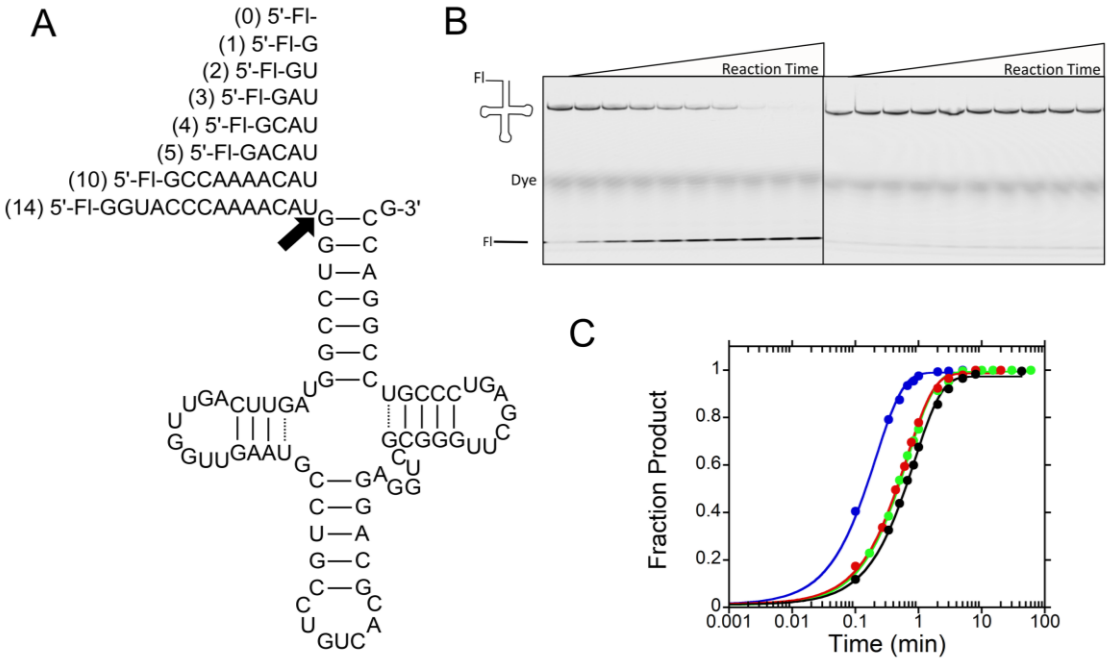

Figure B-3. PRORP1 single-turnover activity with *B. subtilis* pre-tRNA containing varying leader lengths. A. *B. subtilis* pre-tRNA^{Asp} (B.s.) with varying leader lengths used in this study. The 5' end is labeled with fluorescein (Fl). The arrow indicates the RNase P cleavage site. B. Representative single-turnover gels. Left panel show the reaction performed with 1:1 B.s. pre-tRNA and 5 µM PRORP1 and right panel shows an assay performed with 0:1 pre-tRNA and 5 µM PRORP1. C. Representative single-turnover plots for 1:1 Blue, 5:1 Green, 10:1 Red, 14:1 Black pre-tRNAs, performed as described in B.

Table B-2. Observed single-turnover rate constants for PRORP1 catalyzed pre-tRNA cleavage [a]

Pre-tRNA[b]	k_{obs} (min^{-1})	Fold [c]
1	4.7	3.9
2	9.4	7.8
3	1.9	1.6
4	1.5	1.3
5	1.5	1.3
10	1.5	1.3
14	1.2	1

[a]As measured in Figure B-3.
[b]Leader nt length
[c]as compared to 14:1

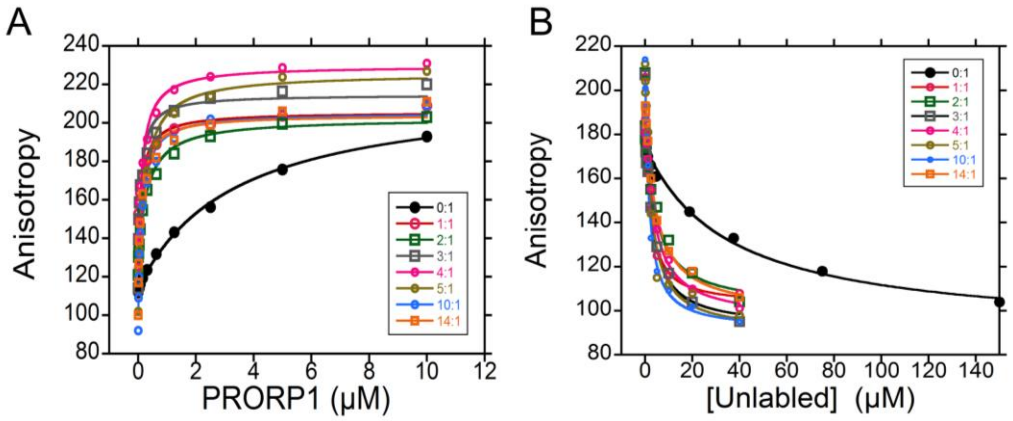

Figure B-4. Fluorescence anisotropy binding assays to measure PRORP1 binding affinity for B.s. pre-tRNA with varying leader lengths. A. Direct binding assays were performed with 5 nM Fl-labeled pre-tRNA and varying concentrations of PRORP1 in the presence of 1 mM $CaCl_2$, 20 mM Mops pH 7.8, 300 mM NaCl, and 1 mM TCEP at room temp. B. Competition binding assays. An ES complex was formed in the presence of Ca^{2+} with 5 nM 5:1 pre-tRNA and 1 μM PRORP1 and titrated against unlabeled pre-tRNAs. Dissociation constants and K_{DApp} are reported in table B-3.

Table B-3. Dissociation constants (K_D in nM) for PRORP1 binding to pre-tRNAs[a]

	Direct		Competition	
Leader	K_D (nM)[b]	Fold[c]	K_D^{app} (μM)	Fold[c]
0	3,400 ± 400	34	36	21
1	150 ± 60	1.5	2	1.2
2	310 ± 20	3.1	4.3	2.5
3	140 ± 40	1.4	2.8	1.6
4	150 ± 40	1.5	3.5	2
5	190 ± 60	1.9	2.3	1.4
10	100 ± 50	1	1.7	1
14	100 ± 30	1	4.2	2.5

[a]as measured in Figure B-4.
[b]Mean and standard deviation of two independent experiments is reported.
[C]as compared to the 10 nt leader pre-tRNA

To determine if the trailer sequence is an important determinant for PRORP1 recognition, I assayed the STO activity of PRORP1 with Cys-Mito containing various trailer lengths or sequences (only pre-tRNAs that did not display significant STO biphasic kinetics are reported). Variation of the trailer sequence length does not alter the binding affinity or STO cleavage rate constant, suggesting that PRORP1 does not make significant contacts with the 3' leader sequence (Table B-4). The Cys-Mito pre-tRNA containing a CCA sequence within the trailer shows a reduced STO cleavage rate constant, possibly by decreasing binding affinity. The binding affinity of some these substrates still needs to be examined (Table B-4).

Table B-4. Single turnover rate constants for pre-tRNA Cys-Mito with varying trailers

Pre-tRNA	k_{obs} (min^{-1})	Fold[c]	K_D (nM)[b]
5:1	2.4 ± 0.1	1	65 ± 5
5:0	1.7 ± 0.1	0.7	-
5:24	2.0 ± 0.1	0.8	70 ± 10
5:ACCA	0.5 ± 0.02	0.2	-
5:AGGU	2.0 ± 0.3	0.7	-

[a]as measured in figure B-1.
[b]as measured in Figure B-4A except in 100 mM NaCl.
[c]as compared to 5:1.

Pre-tRNA Crosslinking to PRORP1

To determine sites of interaction between PRORP1 and pre-tRNA I performed crosslinking experiments between PRORP1 and photoactivatable crosslinkers attached or incorporated within pre-tRNA. I created two different version of 5:1 pre-tRNA Cys-Mito containing either bromouridine (BrU) or azidophenacyl (AzP) crosslinkers. Bromouridine was incorporated at every uridine position within pre-tRNA Cys-Mito through *in vitro* transcription (i.e. the transcription reaction contained BrU instead of uridine triphosphate). The 5' end of pre-tRNA Cys-Mito was labeled with 4-azidophenacyl by reacting 4-Azidophenacyl bromide with pre-tRNA Cys-Mito containing GMPS at the 5' end. An ES complex was formed in the presence of Ca^{2+} using both labeled pre-tRNAs and irradiated with 312 nm light for various lengths of time, quenched and resolved on SDS-urea PAGE (Figure B-5). A crosslinked band is observed only in the presence of labeled pre-tRNA and time. The crosslinked band was extracted and treated with trypsin and RNase T1 for mass spectrometry analysis in collaboration with Dr. Håkansson lab. Samples are waiting analysis.

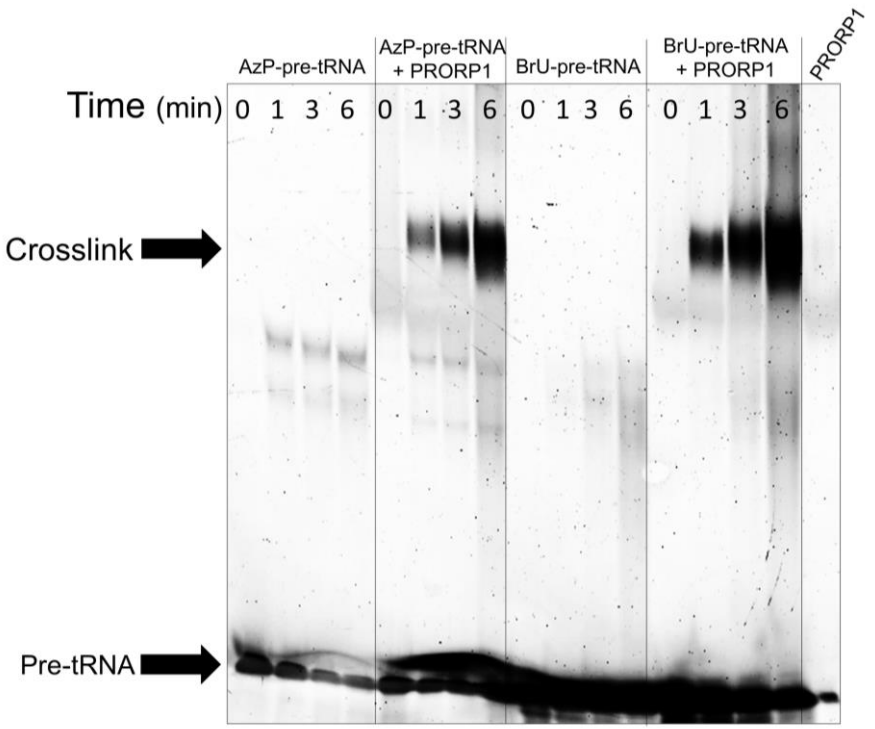

Figure B-5. PRORP1 crosslinking to AzP or BrU containing pre-tRNA Cys-Mito. 10 µM PRORP1 was incubated with 15 µM indicated pre-tRNA in the presence of 5 mM Ca^{2+}, irritated with 312 nm light for indicated times, and time points were separated on a 6% SDS-urea PAGE and stained with SYBER-gold.

PRORP1 Fluorescent Stopped-flow

Determining the kinetic binding mechanism will provide insight into the molecular recognition strategies used by PRORP1 and help delineate the contribution of domains/ residues on the individual steps of the reaction. Preliminary fluorescence stopped-flow experiments using 1 nt leader pre-tRNA labeled at the 5' end with fluorescein in the presence of Mg^{2+} revealed two phases. The dependence of the observed rate constants on PRORP1 concentration are shown in (Figure B-6). The first phase shows a hyperbolic dependence on PRORP1 concentration suggesting that it is limited by a conformational change step and not reporting on the bimolecular step. The second phase also shows a hyperbolic dependence on PRORP1 and has an observed rate constant similar to the cleavage rate constant measured by gel assays (0.08 s^{-1} by gel). Furthermore, this phase does not appear in the presence of Ca^{2+}, where pre-tRNA cleavage does not occur

(Figure B-6). Taken together these data suggest a two-step binding mechanism where an initial ES complex is formed that is not detectable by stopped-flow (possibly occurring within in the dead-time of the instrument), followed by a conformational change step (Scheme 1). Consistent with this proposal the starting fluorescence value of the first phase increases with increasing concentrations of PRORP1 suggesting that the formation of the initial ES complex has already occurred. Further experiments should include lowering the temperature to slow the reaction down in an attempt to capture the bimolecular step and modeling the reaction with Kintec Explorer or Berkeley Madonna to determine the microscopic rate constants and/or equilibrium constants. An alternative

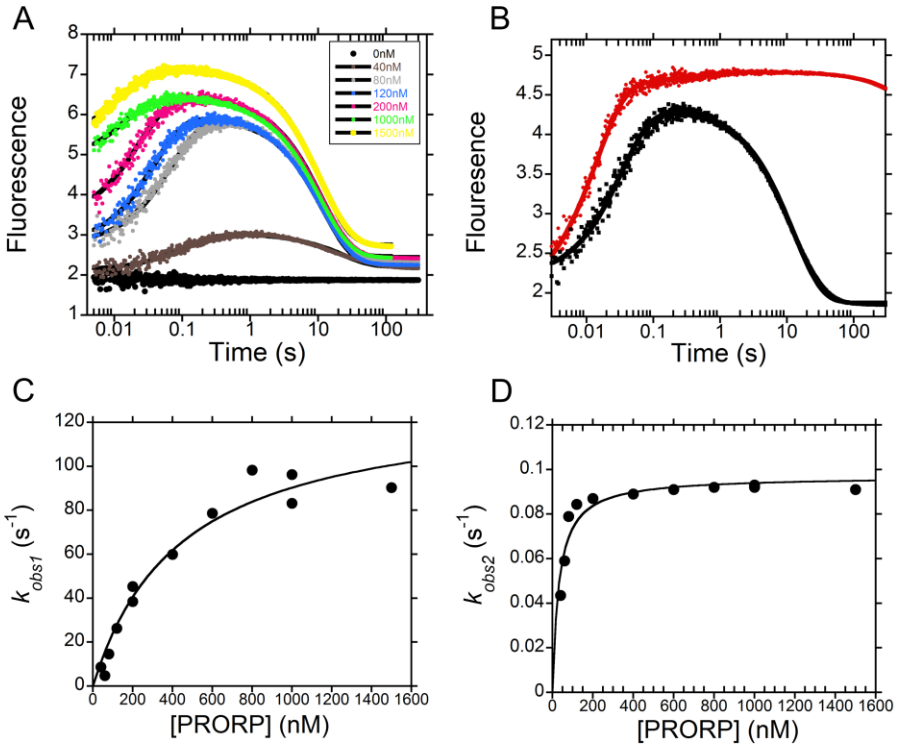

Figure B-6. Stopped-flow studies with PRORP1 and 1:1 B.s. pre-tRNA. A. Representative stopped-flow traces of varying concentrations of PRORP1 binding to 1:1 B.s. pre-tRNA (substrate concentration 15 nM) in 1 mM $MgCl_2$, 30 mM Mops pH 7.8, 150 mM NaCl, 1 mM TCEP at 25°C (black is 0 nM PRORP1, 80 nM: gray, blue: 200 nM, pink:500 nM. Traces were fit to a double exponential equation. B. 200 nM PRORP1 binding to 1:1 B.s. in the presence of 1 mM Ca^{2+} (red trace) or Mg^{2+} (black trace). C. The first observed rate constant plotted vs PRORP1 concentration. The data is fit to a hyperbolic function with k_{obs1} 108 ± 8 s^{-1} and $K_{1/2}$ 400 ± 80 nM. The Y-intercept has high error (-14 ± 9). D. The second observed rate constant plotted vs PRORP1 concentrations and fit to a hyperbola. The $K_{1/2}$ is 32 ± 6 nM and $k_{obs,2}$ max is 0.1 ± 0.001 s^{-1}.

explanation is that the first observable phase actually is the bimolecular step but enzyme stability or aggregation is creating artifactual data.

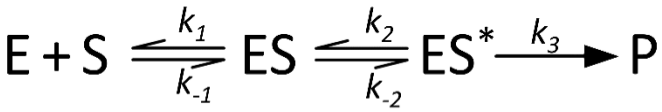

Scheme 1

Appendix C

NYN-domain Containing Proteins

The NYN domain of PRORP is a novel metallonuclease domain sharing homology to the PilT N-terminus (PIN) and flap nuclease families. This domain is also present in at least seven other genes within humans (1). These proteins generally have multi-domain architectures including various RNA-binding domains, suggesting their importance in RNA processing. One of these proteins, Regnase-1/Zc3H12a/MCPIP-1, was identified in a screen for genes that are over-expressed when macrophages are stimulated with lipopolysaccharides (LPS) or Monocyte Chemoattractant Protein-1 (MCP-1) (2-4). Subsequent studies revealed that Regnase-1 negatively regulates the immune response through endonucleolytic cleavage within the 3' UTRs of cytokine transcripts (4). Regnase-1 is essential for organism-level homeostasis. In mice, deletion of Regnase-1 results in severe systemic inflammation and anemia, with most dying within 12 weeks of birth (4,5). Furthermore, Regnase-1 restricts viral infection through cleavage of viral RNA and suppresses microRNA biogenesis through endonucleolytic processing of precursor miRNA (6-8). A molecular understanding of the function of Regnase-1 remains largely unknown. In particular, the molecular features of the RNA targets and their recognition by Regnase-1 are unknown. Revealing the specificity of Regnase-1 would help define a novel mechanism of mRNA turnover at the molecular level, provide insight into host defense mechanisms against viruses, and elaborate on the regulation of miRNA generation.

Typical eukaryotic mRNA decay involves shortening of the 3' poly-A tail and removal of the 5' cap (9). Elimination of these elements inhibits translation and promotes destruction of a transcript through the activity of 3' and 5' exonucleases. Alternatively, some mRNAs are processed through endonucleolytic cleavage within their 3' UTR, generating free 5' and 3' ends in a single step (10). For example, Regnase-1 negatively regulates the

expression of IL-6, IL-2, and its own mRNA through such a cleavage event (11-13). Unlike other regulatory proteins that bind within the 3' UTR and act as scaffolds for recruiting decay factors (14-16), Regnase-1 contains an endoribonuclease domain and cleaves mRNA to modulate protein expression. I hypothesize that Regnase-1 recognizes a stem-loop, termed a Regnase-reponsive element (RRE), within the 3' UTR of target RNAs through its CCCH-Zn^{2+} binding domain.

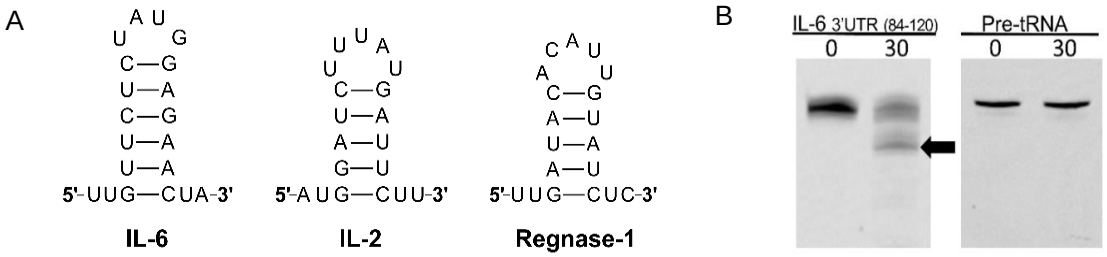

Figure C-1. Predicted secondary structures of Regnase-1 responsive elements (RREs) found within respective 3' UTRs and identified by luciferase reporter assays. 3' UTR regions indicated are: IL-6 (81-100), IL-2 (131-150), Regnase-1 (131-150).B. Reginase-1 was cloned, expressed in E. coli, purified and incubated with 20 nM fluorescein-labeled IL-6 (3' UTR 84-120) or Fl-pre-$tRNA^{Asp}$ as a control. Reactions were quenched at 30 min, resolved on urea-PAGE and imaged using a PhosporImager. Arrow indicates cleavage product.

Regnase-1 catalyzes the decay of IL-6, IL-2 and Regnase-1 (its own transcript) mRNAs via cleavage within the 3' UTR (11-13). Cell-based reporter assays have identified a ~20 nt sequence within the 3' UTR of these mRNAs that confer Regnase-1 specific turnover (11-13). These regions are predicted to form stem-loop structures (Figure 5-1) and may represent the molecular determinant for Regnase-1 specificity. To begin to test this proposal, I purified recombinant human Regnase-1 and examined its ability to catalyze cleavage of a putative RRE within IL-6 mRNA (Figure 5-1B). Future experiments could include determining the cleavage site by comparing cleavage products to alkaline hydrolysis ladders on high-resolution gels. Substrate affinity can be measured using an anisotropy binding assay. RNA sequences can be added and/or truncated from both 5' and 3' ends until Regnase-1 binding and cleavage activity is optimal. My data (Figure 5-

1), suggest that Regnase-1 catalyzes phosphodiester bond hydrolysis of a single site within the IL-6 3' UTR.

Additionally, Regnase-1 has also been proposed to negatively regulate the expression of C-Rel, Calcr, and IL-12B transcripts (11). However, direct evidence for cleavage of these substrates by Regnase-1 is lacking. To test this, Regnase-1-catalyzed cleavage of the 3'UTRs of these RNAs *in vitro* could be examined as discussed above. These studies would expand the substrate set and help define the molecular recognition strategies and biological function of Regnase-1.

To determine the secondary structure of the RREs in the 3' UTR of IL-6, IL-2, and Regnase-1, enzymatic probing techniques could be used (17). Fluorescently labeled *in vitro* transcripts could be incubated individually with nuclease S1 (cleaves ssRNA) and Ribonuclease V1 (dsRNA) and resolved on a high resolution gel next to alkaline ladders to determine sites of reactivity (17).

Sequence alignment and domain analysis indicates that Regnase-1 has five domains/conserved regions, including a $C(X)_5C(X)_5C(X)_3H$ (CCCH) Zn-binding site (Figure 5-2). In tristetraprolin (TPP) protein, a CCCH-Zn^{2+} binding site mediates binding to AU-Rich elements (AREs) within 3' UTRs to modulate mRNA decay (18,19). By extension, I propose that the CCCH-Zn^{2+} binding site within Regnase-1 also confers RNA binding. To test this hypothesis, Zn^{2+} binding ligands (C306, C312, C318, and H322) and residues conserved near the CCCH-Zn^{2+} binding site (Y308, R310, K317, R319, F320) could be mutated to alanine. Variants could then be analyzed for their ability to bind and cleave RREs compared to WT using anisotropy binding and cleavage assays.

Figure C-2. Regnase-1 contains five domains. The NYN metallonuclease domain is responsible for catalyzing phosphodiester bond hydrolysis. The Zn domain binds a Zn atom through conserved CCCH ligands. The roles of ubiquitin associated (UBA), proline rich motif (Pro), and the conserved c-terminal (CCR) domains in Regnase-1 function are unknown. The crystal structure of the NYN domain from Regnase-1 has been determined (Xu, J. et al., NAR, 2012).

Crosslinking experiments using incorporation of photo-reactive amino acids could be performed for Regnase-1 to further map RNA binding sites. Briefly, reactive crosslinking groups could be inserted using non-natural amino acid incorporation within the NYN domain (R214, R215, R220, and/or K219) and within the CCCH-Zn^{2+} binding site (Y308 and F320). Crosslinked RNA could be purified and crosslinked sites identified by reverse transcription.

References

1. Anantharaman, V. and Aravind, L. (2006) The NYN domains: novel predicted RNAses with a PIN domain-like fold. *RNA Biol*, **3**, 18-27.
2. Zhou, L., Azfer, A., Niu, J., Graham, S., Choudhury, M., Adamski, F.M., Younce, C., Binkley, P.F. and Kolattukudy, P.E. (2006) Monocyte chemoattractant protein-1 induces a novel transcription factor that causes cardiac myocyte apoptosis and ventricular dysfunction. *Circ Res*, **98**, 1177-1185.
3. Liang, J., Wang, J., Azfer, A., Song, W., Tromp, G., Kolattukudy, P.E. and Fu, M. (2008) A novel CCCH-zinc finger protein family regulates proinflammatory activation of macrophages. *J Biol Chem*, **283**, 6337-6346.
4. Matsushita, K., Takeuchi, O., Standley, D.M., Kumagai, Y., Kawagoe, T., Miyake, T., Satoh, T., Kato, H., Tsujimura, T., Nakamura, H. *et al.* (2009) Zc3h12a is an RNase essential for controlling immune responses by regulating mRNA decay. *Nature*, **458**, 1185-1190.
5. Zhou, Z., Miao, R., Huang, S., Elder, B., Quinn, T., Papasian, C.J., Zhang, J., Fan, D., Chen, Y.E. and Fu, M. (2013) MCPIP1 deficiency in mice results in severe anemia related to autoimmune mechanisms. *PLoS One*, **8**, e82542.
6. Lin, R.J., Chu, J.S., Chien, H.L., Tseng, C.H., Ko, P.C., Mei, Y.Y., Tang, W.C., Kao, Y.T., Cheng, H.Y., Liang, Y.C. *et al.* (2014) MCPIP1 suppresses hepatitis C virus replication and negatively regulates virus-induced proinflammatory cytokine responses. *J Immunol*, **193**, 4159-4168.
7. Liu, S., Qiu, C., Miao, R., Zhou, J., Lee, A., Liu, B., Lester, S.N., Fu, W., Zhu, L., Zhang, L. *et al.* (2013) MCPIP1 restricts HIV infection and is rapidly degraded in activated CD4+ T cells. *Proc Natl Acad Sci U S A*, **110**, 19083-19088.
8. Lin, R.J., Chien, H.L., Lin, S.Y., Chang, B.L., Yu, H.P., Tang, W.C. and Lin, Y.L. (2013) MCPIP1 ribonuclease exhibits broad-spectrum antiviral effects through viral RNA binding and degradation. *Nucleic Acids Res*, **41**, 3314-3326.
9. Garneau, N.L., Wilusz, J. and Wilusz, C.J. (2007) The highways and byways of mRNA decay. *Nature reviews Molecular cell biology*, **8**, 113-126.
10. Schoenberg, D.R. (2011) Mechanisms of endonuclease-mediated mRNA decay. *Wiley interdisciplinary reviews. RNA*, **2**, 582-600.
11. Matsushita, K., Takeuchi, O., Standley, D.M., Kumagai, Y., Kawagoe, T., Miyake, T., Satoh, T., Kato, H., Tsujimura, T., Nakamura, H. *et al.* (2009) Zc3h12a is an RNase essential for controlling immune responses by regulating mRNA decay. *Nature*, **458**, 1185-1190.
12. Li, M., Cao, W., Liu, H., Zhang, W., Liu, X., Cai, Z., Guo, J., Wang, X., Hui, Z., Zhang, H. *et al.* (2012) MCPIP1 down-regulates IL-2 expression through an ARE-independent pathway. *PloS one*, **7**.
13. Iwasaki, H., Takeuchi, O., Teraguchi, S., Matsushita, K., Uehata, T., Kuniyoshi, K., Satoh, T., Saitoh, T., Matsushita, M., Standley, D.M. *et al.* (2011) The IκB kinase complex regulates the stability of cytokine-encoding mRNA induced by TLR-IL-1R by controlling degradation of regnase-1. *Nature immunology*, **12**, 1167-1175.
14. Brooks, S.A. and Blackshear, P.J. (2013) Tristetraprolin (TTP): interactions with mRNA and proteins, and current thoughts on mechanisms of action. *Biochimica et biophysica acta*, **1829**, 666-679.
15. Van Etten, J., Schagat, T.L., Hrit, J., Weidmann, C.A., Brumbaugh, J., Coon, J.J. and Goldstrohm, A.C. (2012) Human Pumilio proteins recruit multiple deadenylases to efficiently repress messenger RNAs. *The Journal of biological chemistry*, **287**, 36370-36383.
16. Leppek, K., Schott, J., Reitter, S., Poetz, F., Hammond, M.C. and Stoecklin, G. (2013) Roquin promotes constitutive mRNA decay via a conserved class of stem-loop recognition motifs. *Cell*, **153**, 869-881.
17. Messmer, M., Pütz, J., Suzuki, T., Suzuki, T., Sauter, C., Sissler, M. and Catherine, F. (2009) Tertiary network in mammalian mitochondrial tRNAAsp revealed by solution probing and phylogeny. *Nucleic acids research*, **37**, 6881-6895.

18. Lai, W.S., Kennington, E.A. and Blackshear, P.J. (2002) Interactions of CCCH zinc finger proteins with mRNA: non-binding tristetraprolin mutants exert an inhibitory effect on degradation of AU-rich element-containing mRNAs. *The Journal of biological chemistry*, **277**, 9606-9613.
19. Lai, W.S., Perera, L., Hicks, S.N. and Blackshear, P.J. (2014) Mutational and structural analysis of the tandem zinc finger domain of tristetraprolin. *The Journal of biological chemistry*, **289**, 565-580.